Increasing oncoselectivity of virotherapy: Receptor targeted viruses against CD30-positive malignancies

Dem Fachbereich Biologie der Technischen Universität Darmstadt

zur Erlangung des akademischen Grades

eines Doctor rerum naturalium

vorgelegte Dissertation von

Diplom Biochemikerin

Julia Hanauer

aus Frankfurt am Main

Erstgutachterin: Prof. Dr. Beatrix Süß

Zweitgutachter: Prof. Dr. Alexander Löwer

Drittgutachter: Prof. Dr. Christian Buchholz

Darmstadt 2018

Hanauer, Julia: Increasing oncoselectivity of virotherapy: Receptor targeted viruses against CD30-positive malignancies

Darmstadt, Technische Universität Darmstadt

Jahr der Veröffentlichung der Dissertation auf TUprints: 2018

Tag der mündlichen Prüfung: 23.11.2018

Die vorliegende Arbeit wurde unter der Leitung von Prof. Dr. Christian Buchholz in der Arbeitsgruppe „Molekulare Biotechnologie und Gentherapie“ am Paul-Ehrlich-Institut in Langen angefertigt.

Die Betreuung seitens der Technischen Universität Darmstadt erfolgte durch Prof. Dr. Beatrix Süß vom Fachbereich Biologie.

Ein Gelehrter in seinem Laboratorium ist nicht nur ein Techniker;
er steht auch vor den Naturgesetzen wie ein Kind vor der Märchenwelt.

- Marie Curie

Table of contents

Zusammenfassung

Beim klassischen Hodgkin Lymphom (cHL) handelt es sich um eine maligne Erkrankung des hämatopoetischen Systems, die durch ein einzigartiges histologisches Muster charakterisiert ist. Die Tumormasse ist hauptsächlich aus infiltrierten Lymphozyten und anderen Zellen hämatologischen Ursprungs zusammengesetzt, jedoch aus nur sehr wenigen neoplastischen Zellen. cHL-Tumorzellen werden durch CD30 als wichtigsten immunologischen Marker charakterisiert. Die Mehrheit der Patienten mit cHL in einem frühen Stadium können durch Standardtherapie, einer Kombination aus multimodaler Chemotherapie und Radiotherapie, behandelt werden. Jedoch sind Behandlungsmöglichkeiten für Patienten, die nicht empfänglich für die Standardtherapie sind oder ein Rezidiv erleiden, noch unzureichend. In den letzten Jahren haben neue Ansätze für die Behandlung von cHL basierend auf Immuntherapie an Bedeutung gewonnen. CD30 ist als Zielmolekül dabei von besonderer Bedeutung, da es auf anderen Zellen nur sehr gering exprimiert wird. Onkolytische Viren (OV) kombinieren die selektive Lyse von Tumorzellen mit der Induktion einer antitumoralen Immunantwort. Da sie jedoch einen relativ breiten Tropismus aufweisen, wurden verschiedene Strategien entwickelt, um die Tumorselektivität zu erhöhen. Ein Ansatz basiert auf dem Retargeting des Zelleintritts viraler Partikel auf einen bestimmten Rezeptor der Wahl durch genetische Modifikation der viralen Hülle.

Die vorliegende Arbeit beschäftigt sich mit einer neuartigen Behandlungsstrategie für cHL, die auf genetisch modifizierten CD30-targetierten OV beruht. Dazu wurden Masernviren (MV) und Vesikuläre Stomatitis Viren (VSV) so verändert, dass sie CD30 als Rezeptor für die Infektion von $CD30^+$ cHL Tumorzellen verwenden. MV-CD30 und VSV-CD30 basieren auf einem kürzlich beschriebenen CD30-spezifischen Einzelkettenantikörperfragment (scFv) und wurden für diese Arbeit zur Verfügung gestellt. Für die Generierung von VSV-CD30 wurde VSV-G deletiert und gegen die modifizierten Glykoproteine von MV-CD30 ersetzt. In der vorliegenden Arbeit wurde zunächst die spezifische Infektion von zwei verschiedenen $CD30^+$ cHL Tumorzelllinien, L-428 und KM-H2 gezeigt. Zusätzlich wurde die onkolytische Aktivität von MV-CD30 und VSV-CD30 *in vitro* untersucht. VSV-CD30 tötete beide cHL Tumorzelllinien nach Infektion ab, wohin gegen gesunde $CD30^+$ T Lymphozyten vor der Infektion mit CD30-targetieren Viren geschützt waren. VSV-CD30 replizierte schneller als MV-CD30 und erreichte höhere Maximaltiter. Darüber hinaus gaben

infizierte Zellen VSV-CD30 deutlich effizienter in das Zellkulturmedium ab als MV-CD30, so dass VSV-CD30 zellfrei aus dem Überstand aufgereinigt werden konnte.

Für präklinische Studien wurden zwei xenograft Tumormausmodelle von humanem cHL in immundefizienten NSG Mäusen etabliert. Zuerst wurde ein lokales Tumormodell etabliert, in dem die Tumorzellen in einem subkutanen (s.c.) Tumor wuchsen. Subkutane KM-H2 Tumore wurden durch die VSV-CD30 Behandlung in ihrem Wachstum verlangsamt, s.c. L-428 Tumore jedoch nicht. Zusätzlich konnte aus s.c. KM-H2 Tumoren replizierendes VSV-CD30 isoliert werden. Das Wachstum der s.c. KM-H2 Tumore wurde durch ein Hydrogel aus künstlicher extrazellulärer Matrix („Matrigel") stabilisiert. Demnach wurde ein Tumormausmodell basierend auf KM-H2 Zellen als am besten geeignet identifiziert. Basierend darauf wurden die antitumoralen Aktivitäten von MV-CD30 im Vergleich zu VSV-CD30 untersucht. Sowohl intratumoral als aus systemisch appliziertes VSV-CD30 verlangsamte das Tumorwachstum der cHL Tumore über mehrere Wochen, was zu einem signifikanten Überlebensvorteil der tumortragenden Mäuse führte. Zusätzlich wurde ein disseminiertes Tumormodell etabliert, um das Tumorwachstum einer klinisch relevanten Situation besser wiederspiegeln zu können. In diesem Modell reagierten ebenfalls einige Mäuse auf die VSV-CD30 Behandlung durch Verlangsamung des Tumorwachstums. Im Unterschied zu cHL waren $CD30^+$ anaplastisch-großzellige Lymphom (ALCL) Tumorzelllinien nicht suszeptibel für eine Infektion mit VSV-CD30, jedoch für die Infektion mit MV-CD30 *in vitro*. Diese Beobachtung zeigt, dass das onkolytische Potential von VSV-CD30 nicht verallgemeinert werden kann und für jede Tumorart einzeln untersucht werden muss.

Die Charakterisierung von VSV-CD30 in dieser Arbeit liefert die Grundlage, auf der weiterführende präklinische Studien durchgeführt werden können für eine Anwendung als Therapeutikum gegen cHL.

Summary

Classical Hodgkin lymphoma (cHL) is a hematopoietic malignancy with a characteristic cellular composition. The tumor mass is made up of infiltrated lymphocytes and other cells of hematologic origin but only very few neoplastic cells that are mainly identified by the diagnostic marker CD30. While most patients with early stage cHL can be cured by standard therapy, treatment options for relapsed or refractory cHL are still inadequate, although immunotherapy-based approaches for the treatment of cHL patients have gained ground in the last decade. As targeting molecule CD30 is in focus since it is only minimally expressed on normal cells. Oncolytic viruses (OV) combine the selective lysis of tumor cells with the induction of an antitumoral response. Due to the broad tropism, strategies to increase tumor specificity were developed. One approach is the retargeting of cell entry of viral particles to a receptor of choice through genetic modification of the viral envelope.

This thesis investigates CD30-targeted oncolytic viruses as novel therapeutic concept against cHL selectively destroying $CD30^+$ tumor cells. CD30-targeted measles virus (MV-CD30) and vesicular stomatitis virus (VSV-CD30) were generated in a previous work and rely on a recently described CD30-specific single chain variable fragment (scFv). For VSV-CD30 the VSV glycoprotein G reading frame is replaced by those of the CD30-targeted MV glycoproteins. In the current thesis, selectivity for the infection of $CD30^+$ cHL cells was demonstrated by infection experiments of two cHL cell lines L-428 and KM-H2. *In vitro* killing capacity of VSV-CD30 vs. MV-CD30 was examined, demonstrating that VSV-CD30 induced more rapid and efficient killing of both cHL cell lines. In contrast, $CD30^+$ activated healthy T lymphocytes were protected from infection with CD30-targeted viruses. Notably, VSV-CD30 yielded much higher titers than MV-CD30 and could be purified out of supernatant of infected cells. For preclinical studies, two xenograft tumor mouse models of human cHL in immunodeficient NSG mice were designed. First, a local subcutaneously growing cHL mouse model was established. Subcutaneous KM-H2 but not L-428 tumors responded to VSV-CD30 treatment with growth inhibition. In addition, replicating virus could be recovered from tumor tissue. After stabilizing tumor growth using “Matrigel” and demonstrating that virus replication is not hindered in this extracellular based hydrogel, KM-H2 was identified as a potentially appropriate tumor model. Using the established local mouse tumor model, antitumoral activities of both MV-CD30 and VSV-CD30 were evaluated.

Remarkably, intratumorally, as well as systemically injected VSV-CD30 significantly slowed down tumor growth of cHL xenografts resulting in a substantially prolonged survival of tumor-bearing mice. Second, a disseminated growing cHL mouse model was established to represent a clinically more relevant tumor burden. At least in some mice, VSV-CD30 treatment induced tumor growth inhibition, again underlining the CD30 targeting capacity. In contrast to cHL, $CD30^+$ anaplastic large cell lymphoma (ALCL) cell lines were not susceptible for the infection with VSV-CD30 but rather for the infection with MV-CD30. These findings demonstrate that oncolytic potential of VSV-CD30 cannot be generalized and has to be separately evaluated for each type of tumor.

In summary, this study is a proof of concept that VSV-CD30 has oncolytic activity against xenograft cHL tumors. It will pave the way for further preclinical investigations to use VSV-CD30 as a novel therapeutic agent for the treatment of cHL.

1 Introduction

1.1 Lymphoma

Lymphomas are part of a heterogeneous group of malignant diseases of the lymphatic system. The lymphatic system includes lymph nodes, spleen, thymus, and bone marrow. Therefore, lymphomas can affect all those lymphatic areas as well as other organs (extranodal). Lymphomas mainly arise from B- or T cells at various stages of development. These lymphocytes change their expression profile and underlie lymphomagenesis. The characteristics of the specific lymphomas correlate to the cell from which they originated.

Lymphomas are divided in two main types: Hodgkin lymphoma (HL) and non-Hodgkin lymphoma (NHL). HL accounts for about 10% of all lymphomas and is primarily defined histologically by the presence of Hodgkin- and Reed-Sternberg (HRS) cells (Pierce and Mehta 2017). Additionally, classical HL (cHL) is defined by a constant CD30 expression. NHL represents a rather wide spectrum of illness and ranges from indolent to aggressive malignancies (Armitage et al. 2017). Approximately 85-90% of NHL are classified as mature B cell neoplasms, whereas the remaining 10-15% are mature T cell and natural killer (NK)-cell neoplasms. The relative frequency of specific subtypes of NHL varies geographically (Armitage et al. 2017). The diffuse large B-cell lymphoma (DLBCL) is the most common subtype of NHL. Besides cHL, also DLCBL and anaplastic large cell lymphoma (ALCL) both as subtypes of NHL express a high amount of CD30 (Pierce and Mehta 2017). For DLBCL the usual treatment relies on standard chemotherapy regimens and radiotherapy, often in combination with the CD20 monoclonal antibody rituximab. The addition of rituximab improves the treatment outcome of DLBCL. Since CD30 is expressed on a variety of lymphoma subtypes, it was recognized as a potential target for therapy.

1.1.1 Hodgkin lymphoma

Classical Hodgkin lymphoma (cHL) was first described by Thomas Hodgkin in 1832 (Hodgkin 1832). It is one of the most frequent lymphomas in the Western world which occurs with an incidence of 3-4 cases per 100.000 persons per year (Küppers 2012). cHL is a malignant disease of the hematopoietic system, but can also affect peripheral lymph nodes and extranodel sites such as liver, lung, and bone marrow (Küppers 2012). Tumor cells of cHL are composed of mononucleated Hodgkin (HL) and bi- or multinucleated Reed-Sternberg (HRS) cells which were first described around 1900 by Dorothy Reed and Carl Sternberg (Figure 1.1 A) (Reed 1902; Sternberg 1898). The most important immunological marker on malignant HL and HRS cells is CD30 (Figure 1.1 B). CD15 is expressed in varying amounts and PAX5 is expressed typically weakly (Mathas et al. 2016). The histopathological appearance of cHL is characterized by a unique pattern: Less than 1% of tumor cells are embedded in a reactive immune cell infiltrate mainly consisting of T lymphocytes, eosinophils, neutrophils, and mast cells (Figure 1.1 C) (Hansen et al. 2016; Pileri et al. 2002). Interaction of HRS cells with cells in the microenvironment is based on cytokine secretion and interaction with surface receptors. The expression of surface receptors varies a lot, while the expression of CD30 is constant. The interaction with rosetting cells is important for survival of HRS cells (Schmitz et al. 2009). Most cHL are derived from B cells, but in rare cases they have a T cell origin.

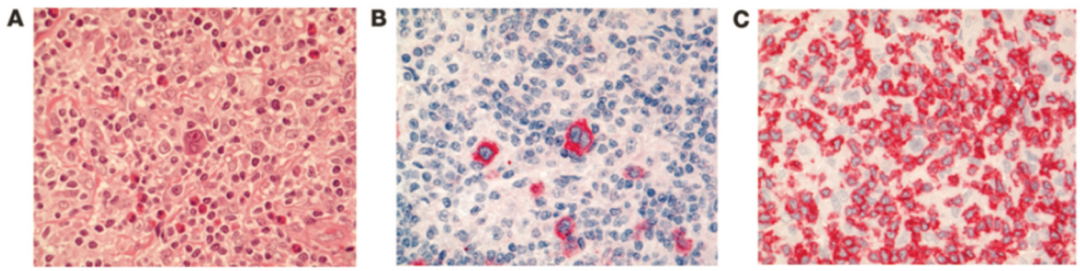

Figure 1.1: Hodgkin- and Reed-Sternberg (HRS) cells in their microenvironment

Morphology and immunhistochemical staining of HRS cells (from cHL of mixed cellularity type) with a bi-nucleated HRS cell in the middle of the image surrounded by T lymphocytes (**A**) Hematoxylin and eosin staining (**B**) CD30 immunostaining (**C**) CD3 immunostaining. Figure is reprinted from (Küppers 2012).

Four subtypes of cHL are classified by the World Health Organization (WHO) based on histological appearance and phenotypes of tumor cells: (1) Nodular sclerosing HL (NSHL), (2) Mixed cellularity (MCHL), (3) lymphocyte-rich cHL (LRCHL), and (4) lymphocyte-depleted HL (LDHL).

In addition, a non-classical subtype of HL is defined as nodular lymphocyte-predominant HL (NLPHL) (Küppers 2012). NSHL is the most frequent subtype in the Western world which mainly occurs as large mediastinal tumors in adolescents. It is histologically defined by fibrotic bands which confine nodular compartments containing the typical infiltrates of HRS cells surrounded by immune cells. MCHL is the second most frequent subtype of cHL which usually occurs in children, elderly people or immunocompromised patients. The peripheral lymph nodes are frequently involved with diffuse infiltrates of mixed inflammatory background without nodular sclerosing fibrosis. LRCHL is a rare subtype of cHL which occurs mostly in adults. It shows a prevalent involvement of cervical lymph nodes and the Waldeyer lymphatic tissue. Histologically, LRCHL is characterized by a monomorphic pattern, with nodules of mantle zone B cells containing HRS cells. Reactive T lymphocytes rosetting HRS cells often express PD-1, which is used as a diagnostic marker. LDHL has become extremely rare, since it can now be better distinguished from PAX5-negative ALCL. It occurs more likely in immunocompromised patients and HRS cells are rather abundant in the histological pattern (Mathas et al. 2016).

Current treatment options for patients with early stage cHL mainly rely on multi-agent chemotherapy (CHOP) and localized radiotherapy (Blank et al. 2017). Patients with chemo-sensitive relapsed cHL are treated by autologous hematopoietic stem cell transplantation (HSCT). This treatment results in long-term progression-free survival in approximately 50% of patients (Kasamon et al. 2017). Recent concepts have started to focus on immunotherapy-based approaches. Based on the strong expression on cHL and low expression on normal cells, CD30 is in focus as targeting molecule for new therapy options (Scott 2017). Brentuximab vedotin (Adcetris®) is an antibody-drug conjugate of a CD30-specific monoclonal antibody coupled with a potent anti-microtubule cytotoxin which received marketing authorization in the EU in 2012 (Scott 2017). Used as salvage therapy for patients with relapsed or refractory cHL after failed HSCT, it induced a 5-year overall survival rate of 41% and thus substantially improved the prospects for cHL patients (Chen et al. 2016). Another new immunotherapy based option is the use of the PD-1-specific immune checkpoint inhibitor nivolumab. It was approved in 2016 for the treatment of patients with relapsed or refractory cHL after failed HSCT and brentuximab vedotin treatment (Kasamon et al. 2017). Using α-PD-1 in these patients, a response rate of 65% was observed.

1.1.2 Anaplastic large cell lymphoma

Anaplastic large cell lymphoma (ALCL) is a subtype of large cell lymphomas and accounts for about 2-3% of all NHL and 12% of T cell NHL (Pierce and Mehta 2017; Ferreri et al. 2013). The definition is based on the frequent proliferation of mainly large lymphoid cells and a constant CD30 expression (Stein et al. 2000). Within ALCL four subtypes are classified: (1) Primary systemic anaplastic lymphoma kinase (ALK)+ ALCL, (2) Primary systemic ALK- ALCL, (3) Cutaneous ALCL, and (4) Breast implant-associated ALCL (Stein et al. 2000; Armitage et al. 2017). All entities usually have a cytotoxic T lymphocyte origin and therefore express T lymphocyte associated and cytotoxic markers (Ferreri et al. 2013). The expression of the ALK protein is mediated by a translocation between chromosome 2 and 5 (t(2;5)) involving the ALK gene (Ferreri et al. 2012). ALK+ and ALK- subtypes of ALCL were classified as separate disease entities by the WHO in 2016 (Savage et al. 2008). ALK+ALCL predominantly occurs in young male patients. It shows a broad morphologic spectrum, where large neoplastic cells usually have an abundant cytoplasm and pleomorphic, horseshoe-shaped nuclei. It is frequently present at an advanced stage with extranodal involvement (Ferreri et al. 2012). ALK- is morphologically not distinguishable from ALK+, but lacks the ALK protein. ALK-ALCL affects older patients of both genders. At diagnosis, it is usually present in lymph nodes and less frequently in extranodal sites (Ferreri et al. 2013). To distinguish both systemic forms of ALCL from cHL, PAX5 is stained which is less present on cHL (Ferreri et al. 2013). Patients with both types of systemic ALCL are treated with standard multi-agent chemotherapy (CHOP) (Pierce and Mehta 2017). Patients with ALK+ ALCL have a superior treatment outcome of the disease with a 5-year overall survival (OS) of 70% compared to those with ALK- ALCL which have a 5-year OS of 49% (Savage et al. 2008). Patients with relapsed or refractory ALCL are treated with HSCT or alemtuzumab, a monoclonal CD52 anitbody. Cutaneous ALCL is usually ALK- and has a good prognosis with a 5-year OS of 90% and without systemic dissemination in most cases (Savage et al. 2008; Ferreri et al. 2012).

Due to the constant CD30 expression on all ALCL subtypes, it is in focus for CD30-targeted therapies. Brentuximab vedotin is currently tested in clinical trials as substitute of one chemotherapeutic drug in the standard chemotherapy regime (Armitage et al. 2017).

1.2 Oncolytic viruses

Oncolytic viruses (OVs) are a novel treatment approach mediating selective lysis of tumor cells while sparing normal cells.

During carcinogenesis, innate immune response pathways would lead to an immune reaction towards tumor cells. To escape from these immune mechanisms, tumor cells have developed aberrant deregulated cell signaling pathways (Berchtold et al. 2013). This includes the activation of the Ras signaling pathway and impaired dsRNA-dependent protein (PKR) kinase activity resulting in deregulated expression of type I interferons (IFN) α and β (Kirn et al. 2001; Noser et al. 2007; Zhang et al. 2010). Due to these deregulated innate immune response pathways many tumor types are sensitive towards infection with RNA viruses in particular (Katze et al. 2002). These viruses can consequently be considered as treatment option for different types of cancer since they replicate in cancer cells but spare normal cells.

In general, OVs can be divided into two groups: Some viruses have an inherent selectivity for tumor cells like parvovirus, reovirus or Newcastle disease virus. Other viruses are adapted and genetically modified to be selective for tumor cells like adenovirus, vaccinia virus or herpes simplex virus (HSV) (Russell et al. 2012). Compared to other anticancer drugs, OVs have a special mode of killing tumor cells. Infected tumor cells are lysed, termed as oncolysis, releasing tumor-associated antigens (Breitbach et al. 2016). Thereby OVs promote different mechanisms of antitumor responses. Direct oncolysis causes tumor debulking and enables the release of viral particles to infect neighboring cells where viral infection amplifies. Furthermore, oncolysis induces a local inflammation with the release of cytokines, recruitment of T lymphocytes and other immune cells to the tumor microenvironment causing an antitumor immune response. Even when the OV is applied locally into the tumor tissue a systemic immune response can be triggered which is crucial for therapy efficacy (Guo et al. 2017). Different transgenes have been incorporated into the genome of several OVs to further improve their therapeutic efficacy. This includes equipping OVs with genes encoding immune activating proteins like the granulocyte-macrophage colony-stimulating factor (GM-CSF). By the expression of GM-CSF, recruitment of dendritic cells into the tumor microenvironment is improved resulting in an increased presentation to T lymphocytes and enhanced antitumor immune responses (Hughes et al. 2014).

1.2.1 Oncolytic measles virus

The measles virus (MV) is a spherical, non-segmented, single-stranded, negative sense RNA (ss(-)RNA) virus and belongs to the order *Mononegavirales*, family *Paramyxoviridae* and genus of *Morbillivirus*. The linear genome consists of 15.894 nucleotides, ordered in six genes that encode eight known proteins (Patterson et al. 2000). With the leader and trailer regulatory sequences the genome is in the order 3'-(leader)-N-P/C/V-M-F-H-L-(trailer)-5'.

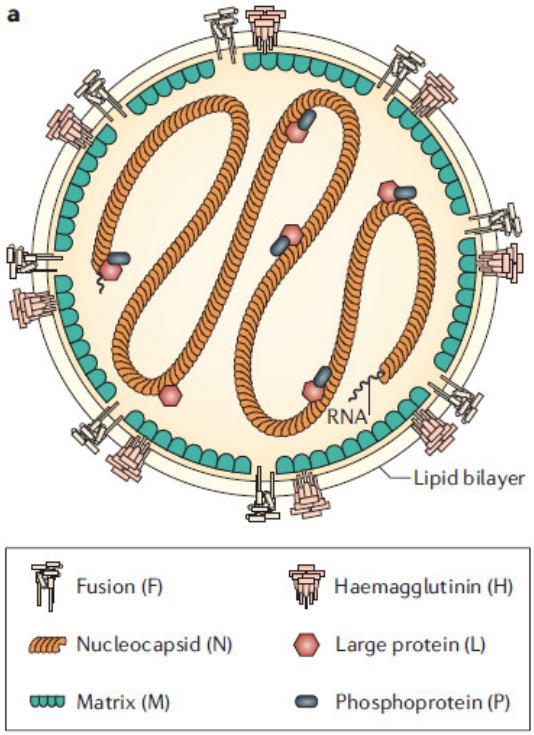

Figure 1.2: Schematic view of a MV virion

N, L, and P associate together with the RNA genome to the RNP-complex. M clusters to the RNP-complex and forms the viral envelope together with the glycoproteins H and F. Figure is reprinted from (Moss and Griffin 2006).

The viral RNA is tightly associated with the nucleocapsid (N) protein to form a nuclease-resistant helical structure where one N protein binds to six nucleotides (Calain and Roux 1993; Aref et al. 2016) (Figure 1.2). This N decorated RNA forms the functional template for MV RNA synthesis. It binds to the RNA-dependent RNA-polymerase (RdRp), which consists of the large polymerase (L) as catalytic active subunit and the phosphoprotein (P) as cofactor protein. The N decorated RNA forms the ribonucleoprotein (RNP) complex together with L and P as minimal infection unit (Moss and Griffin 2006).

The MV P gene encodes two additional non-structural gene products, termed C and V proteins (Iwasaki et al. 2009). Both are accessory proteins which are virulence factors and involved in the pathogenesis of MV for counteracting innate immune defenses (Patterson et al. 2000). The RNP-complex is linked to the matrix (M) protein via the N protein (Iwasaki et al. 2009). M is associated with the inner surface of the plasma membrane which is formed from lipids of the host cell membrane. Additionally, M interacts with the cytoplasmic tails of the two MV glycoproteins hemagglutinin (H) and fusion protein (F). Both glycoproteins together with the M protein build the viral envelope. F mediates membrane fusion of the viral envelope with the host cell membrane after the receptor binding of H has induced conformational changes. F is synthesized as an inactive precursor form F_0. While passing the trans-Golgi network, F_0 is proteolytically cleaved by Furin into F_1 and F_2. Both fragments remain linked by a disulfide bond (Mühlebach et al. 2008).

The tropism of MV is mediated through the receptor binding of H. Wildtype MV enters host cells through the receptors SLAM (Signaling Lymphocyte Activation Molecule) (Hsu et al. 2001) or Nectin-4 (Noyce et al. 2011). SLAM is expressed on activated B- and T-lymphocytes, dendritic cells, and macrophages (Tatsuo et al. 2000). By infection of $SLAM^+$ cells, the first systemic spread of MV takes place. Nectin-4 is expressed on the baso-lateral side of epithelial cells in the lung (Mühlebach et al. 2011). Thus, MV particles are released from lung cells to enable infection of other individuals after systemic spread. Moreover, Nectin-4 is highly expressed in lung, breast, and ovarian cancer (Mühlebach et al. 2011). The viral replication cycle of MV starts with the receptor attachment mediated by H. Then, a pH-independent fusion mediated by F of the viral envelope with the host cell membrane is initiated. The viral RNP-complex is released into the cytoplasm of the host cell where it acts as a template for primary transcription of mRNAs as well as replication into positive-stranded anti-genomic RNA (Bankamp et al. 2011). The polymerase entry site is located at the 3'-end of the genome in the 3' leader sequence. The genome is organized in six expression cassettes where each of them has an initiation sequence and a poly-A termination sequence in the intergenic region for transcriptional regulation (Parks et al. 2001). The polymerase stops at the end of a gene and reinitiates transcription of the next gene. Thus, single distinct mRNAs from each expression cassette are transcribed. With a certain frequency, the polymerase detaches and fails to reinitiate transcription of the following downstream genes. This way a transcription gradient with high amounts of N protein mRNA and lower amounts of L protein mRNA forms, which directly influences

the amount of expressed proteins (Cattaneo et al. 1987; Plumet et al. 2005). Newly transcribed mRNAs are capped, polyadenylated and immediately decorated with N proteins. From synthesized mRNA templates proteins are translated at the cellular ribosomes. Glycoproteins H and F are transported to the host cell membrane via the secretory pathway. Since the RNA is associated with N proteins, the transcription stops when sufficient N protein is present in the cell. Then the polymerase transcribes a full-length positive sense anti-genomic intermediate. This serves as template for the replication of a full-length negative sense genomic RNA (Radecke et al. 1995; Bankamp et al. 2011). The genomic RNA forms the RNP complex with the translated N, P and L proteins. Via the M protein the RNP complex is connected to the membrane, where H and F are expressed. Finally, all assembled components bud from the plasma membrane to complete the replication cycle. Dependent on cell type, approximately 30 hours post infection, new viral particles are released (Plumet et al. 2005). Due to the expression of H and F on the plasma membrane, MV receptor positive neighboring cells are recognized and the formation of multinucleated giant cells, termed as syncytia, is induced (Duprex et al. 1999; Aref et al. 2016). Using this characteristic cytopathic effect, MV can also spread from cell-to-cell and is not exclusively dependent on viral particles.

For vaccination, live attenuated vaccine strains based on the MV Edmonston (MV-Edm) strain are used since 1963 (Hilleman 2001). MV-Edm was isolated from a patient called David Edmonston by Enders and Peebles in 1954 (Enders and Peebles 1954). Several MV vaccine strains were attenuated by extensive passaging of the isolated virus in cell culture. Moraten and Schwarz strains are mostly used for vaccination in the Western world and show a high safety profile (Bankamp et al. 2011). From these vaccine strains a variety of recombinant laboratory MV clones have been generated, e.g. MV_{Schw}, MV_{vac2} and MV_{NSe}. Elimination of endonuclease recognition sites generated MV_{NSe} (NSe = NarI-and-SpeI- eliminated). MV_{NSe} is described to be more fusogenic than the Moraten strain (Devaux et al. 2007). MV vaccine strains have an additional tropism for CD46 compared to wildtype MV. The additional receptor usage is based on mutations in the H protein obtained during extensive passaging for attenuation (Bankamp et al. 2011). CD46 itself is a member of the regulators of complement activation and ubiquitously expressed on all human nucleated cells (Dörig et al. 1993). On a variety of different malignant diseases CD46 is overexpressed, primarily to evade complement-mediated lysis (Fishelson et al. 2003). Due to the high expression of CD46 on malignant cells, MV

vaccine strains have a high tumor selectivity (Galanis 2010). The formation of syncytia can significantly enhance the antitumoral effect of MV since for each infected cell, many neighboring cells can fuse to form syncytia followed by apoptotic cell death (Galanis et al. 2001).

To generate recombinant MVs, a reverse genetic system was developed (Radecke et al. 1995; Takeda et al. 2000). Using this system, it was possible to engineer the virus genome and rescue viruses in cell culture. MV used as OV in clinical trials is a modified version of the recombinant MV vaccine strain MV_{NSe}. By insertion of transgenes, the viral gene expression can be monitored *in vivo*. Recombinant MVs were generated encoding for the sodium iodine symporter (NIS) (Galanis 2010). NIS transports and accumulates radioactive ^{99m}TC or ^{125}I in infected cells. It can be detected by computed tomography/single-photon emission computed tomography (SPECT-CT) or γ-camera imaging (Galanis 2010). Selective infection and lysis of myeloma plasma cells induced by MV-NIS was demonstrated. Recently, MV-NIS was tested in a phase I clinical trial by treating two MV-seronegative patients with relapsing drug-refractory myeloma. Both patients received a systemic administration of 10^{11} $TCID_{50}$ infectious units of MV-NIS in 100 ml and responded to the therapy. One patient showed durable complete remission at all disease sites, while toxicities resolved within the first week after therapy (Russell et al. 2014).

1.2.2 Oncolytic vesicular stomatitis virus

The vesicular stomatitis virus (VSV) belongs to the order of *Mononegavirales* being a non-segmented, single-stranded, negative sense RNA (ss(-)RNA) virus as is MV. In contrast to MV, it is a bullet-shaped virus, belonging to the family *Rhabdoviridae* and genus of *Vesiculovirus*. The rather compact linear genome consists of approximately 11.000 nucleotides, ordered in five genes that encode five known proteins (Lichty et al. 2004).

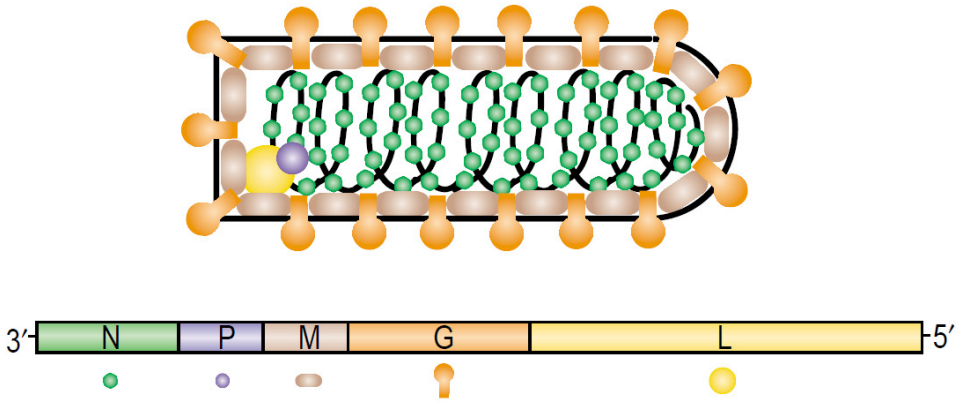

Figure 1.3: Schematic view of a VSV virion

The genome encodes the five gene products: N (nucleoprotein), P (phosphoprotein), M (matrix protein), G (glycoprotein) and L (large polymerase). N, L, and P associate together with the RNA genome to the RNP-complex. M clusters to the RNP-complex and builds together with the glycoprotein G the viral envelope. Figure is reprinted from (Lichty et al. 2004)

The RNA genome is tightly decorated with the nucleoprotein (N) (Figure 1.3). The RdRp, which is highly homologous within the order of *Mononegavirales*, consists of the large polymerase (L) as catalytic active subunit and its co-factor the phosphoprotein (P) (Hastie and Grdzelishvili 2012). The N decorated RNA genome is associated with the RdRp to an RNP complex. The RNP complex in turn is connected with the matrix (M) protein, which is located at the lipid bilayer on the cytosolic site. The M protein has multiple functions in addition to the role during assembly and budding of new viral particles (Barr et al. 2002). First, it partially regulates the transcription of VSV genes by RdRp (Lichty et al. 2004). Second, it prevents that VSV is recognized by cellular antiviral programs. More precisely, the cellular transcription programs are interrupted and the cellular mRNA export from the nucleus is blocked (Petersen et al. 2000; Ahmed et al. 2003; Lichty et al. 2004). Hence antiviral genes like IFN-β are blocked and VSV can replicate unabated (Ahmed et al. 2003). Third, the M protein is responsible for cell rounding as cytopathic effect leading to apoptotic cell death of susceptible host cells (Lichty et al. 2004).

Unlike MV, VSV has only one glycoprotein (G) which mediates receptor binding and fusion of viral and cellular membranes (Sun et al. 2010). G has a trimeric structure and binds to the low density lipoprotein (LDL) receptor, which is ubiquitously expressed (Finkelshtein et al. 2013). Therefore, VSV has a very broad tropism and can infect virtually all animal cells (Lichty et al. 2004). Other than MV, VSV enters the cell via pH-dependent clathrin-mediated endocytosis after receptor binding (Sun et al. 2005).

The virus is engulfed, then trafficked into endosomal vesicles and released during subsequent acidification of the endosome (White et al. 1981; Sun et al. 2010). The pH drop triggers a conformational change in the G protein which catalyzes the fusion of viral envelope and endosomal membrane (Sun et al. 2010). This way the RNP complex is released into the cytoplasm and replication is initiated. Similar to the replication cycle described for MV, the polymerase complex for transcription of the genome is delivered with the RNP complex. The single polymerase entry site is located at the 3'-end of the genome, which makes the transcription obligatory sequential (Ball and White 1976; Emerson 1982; Bishnoi et al. 2018). Between the five expression cassettes, cis-elements serve as start/stop sequences to regulate transcription (Barr et al. 2002). First, individual mRNAs for each viral gene are transcribed. A transcription gradient due to the re-initiation fail of the polymerase is present as well, which leads to lower amounts of proteins expressed from downstream genes (Iverson and Rose 1981; Hastie and Grdzelishvili 2012). Viral mRNAs are translated into proteins by the host ribosomes. At later stages, the polymerase complex switches from transcription to replication. Here, for replication of the negative-sense RNA genome, a positive-sense anti-genome as intermediate is synthesized by the polymerase as well. The assembly of the first batch of progeny virions is coincidental to the secondary viral genome transcription (2-3 hours post infection) (Bishnoi et al. 2018). Finally, all assembled components are packaged into new progeny VSV virions.

Using reverse genetic tools recombinant VSV has been generated *de novo* in cell culture (Schnell et al. 1994; Bishnoi et al. 2018). This was the prerequisite to modify VSV and develop promising candidates to use as oncolytic virus. VSV is non-pathogenic to humans, has a well-studied biology and a genome that is easily manipulable, has a rapid replication cycle and can be produced in high viral titers. Furthermore, VSV has high tumor selectivity due to its high sensitivity towards IFN. However, the main issue of VSV is its inherent neurotoxicity. Neurotropism is primarily mediated by the G protein and partly by the M protein (Bishnoi et al. 2018). VSV application in different *in vivo* models leads to an invasion of the central nervous system following severe neurological diseases (Johnson et al. 2007; Muik et al. 2012; Shinozaki et al. 2005). Several modifications of VSV were done to increase the safety, resulting in the generation of different recombinant VSV bearing certain mutations in a viral gene or expressing a foreign antigen (Lichty et al. 2004). One approach to increase oncoselectivity is the use of VSV-MΔ51. The methionine at position 51 of the M protein is

mutated, thus unblocking the nucleocytoplasmic transport of host mRNA. This way, IFN from non-cancer cells is produced protecting them from infection with VSV (Stojdl et al. 2003). Another approach to attenuate VSV replication in healthly tissue is the development of a recombinant VSV encoding IFN-β (Obuchi et al. 2003). Preclinical studies showing off-target free toxicity in malignant cells are promising and therefore VSV-IFNβ is investigated in ongoing clinical trials (ClinicalTrials.gov Identifier: NCT03017820, NCT02923466). To neutralize neurotoxicity of VSV, one approach is the exchange of VSV-G glycoprotein as key determinant of VSV neurovirulence. It was shown that by exchanging the glycoprotein of VSV with the glycoprotein of lymphocytic choriomeningitis virus (LCMV) in different *in vivo* models, neurotoxicity can be eliminated (Muik et al. 2011; Muik et al. 2014).

1.3 Receptor targeting of oncolytic RNA viruses

Viral tropism is determined through the susceptibility and permissiveness of a host cell for an infection. This means, that the virus binds to a surface receptor through its viral glycoproteins for cell entry on a susceptible target cell. Post entry, the permissive host cell provides transcription factors and nutrients to allow viral replication. To target viruses to certain cell types, there are two main strategies: First, the cell entry of viral particles can be targeted to a receptor of choice through genetic modification of the viral envelope. Second, the viral replication in healthy tissue can be inhibited on post-entry level by silencing viral mRNA translation. This can be achieved i.a. by the insertion of microRNA target sites into the genome of MV (Leber et al. 2018; Edge et al. 2008). This thesis is focusing on retargeting the viral cell entry of MV and VSV to a receptor of choice by modifications of the viral envelop.

1.3.1 Receptor targeting of measles virus

Targeting of MV to a receptor of choice is well characterized and established. First of all, a specific binding ligand needs to be fused to MV-H, mediating receptor attachment. Since the fusion of a large antibody with tetrameric structure and disulfide bonds is not possible, engineered binding domains are used. In the beginning of targeting approaches, a ligand (Schneider et al. 2000), a peptide (Hallak et al. 2005) or a single chain variable fragment (scFv) (Hammond et al. 2001) was fused to the extracellular part of MV-H protein to achieve an extended tropism. For complete retargeting of MV, the inherent binding sites for the natural receptors need to be erased. Thus, MV-H is blinded by the insertion of four specific point mutations in the receptor binding sites for CD46, SLAM and Nectin-4 (abbreviated as H_{mut}). Subsequently a targeting domain with a specificity of choice is fused to H_{mut} (Nakamura et al. 2005). For this approach frequently used targeting domains are scFv. They contain the antigen-binding variable regions of the heavy and light chains of an antibody and retain complete antigen specificity. These modifications of H_{mut} leads to MV particles that do no longer bind to natural MV receptors, but with high affinity to the receptor of choice which is targeted by the scFv. Utilizing this retargeting concept, a series of MV were generated each using a particular type of tumor surface marker as entry receptor (Aref et al. 2016). One example is an oncolytic MV specifically retargeted to $CD133^+$ tumor-initiating cells, which are described for various tumor entities, including hepatocellular carcinoma and glioblastoma. MV-CD133 selectively eliminated $CD133^+$ tumor cells and was more effective in prolonging survival of tumor bearing mice compared to MV_{NSe}. (Bach et al. 2013)

Besides scFv, artificial binding domains based on designed ankyrin repeat proteins (DARPins) are used as targeting domains with antibody-like specificity for retargeting MV. Using DARPins, oncolytic MV retargeted to three different tumors markers (Epidermal growth factor receptor (EGFR), human epidermal growth factor 2 (Her2/neu) and epithelial cell adhesion molecule (EpCAM)) were generated and shown to eliminate tumor xenografts. To circumvent therapy resistance based on down regulation of a tumor marker, a bispecific targeting of MV using DARPins was demonstrated as well. (Friedrich et al. 2013)

1.3.2 Receptor targeting of vesicular stomatitis virus

Until now, complete retargeting of VSV using the inherent glycoprotein VSV-G was not possible. However, VSV tolerates the incorporation of glycoproteins from other virus families very well. In 2006, a recombinant, replication competent VSV that preferentially infects Her2/neu-positive breast cancer cells, was generated. This was achieved by generating a VSV-Sindbis pseudotype. The native VSV-G glycoprotein was deleted and instead a chimeric Sindbis glycoprotein which included a scFv specific for Her2/neu was inserted. However, after several cycles of passaging on a target cell line, viral replication was reduced and viral yield was poor (Gao et al. 2006). A different approach to retarget VSV to tumor vasculature associated integrins using VSV-G itself was investigated in 2013. A replication competent VSV displaying different tumor-targeting ligands on the surface of VSV-G was generated. The feasibility of the approach for the insertion of two integrin-binding peptides was demonstrated. First a 9-amino-acid cyclic RGD peptide, second a 49-amino-acid echistatin domain was fused. Both ligand-displaying VSV replicated as efficiently as parental VSV and showed specificity to bind to targeted integrins. Furthermore, the authors investigated the insertion of scFv specific for EGFR or Her2/neu. However, VSV displaying scFv grew to lower maximum titers than unmodified VSV and the EGFR-scFv was partially cleaved from the G-protein (Ammayappan et al. 2013). In 2012, Ayala-Breton et al. for the first time generated a fully retargeted, but replication deficient VSV-MV pseudotype. VSV-G was deleted and a chimeric MV-H fused to a scFv specific for EGFR, FR or PSMA together with MV-F were inserted. Viral particles were produced, but viral titers were moderate. Specificity of all viruses for receptor positive tumor cells was shown on transgenic cell lines *in vitro* as well as in human xenograft tumors *in vivo* (Ayala-Breton et al. 2012). A replication competent VSV-MV pseudotype was investigated in 2013 and 2014. Here, VSV-G was deleted and unmodified MV glycoproteins were inserted. The generated VSV-MV chimera infected MV-receptor positive tumor cells and formed syncytia *in vitro*. The authors claimed that VSV-MV harnessed the safety of oncolytic MV and spread with VSV-like kinetics. In a myeloma xenograft model VSV-MV showed higher oncolytic activity compared to MV or VSV-MΔ51. Due to the deletion of VSV-G it proved not to be neurotoxic. Generating this kind of VSV-MV chimera was the basis for a fully retargeted replication competent VSV (Ayala-Breton et al. 2013; Ayala-Breton et al. 2014).

1.4 Objectives

Aim of this study was the characterization of two CD30-targeted oncolytic viruses with respect to their antitumoral activity against cHL and ALCL cell lines. Until now, oncolytic virotherapy has not been considered for the treatment of cHL. Compared to other tumor entities, the frequency of tumor cells in the affected tissue of cHL is low, which makes the use of conventional oncolytic viruses challenging. Additional layers of tumor cell targeting may be beneficial to establish an effective virotherapy strategy for cHL. Since tumor cells of cHL constantly express CD30, this surface molecule is in focus for new therapy approaches of cHL. For this purpose both, a CD30-targeted MV and for the first time a completely retargeted VSV-MV chimera had been generated (Hanauer 2015). CD30-targeted viruses are designed to induce oncolysis in $CD30^+$ tumor cells leading to apoptotic cell death and tumor shrinkage. Using a CD30-targeted VSV as oncolytic agent is thought to be beneficial compared to MV due to its faster replication kinetics.

New virus stocks had to be produced and characterized for their potential application *in vivo.* This involved the analysis of the particle assembly as well as their ability to induce cell killing of two different cHL cell lines *in vitro*. Next, a suitable cHL xenograft tumor mouse model had to be established for the evaluation of CD30-targeted viruses *in vivo*. For this purpose, two different cHL cell lines were investigated in regard to formation of a s.c. tumor and their susceptibility for the infection with CD30-targeted viruses. Using the established s.c. tumor mouse model, the oncolytic activities of both MV-CD30 and VSV-CD30 had to be evaluated using different virus application routes. In addition, a multifocal growing cHL tumor mouse model reflecting the clinically relevant tumor burden had to be established. First, a cHL cell line allowing tumor development observation *in vivo* had to be generated and analyzed for its susceptibility to VSV-CD30. Second, the established multifocal tumor model had to be used to evaluate the oncolytic activity of VSV-CD30 as well. Finally, the susceptibility of different $CD30^+$ ALCL cell lines had to be investigated *in vitro*.

2 Material and methods

2.1 Material

2.1.1 Instruments

Table 1: Instruments

Name	Manufacturer
Centrifuge: Multifuge X3R	Heraeus, Thermo Scientific
Cryo freezing container	Nalgene
Cryostat: CM1900	Leica
Digital caliper	PMS
Flowcytometer: MACSQuant Analyzer 10	Miltenyi Biotec
Fluorescence microscope: Axio Observer X1, ApoTome optical sectioning unit	Carl Zeiss, Jena
Fluorescence microscope: Axiovert 200, AxioCam	Carl Zeiss, Jena
Humidified CO2-incubator: BBD6220	Heraeus, Thermo Scientific
In vivo Imaging System: IVIS Spectrum	Perkin Elmer
Laminar Flow Cabinet Class II	The Baker Company
Light microscope: Axiovert 25	Carl Zeiss, Jena
Microplate luminometer: Microlumat Plus LB 96V	Berthold Technologies
Microcentrifuge: Biofuge fresco	Heraeus, Thermo Scientific
Micropipettes (10 µl, 100 µl, 1000 µl)	Brand/Eppendorf
Multichannel pipettes: Eppendorf Research plus	Eppendorf
Pipetting assistance: Accu-jet	Brand
Semi-dry blotter: Transfer Cell SD	Bio-Rad
Small animal anesthetic device: indulab-vet	HME-Highland Medical Equipment
Western Blot film processor: Curix 60	Agfa

2.1.2 Consumables

Table 2: Consumables

Name	Vendor
1.5 ml reaction tube	Eppendorf
BD Vacutainer Safety-Lok Blood Collection Set	Becton Dickinson
BD Vacutainer® CPT™ Mononuclear Cell Preparation Tube	Becton Dickinson
Bottle Top Filter 500 ml, 0.45 µm SFCE, Rapid-Flow	Thermo Fisher Scientific
Canulas: Sterican (various types)	Braun
Cell culture dish (15 cm)	TPP
Cell culture microplate, 96 well, µCLEAR®, black	Greiner Bio-One
Cell scraper	TPP
Cell strainer (70 µm)	BD Biosciences
Cryovial (2 ml)	Greiner Bio-One
FACS tubes (1.4 ml)	Micronic
Falcons, CellStar Tubes (15 ml, 50 ml)	Greiner Bio-One
High performance chemiluminescent films	GE Healthcare
Nitro cellulose membrane, Hybond ECL	GE-Healthcare
Pipette tips, filtered (10 µl, 100 µl, 300 µl, 1000 µl)	Nerbe Plus, Biotix, Biozym
Serological pipettes (2 ml, 5 ml, 10 ml, 25 ml)	Greiner Bio-One
Size exclusion filter, Amicon Ultra-15, 100 kDa	Merck
Slides, Superfrost Plus	Menzel
Syringe filters, Minisart PTFE (0.45 µm, 0.2 µm)	Satorius
Syringe: Omnifix® (1 ml, 5 ml, 10 ml, 20 ml)	Braun
Syringe: BD MicroFine, 1 ml, U100, 29G Insulin	BD Biosciences
Tissue culture flask (T25, T75, T175)	Greiner Bio-One
Tissue culture plates (96-, 48-, 24-, 12-, 6-well)	Nunc, Thermo Fisher Scientific

2.1.3 Reagents

Table 3: Reagents

Reagent	Vendor
Acrylamide (Rotiphorese® Gel 30)	Carl Roth
Ammonium persulfate (APS)	Sigma-Aldrich
Bovine Serum Albumin (BSA)	Sigma-Aldrich
CD30-Fc protein	(Friedel et al. 2015)
Corning® Matrigel® Basement Membrane Mix	Thermo Fisher Scientific
Dimethylsulfoxide (DMSO), 99.9% p.a.	Sigma-Aldrich
Dithiothreitol (DTT)	Sigma-Aldrich
Donkey serum	Chemicon
Dulbecco's Modified Eagle Medium (DMEM)	Lonza, Biowest
FcR blocking reagent, murine	Miltenyi Biotech
Fetal calf serum (FCS)	Biochrome
Fluoroshield™ DAPI (4 ,6-diamidino-2-phenylindole)	Sigma-Aldrich
Formaldehyde, 37% p.a. (ROTIPURAN®)	Carl Roth
Glycerol	Sigma-Aldrich
H_2O (tissue culture grade)	Sigma-Aldrich
HEPES solution	Sigma-Aldrich
Interleukin-2 (IL-2), human	Miltenyi Biotech
Isoflurane CP	CP-Pharma
Isopropanol	VWR Chemicals
L-glutamine	Sigma-Aldrich
Methanol	VWR Chemicals
N,N,N',N' Tetramethylenediamine (TEMED)	Carl Roth
OptiMEM®	Gibco, Life Technologies

PageRuler™ Plus Prestained Protein Ladder	Thermo Fisher Scientific
PBS (w/o Mg^{2+}/Ca^{2+})	Lonza
Penicillin/Streptomycin (PenStrep)	Paul-Ehrlich-Institut
Pierce™ ECL Western Blotting Substrate	Thermo Fisher Scientific
Powdered milk, low fat	Carl Roth
Puromycin	Gibco, Life technologies
Roti®-Histofix 4%	Carl Roth
RPMI 1640 medium	Biowest
Sodium dodecyl sulfate (SDS)	Carl Roth
Sucrose	Sigma-Aldrich
Tissue-Tek® O.C.T. Compound	Sakura® Finetek
Triton X-100	Sigma-Aldrich
Trypan blue	Sigma-Aldrich
Trypsin 2.5%	Paul-Ehrlich-Institut
Tris	Paul-Ehrlich-Institut
Tween-20	Sigma-Aldrich
Urea, p.a.	Sigma-Aldrich
VP-SFM (virus production serum free medium)	Life technologies
Xenolight D-Luciferin	Perkin Elmer

2.1.4 Commercially available kits

Table 4: Commercially available kits

Name	Vendor
eBioscience™ Fixable Viablity Dye eFluor™ 450	Thermo Fisher Scientific
RealTime-Glo™ MT Cell Viability Assay	Promega
LIVE/DEAD Fixable Violet Dead Cell Stain Kit	Molecular Probes

2.1.5 Software

Table 5: Software

Name	Vendor
Axio Vision 4.8	Carl Zeiss, Jena
Citavi 6.0	Swiss Academic Software
FCS-Express 6.0	De Novo Software
GraphPad Prism 7.0	Graph Pad Software
Living Image 4.2	Perkin Elmer
Microsoft Office 2010	Microsoft
WinGlow 1.25	Berthold Technologies

2.1.6 Media and Buffers

Table 6: Media and Buffers

Name	Composition
Ammoniumchloride	0.86% ammoniumchloride in H_2O
Blocking buffer (WB)	5% powdered milk in TBS-T
FACS fixation buffer	1% formaldehyde in PBS w/o Mg^{2+}/Ca^{2+}
FACS wash buffer	2% FCS 0.1% NaN_3 in PBS w/o Mg^{2+}/Ca^{2+}
Freezing medium	10% DMSO 90% FCS
PBS/EDTA	2 mM EDTA in PBS w/o Mg^{2+}/Ca^{2+}

SDS loading buffer (4x)	250 mM Tris/HCL (pH 6.8) 4% SDS 20% glycerol 20 mg bromophenol blue 10% β-Mercaptoethanol in H_2O
SDS running buffer	25 mM Tris 192 mM glycine 1% SDS in H_2O
Sucrose	30% Sucrose in PBS w/o Mg2+/Ca2+
T cell medium	10% FCS 2 mM L-glutamine 25 mM HEPES 0.4% Penicillin/Streptomycin in RPMI 1640
TBS buffer	50 mM Tris 150 mM NaCl in H_2O
TBS-T I buffer	0.1% Tween-20 in TBS buffer
TBS-T II buffer	0.2% Triton X-100 in TBS buffer
Transfer buffer (WB)	48 mM Tris 39 mM glycine 20% v/v methanol in H_2O
Trypsin working solution	2 mM EDTA 0.25% Trypsin-Melnick

	in PBS w/o Mg^{2+}/Ca^{2+}
Urea-denaturation buffer (2x)	200 mM Tris-HCl 8 M Urea 5% SDS 100 mM EDTA 0.03% bromophenol blue 1.5% (w/v) DTT in H_2O

2.1.7 Antibodies

Table 7: FACS antibodies

Antibody	Clone	Vendor
mouse α-human CD3-Pacific Blue	UCHT1	BD Pharmingen
mouse α-human CD25-APC-Cy7	BC96	BioLegend
mouse α-human CD30-PE	Ki-2	Miltenyi Biotec
mouse α-human CD46-FITC	MEM-258	Biolegend
mouse α-human CD150 (SLAM)-PE	A12 (7D4)	Biolegend

Table 8: Western Blot (WB) antibodies

Antibody	Dilution	Vendor
goat α-rabbit-HRP	1:2.000	DAKO Cytomation
rabbit α-MV-F (1034), polyclonal	1:4.000	Abcam
rabbit α-MV-H (606), polyclonal	1:1.000	Abcam
rabbit α-MV H_{cyt} purified IgG VSEP103081, rabbit 1141 ZDE 10143	1:20.000	Eurogentec

Table 9: T cell activation antibodies

Antibody	Clone	Vendor
mouse α-human CD3	OKT3	Miltenyi Biotec
mouse α-human CD28	15E8	Miltenyi Biotec

Table 10: Immunofluorescence (IF) antibodies

Antibody	Dilution	Vendor
donkey α-rabbit IgG Cy2	1:200	Jackson ImmunoResearch
donkey α-rat IgG Alexa-Fluor647	1:200	Jackson ImmunoResearch
rabbit α-GFP, polyclonal IgG serum	1:200	Invitrogen
rat α-mouse CD31, clone: SZ31	1:10	Dianova

2.1.8 Viruses

Table 11: Viruses

Name	Description
MV	Parental MV_{NSe}, recombinant clone of MV laboratory strain derived from Edmondston B vaccine strain, encodes for eGFP(N), (Radecke et al. 1995)
MV-CD30	Transgenic MV_{NSe} encodes for HRS3opt2#2-scFv (H_{mut}-CD30scFv) and eGFP(N), (Hanauer 2015)
VSV-MV	Parental VSV-MV, based on VSV Indiana serotype, encodes for MV glycoproteins F and H as well as eGFP, (Ayala-Breton et al. 2014)
VSV-CD30	Transgenic VSV-MV, encodes for MV glycoproteins F and H_{mut}-CD30-scFv as well as eGFP, (Hanauer 2015)

2.1.9 Cell lines

Table 12: Cell lines

Name	Description	Origin
HT1080-CD30	Human fibrosarcoma cell line genetically engineered to express human CD30	(Friedel et al. 2015)
Karpas299	Human anaplastic large cell lymphoma (ALCL) cell line (ALK+)	German Collection of Microorganisms and Cell Cultures, Braunschweig
KM-H2	Human classical Hodgkin lymphoma (HL) cell line (Subtype: mixed cellularity)	German Collection of Microorganisms and Cell Cultures, Braunschweig
KM-H2-luc	Human classical Hodgkin lymphoma (HL) cell line genetically engineered to express firefly luciferase	This thesis
L-428	Human classical Hodgkin lymphoma cell line (Subtype: nodular sclerosis)	German Collection of Microorganisms and Cell Cultures, Braunschweig
MAC-1	Human anaplastic large cell lymphoma (ALCL) cell line (ALK-, cutaneous T cell ALCL)	(Kadin et al. 1994)
SUDHL-1	Human anaplastic large cell lymphoma (ALCL) cell line (ALK+)	German Collection of Microorganisms and Cell Cultures, Braunschweig
Vero-αHis	Kidney epithelial cells from *Cercopithecus aethiops* genetically engineered to express a αHis6-tag-scFv displayed on the PDGFR TM domain	(Nakamura et al. 2005)

2.2 Protein biochemical methods

2.2.1 SDS-PAGE

SDS-PAGE (sodium dodecyl sulfate polyacrylamide gel electrophoresis) is a method to electrophoretically separate SDS-decorated proteins according to their molecular weight using a polyacrylamide gel. Protein samples (here: virus stocks) were mixed with 2x urea-denaturation butter or 4x SDS loading buffer and incubated for 10 min at 95°C for denaturation. Samples were loaded to 10% SDS polyacrylamide gels and separated using a gel electrophoresis chamber filled with 1x SDS running buffer. The polyacrylamide gels used for separation were prepared as described in Table 13.

Table 13: Composition of polyacrylamide stacking and separation gel

Components	Stacking gel (5%)	Separation gel (10%)
30% acrylamide (Rotiphorese® Gel 30)	1.65 ml	6.6 ml
1 M Tris, pH 8.8	-	7.8 ml
1 M Tris, pH 6.8	1.25 ml	-
50% glycerol	-	1.64 ml
10% SDS	100 µl	220 µl
H_2O	7.00 ml	3.70 ml
TEMED	26 µl	26 µl
20% APS	52 µl	52 µl

Electrophoretic separation was performed at 100 V until the running front reached the resolving gel, then proteins were further separated with 120 V until the desired marker proteins reached the end of the resolving gel. As size standard for comparison of the applied samples, the PageRuler™ Plus Prestained Protein Ladder (Thermo Fisher Scientific) was used.

2.2.2 Western Blot analysis

After electrophoretic separation (2.2.1), proteins were transferred onto a nitrocellulose membrane and used there for immunodetection by Western Blot. Proteins were transferred electrically using a semi-dry blotter. Filter (Whatman) paper, nitrocellulose membrane and the polyacrylamide gel were pre incubated in Transfer buffer. Next, all components were stacked carefully onto the electrode of the blotter machine. Proteins were transferred at 0.18 A for 90 min. Afterwards, proteins on the membrane were blocked with TBS-T containing 5% milk powder for 30 min. Subsequently, the membranes were incubated with primary antibodies diluted in blocking buffer and incubated at 4°C over night. Antibody solution was removed following the incubation time and membranes were washed three times with TBS-T. Horseradish peroxidase (HRP)-conjugated secondary antibodies were diluted in blocking solution and used for membrane incubation at room temperature for 30 min. Antibody solution was removed and membranes were washed three times with TBS-T. Protein signals were detected using the Pierce™ ECL Western Blotting Substrate (Thermo Fisher Scientific).

2.3 Cell culture methods

2.3.1 Cultivation of eukaryotic cell lines

Eukaryotic cell lines were cultivated under standard cultivation conditions at 37°C in an atmosphere containing 5% CO_2 and 95% humidity. Cells were cultured in DMEM or RPMI media supplemented with 10% heat-inactivated FCS and 2 mM L-glutamine (10% FCS, 1% L-glutamine) and cultured in T175, T75 or T25 cell culture flasks. Depending on cell growth, cells were split twice a week in different ratios to maintain confluence of 80-90%. Medium from cells was removed and cells were washed with PBS. To detach adherent cells from the cell culture flask, PBS-Trypsin-EDTA was added to remaining cells and incubated at 37°C until cells detached. By resuspending the cells in fresh media, the detachment process was stopped. A part of the cell suspension was then discarded or used for subsequent experiments. The remaining cells were supplied with fresh media and distributed to new cell culture flasks. All cell lines were checked for contaminations with mycoplasma by PCR on a regular basis.

2.3.2 Freezing and thawing of cells

To freeze cells, the cell culture was expanded at a minimum of four T175 cell culture flasks. At a confluence of 80%, cells were detached, pooled and centrifuged for 5 min at 300xg and 4°C. The remaining cell pellet was then resuspended in ice cold freezing medium, aliquoted into cryovials (1 ml/vial) and frozen at -80°C using a Mr. Frosty Freezing Container (Nalgene) filled with Isopropanol. On the next day, cells were transferred to the gas phase of a liquid nitrogen tank and stored at -155°C.

For thawing cells, a cryovial containing cells was thawed at room temperature or in the water bath at 37°C. Immediately after thawing, cell suspension was transferred to a reaction tube filled with pre-warmed medium and centrifuged for 5 min at 300xg and 4°C. The cell pellet was then resuspended in appropriate pre-warmed culture medium (10% FCS, 1% L-glutamine) and cells were seeded in a T75 cell culture flask. On the next day, cell culture medium was exchanged.

2.3.3 Isolation and activation of human peripheral blood mononuclear cells

Primary human peripheral blood mononuclear cells (PBMC) were isolated from fresh healthy human donor blood by density centrifugation. To do so, Vacutainer® CPT™ Mononuclear Cell Preparation Tubes (Becton Dickinson) were used according to the manufacturer's protocol. Following density centrifugation, erythrocytes and granulocytes were pelleted. The layer containing the mononuclear lymphocytes, monocytes and macrophages was aspirated from the interphase. Obtained PBMC were washed twice with PBS. Remaining erythrocytes were lysed for 10 min at 37°C using 0.86% ammonium chloride. After two additional washing steps with PBS, cells were counted and resuspended in T cell medium supplemented with 100 U/ml interleukin-2 (IL-2) (Miltenyi Biotec). For activation, PBMC were seeded in plates pre-coated with 1 µg/ml α-human CD3 antibody (Miltenyi Biotec) and 3 µg/ml α-human CD28 antibody (Miltenyi Biotec) and cultured for 72 h. After infection, cells were cultured in T cell medium supplemented only with IL-2.

2.3.4 Generation of stably transgenic cell lines

Cell stably expressing an introduced transgene were generated by transduction with a lentiviral vector (LV) encoding for the transgene and a puromycin resistance gene.

KM-H2-luc cells were generated by transduction with a VSV-G-HIV1-Puro-Luc LV transferring the luciferase transgene and a puromycin resistance gene. For transduction of parental KM-H2 cells unconcentrated supernatant of LV producer cells was used. To do so, 1 x 10^5 cells were seeded in a 48-well plate and transduced with different volumes of vector stock (10-100 µl). After 24 h of transduction, 1 ml of RPMI (10% FCS, 1% L-glutamine) was added to the cells. Selection of transgene expressing cells was achieved by supplementing the cell culture medium with 10 µg/ml puromycin three days after transduction. KM-H2-luc cells were selected for two weeks and afterwards verified for luciferase expression using the luciferase assay system (Promega) according to the manufacturer's protocol. KM-H2-luc cells showing luciferase activity were expanded and frozen.

2.3.5 Surface staining and flow cytometry analysis

For staining, cell suspension was transferred to micronic tubes. Next, cells were washed twice with FACS washing buffer and centrifuged for 3 min at 300xg and 4°C. Cells were incubated with an appropriate dilution of antibody in FACS washing buffer and incubated for 30 min at 4°C. To remove unbound antibody, cells were washed again twice with FACS washing buffer and were then fixed with 200 µl FACS Fix buffer. Flow cytometry analysis was performed at the MACSQuant Analyzer 10 (Miltenyi Biotec) and data were analyzed using FCS express V4 and V6 (De Novo Software).

2.4 Virological methods

2.4.1 Preparation of cell-associated MV stocks

1.5 x 10^7 Vero-αHis cells were seeded in 15 cm cell culture dishes in DMEM (10% FCS, 1% L-glutamine) and infected with an MOI of 0.03. Infected cells were cultivated for 48 h at 37°C until at least 50% of the area was covered by syncytia. To harvest cell-associated MV, supernatant of infected cells was discarded and 1 ml of OptiMEM was added per cell culture dish. Adherent cells were detached using a cell scraper and cell suspension from several dishes was pooled in a 15 ml falcon tube. After snap-freezing the tube in liquid nitrogen, cell suspension was thawed at 37°C. Cell debris was removed by centrifugation for 5 min at 750xg and 4°C. Virus-containing supernatant was aliquoted into cryovials and frozen at -80°C for storage.

2.4.2 Preparation of supernatant VSV stocks

1.5 x 10^7 Vero-αHis cells were seeded in T175 cell culture flasks in VP-SFM (1% L-glutamine) and infected with an MOI of 0.01. Infected cells were cultured for 24 h at 37°C, followed by incubation for 24 h at 32°C until at least 50% of the area was covered by syncytia. Supernatant (SN) of infected cells was collected and pooled. Cell debris in the supernatant were first removed via centrifugation for 5 min at 3000xg and second by filtration through a 0.45 µm bottle top filter. Concentration of virus containing supernatant was performed using an Amicon 100K size exclusion filter (Merck). Volume was concentrated to 500 µl per size exclusion filter after centrifugation at 3000xg for 1.5 h. After concentration, virus stocks were sterile filtrated through a 0.22 µm filter. Virus-containing supernatant was aliquoted into cryovials and frozen at -80°C for storage.

2.4.3 Determination of the $TCID_{50}$/ml

Viral titers of MV or VSV-MV were calculated by the 50% Tissue Culture Infective Dose ($TCID_{50}$/ml). First, 1 x 10^4 permissive Vero-αHis cells were seeded in a 96-well-plate. The viral suspension of unknown titer was diluted in two individual dilution series ranging from 10^{-1} to 10^{-8} in DMEM. Vero-αHis cells were infected with 30 µl of each dilution step in eight replicas and cultivated at standard cultivation conditions. Depending on the viral kinetic, cells were analyzed for syncytia formation 48-96 h post titration via fluorescence microscopy.

Based on syncytia-positive counted wells, the viral titer was calculated using the equation of Spearman and Kärbers with a detection limit of 1 x 10^2 $TCID_{50}$/ml:

$$\frac{TCID50}{ml} = x \cdot 10^{-(log_{10}A-(B-0.5))}$$

x: Extrapolation factor arising from the volume of virus dilution used per well
A: Value of the last dilution step where all eight wells showed syncytia formation
B: Summation of the proportion of positive wells including both the last 100% up to the first 0% infectious dilution

2.4.4 Cell viability assay

For viability analysis of virus infected cells, the RealTime-Glo™ MT Cell Viability Assay (Promega) was used according to the manufacture's protocol. 2 x 10^4 L-428 or KM-H2 cells were seeded into 96-well plates. Cells were infected in triplicates with an MOI of 1 with VSV-CD30 or MV-CD30.

In addition, cells were treated with OptiMEM or VP-SFM as mock control. 4 h post infection, NanoLuc® luciferase and the cell-permeant pro-substrate MT Cell Viability Substrate were added and incubated at 37°C. To monitor cell viability, luciferase signals were quantified at the microplate luminometer (Berthold Technologies) 24 h and 48 h post infection. Pure medium served as blank and cell viability was normalized to uninfected control cells.

2.5 Experimental mouse work

All animal experiments were carried out in compliance with the regulations of the German animal protection law. 6-8 weeks old female NOD.Cg.Prkdc^{scid}IL2rg^{tmWjl}/SzJ (NSG) mice were purchased from Charles River. Mice were housed in the animal facility in individually ventilated cages and handled under a laminar flow hood.

2.5.1 Administration of tumor cells

L-428 and KM-H2 tumor cells were cultured as described in chapter 2.3.1. Then, desired amount of cells were pooled, pelleted at 300xg for 5 min and washed with PBS. Cell number was determined and resuspended in a defined volume of PBS to the desired cell density for implantation. To implant subcutaneous (s.c.) tumors, mice were anesthetized with 2% isoflurane using an anesthetic machine with an isoflurane vaporizer and oxygen concentrator (indulab-vet). 100 µl of tumor cell suspension were s.c. injected into the flank using a BD MicroFine 1 ml U100 29G Insulin syringe. For pilot experiments, 5x10^6 KM-H2 or L-428 were s.c. injected per NSG mouse. For main experiments, 1x10^7 KM-H2 cells pre-mixed with an equal amount of Corning® Matrigel® Basement Membrane Mix were s.c. injected per NSG mouse. Tumor growth was monitored by palpation and later using a digital caliper. Tumor size was calculated according to the volume of an ellipsoid by the following equation:

$$tumor\ volume\ [mm^3] = \frac{length[mm] \times (heigth[mm])^2}{2}$$

For implantation of disseminated tumors, NSG mice were pre-warmed using an infrared lamp in order to dilate the veins and transferred to a mouse-restrainer. 200 µl of tumor cell suspension containing $2x10^6$ KM-H2-luc cells was intravenously (i.v.) injected into one of the lateral tail veins using a BD MicroFine 1 ml U100 29G Insulin syringe. The extent of tumor progression was analyzed by in vivo imaging (Chapter 2.5.3).

Differences in tumor growth were quantified afterwards via calculation of area under the curve (AUC) (Duan et al. 2012).

2.5.2 Virus administration

When s.c. L-428 and KM-H2 tumors reached a specified volume, they were intratumorally (i.t.) injected with VSV-CD30 or MV-CD30. The desired amount of virus was diluted in VP-SFM (VSV-CD30) or OptiMEM (MV-CD30) to a total volume of 50 µl per tumor. Mice were anesthesized with 2% isoflurane using an anesthetic machine with an isoflurane vaporizer and oxygen concentrator (indulab-vet).

For i.v. injections, 200 µl VSV-CD30 was injected into one of the lateral tail veins as described in the previous chapter. VP-SFM served as mock control.

2.5.3 *In vivo* imaging

In vivo imaging is a method for non-invasively visualization of luciferase expressing cells in living mice. Luciferase signals were measured using the IVIS® Spectrum (Perkin Elmer) and analyzed using the Living Image Software (Perkin Elmer). Prior to measurement, 150 µg D-luciferin per gram body weight was injected intraperitoneally into mice. Mice were anesthetized with 2% isoflurane using a XGI-8 Gas Anesthesia system (Perkin Elmer). Imaging data were obtained 10 min after luciferin injection.

2.5.4 Immunofluorescence staining of cryo slices

Subcutaneous tumors were explanted, cut into two halves and fixed in 4% formaldehyde in PBS (Roti®-Histofix 4%) for at least 24 h. Next, tissue was dehydrated in 30% sucrose (PBS) and then embedded in optimum cutting temperature (O.C.T.) medium for snap freezing. Specimens were stored at -80°C.

Slices of 8 µm thickness were obtained with a cryostat (Leica CM1900) and dried at room temperature overnight. Slices were permeabilized with 0.2% Triton X100/PBS for 10 min and blocked with 5% donkey serum for 30 min at room temperature. For staining against GFP, slices were incubated with the rabbit α-GFP antibody (Invitrogen) overnight at 4°C, followed by incubation with the donkey α-rabbit Cy2-coupled secondary antibody (Jackson ImmunoResearch). For immunofluorescence staining against CD31, slices were incubated with the rat α-mouse CD31 antibody (Dianova) overnight at 4°C, followed by incubation with the donkey α-rat Alexa647-coupled secondary antibody (Jackson ImmunoResearch). Sections were mounted using Fluoroshield™ DAPI containing mounting media (Sigma-Aldrich).

2.5.5 Virus recovery

VSV-CD30 treated s.c. tumor were explanted, placed onto a 70 µm cell strainer and pushed through the cell strainer using the plunger end of a syringe. Next, the strainer was washed with $DMEM^{+PenStrep}$ medium and cells were pelleted for 5 min at 300xg and 4°C. Tumor cell suspension was transferred to Vero-αHis cells and incubated for 48 h at 37°C. After two days, cell culture of Vero-αHis cells and tumor cell suspension was analyzed by fluorescence microscopy for GFP expression.

3 Results

This thesis characterizes two CD30-targeted oncolytic viruses as a new treatment option for CD30$^+$ cHL. One is an oncolytic MV the other is VSV-MV chimera specific for CD30. The generation of those CD30-targeted oncolytic viruses was described in a previous work (Hanauer 2015). After demonstrating their specificity and their ability to infect and lyse CD30$^+$ cHL cell lines *in vitro*, suitable tumor mouse models were set up. Having two cHL xenograft mouse models at hand, the therapeutic activities of both MV-CD30 and VSV-CD30 were investigated via different virus application routes. Finally, the susceptibility of other CD30$^+$ tumor cell lines (anaplastic large cell lymphoma) for the infection with CD30-targeted viruses was evaluated *in vitro*.

3.1 CD30-targeted oncolytic viruses

In the previous work, a CD30-targeted measles virus (MV-CD30) and a vesicular stomatitis virus (VSV-CD30) were generated with the aim of selectively destroying CD30$^+$ cHL cells (Hanauer 2015). Both rely on the recently described scFv HRS3opt2#2 (Friedel et al. 2015) as CD30-specific binding domain. Its coding sequence is fused to that of MV hemagglutinin (H) at the C terminal end. To achieve retargeting, the MV-H is blinded for the attachment to natural MV receptors CD46, Nectin-4 and SLAM (Nakamura et al. 2005). For MV-CD30, the unmodified MV-H gene is exchanged against the coding sequence of H_{mut}-CD30-scFv (Figure 3.1). In case of VSV-CD30 the VSV glycoprotein G gene is replaced by reading frames of the MV fusion protein (F) and H_{mut}-CD30scFv. Recombinant VSV-MV contain an unmodified H protein, as well as MV_{Nse} both serving as parental virus controls. The usage of CD30 as an entry receptor by the generated CD30-targeted viruses had been analyzed before by infection of co-cultures of target and non-target cells as well as through blocking infection by soluble CD30-Fc protein (Hanauer 2015). New virus stocks of both CD30-targeted viruses as well as their parental viruses were produced in the beginning of this thesis.

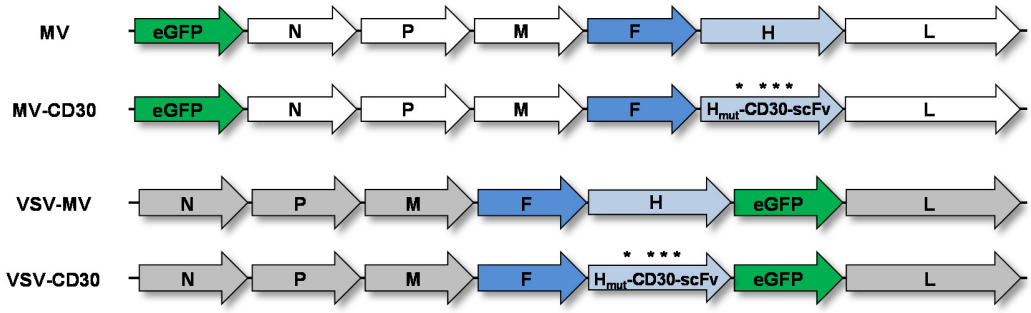

Figure 3.1: Genomic organization of CD30-targeted and untargeted parental viruses

MV-H protein blinded for natural MV receptors CD46 and SLAM (indicated by *) to generate H_{mut} is fused to a CD30-specific scFv with a C-terminal hexa-His-tag (H6) (CD30-scFv). For VSV-MV the VSV glycoprotein G reading frame is replaced with those of MV-F and MV-H, while VSV-CD30 encodes for MV-F and MV-H_{mut}-CD30-scFv. All virus genomes encode the reporter protein eGFP. Modified from (Hanauer 2015; Hanauer et al. 2018).

Following initial rescue of virus particles, single virus clones were generated by picking isolated syncytia after three rounds of passaging as described in chapter 2.4.1 and 2.4.2. Selected clones were further propagated on Vero-αHis cells. These cells are $CD30^-$ but display a Hexa-His-tag (H6)-specific antibody which can be used as entry receptor by both retargeted viruses due to a C-terminal H6 fused to H_{mut}-CD30scFv. All recombinant MV stocks were generated from infected Vero-αHis cell lysates.

Viral growth kinetics of all generated viruses had been investigated (Hanauer 2015). VSV-CD30 replicates with VSV-like kinetics to high titers in supernatant of infected Vero-αHis cells. Therefore, the purification of VSV-CD30 out of supernatant of infected cells was established in this thesis instead of using cell lysates. For this, Vero-αHis cells were seeded in a T175 cell culture flask in VP-SFM supplemented with 1% glutamine and infected with an MOI of 0.01. Infected cells were cultured for 24 h at 37°C, followed by 24 h at 32°C. After incubation, supernatant of infected cells was collected and pooled. Cell debris in the supernatant were first removed via centrifugation for 5 min at 3000xg and second by filtration through a 0.45 µm filter. Concentration of virus containing supernatant was performed using an Amicon 100K size exclusion filter. Volume was concentrated to 500 µl per size exclusion filter after centrifugation at 3000xg for 1.5 h. After concentration, virus stocks were sterile filtrated through a 0.22 µm filter and titrated on Vero-αHis cells.

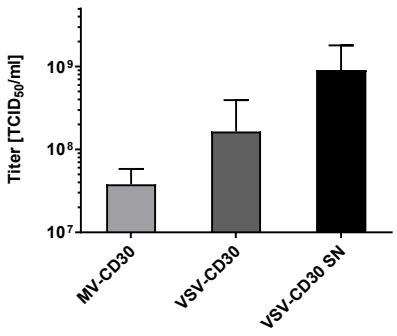

Figure 3.2: Viral titers of CD30-targeted viruses

Cell-associated and supernatant (SN) titers of MV-CD30 and VSV-CD30 stocks represented by the 50 % Tissue Culture Infective Dose ($TCID_{50}$/ml). n=6, error bars: mean ± SD.

Recombinant cell-associated VSV-CD30 was produced to titers up to 5.0 x 10^8 $TCID_{50}$/ml (Figure 3.3), whereas VSV-CD30 purified out of supernatant grew to highest titers up to 1 x 10^9 $TCID_{50}$/ml. In contrast, MV-CD30 grew to maximal titers in the range of 1 x 10^8 $TCID_{50}$/ml.

3.1.1 Characterization of CD30-targeted viruses

After generation of CD30-targeted viruses, the molecular composition of viral particles was analyzed. For this purpose, Western blot analysis for verification of the incorporation of MV-H and –F proteins was performed.

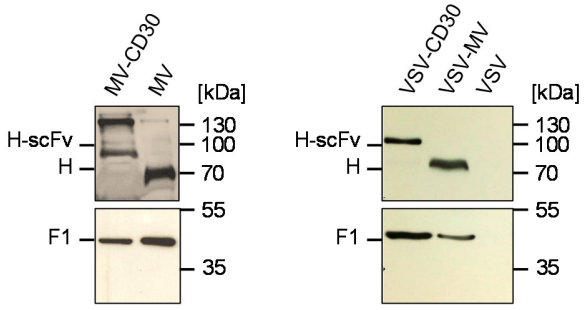

Figure 3.3: MV-glycoprotein expression of CD30-targeted viruses

Western blot analysis of 5 x 10^5 $TCID_{50}$ virus stock solution of CD30-targeted (MV-CD30, VSV-CD30) and untargeted (MV, VSV-MV) viruses for expression of MV-H and –F protein using antibodies recognizing the cytoplasmic tail of MV-H or MV-F. As negative control, wildtype VSV was used. Modified from (Hanauer et al. 2018).

Immunoblots of viral stocks revealed that VSV-CD30 and VSV-MV both contained the MV glycoproteins H and F (Figure 3.3).

Due to the fusion of the CD30-scFv protein, electrophoretic mobility of H_{mut}-CD30-scFv was reduced compared to H, resulting in a typical signal shift. This was also the case for stocks of MV-CD30 which were analyzed along with MV stocks.

3.1.2 Susceptibility of human classical Hodgkin lymphoma cell lines

After assessing the selectivity of CD30-targeted viruses, the next focus was the susceptibility of cHL cells. Since primary HRS-cell cultures are unavailable, cHL-derived, continuously growing cell lines were used as a model. The selected cell lines are covering two different subtypes of cHL, nodular sclerosis (L-428) and mixed cellularity (KM-H2) and are long-standing adequate models for HRS cell physiology with tumorigenic potential (Mathas et al. 2006; Steidl et al. 2011; Tiacci et al. 2012). First, the expression levels of the target receptor CD30 and the natural MV receptors SLAM and CD46 on L-428 and KM-H2 cells were determined by flow cytometry. Both cell lines were infected with CD30-targeted and the parental viruses.

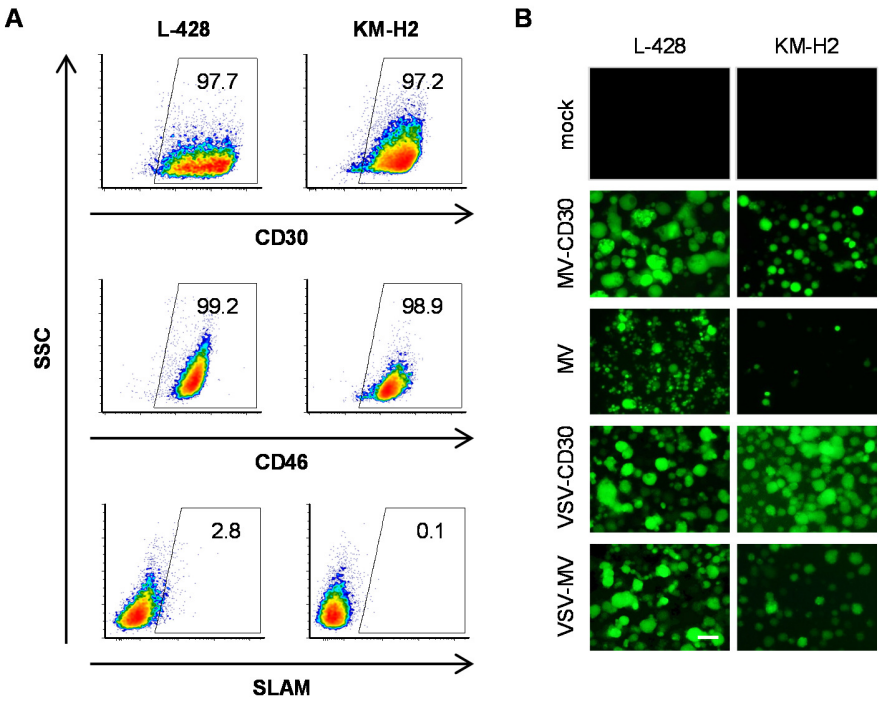

Figure 3.4: Susceptibility of human cHL cell lines L-428 and KM-H2

(**A**) Flow cytometry analysis of human cHL cell lines L-428 and KM-H2 for CD30, CD46 and SLAM expression. Cells were stained with a PE-labeled mouse CD30 antibody, a PE-labeled mouse CD150 (SLAM) antibody and a (FITC)-labeled mouse CD46 antibody. (**B**) Human cHL cell lines L-428 and KM-H2 were infected with CD30-targeted viruses and untargeted parental viruses at an MOI of 1 and analyzed by fluorescence microscopy 24 hours (VSV/MV, VSV-CD30) or 72 hours (MV, MV-CD30) post infection. Scale bar=200 µm. Modified from (Hanauer et al. 2018).

Flow cytometry analysis showed that L-428 and KM-H2 cells expressed CD30 as well as CD46 in a similarly high amount, but hardly any SLAM (Figure 3.4A). Both CD30-targeted viruses as well as their untargeted parental viruses readily infected both cHL cell lines and induced the formation of large syncytia (Figure 3.4B). Finally, the cytotoxic activity of MV-CD30 and VSV-CD30 infection on both cHL lines were evaluated.

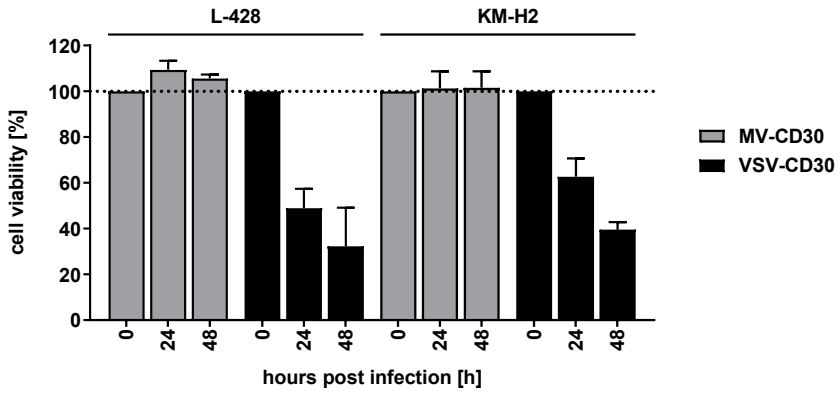

Figure 3.5: Killing assay of human cHL cell lines L-428 and KM-H2

Cell viability of human classical HL cell lines L-428 and KM-H2 after infection with MV-CD30 or VSV-CD30 with an MOI of 1. Viability was determined until 48 h post infection using the RealTime-Glo MT Cell Viability Assay and is presented as percentage to mock control. n=3, error bars: mean ± SEM. Modified from (Hanauer et al. 2018).

MV-CD30 infection did not kill L-428 cells within 48 h, while VSV-CD30 infection reduced cell viability to 50% after 24 h and to 30% after 48 h (Figure 3.5). Similar to what observed with L-428 cells, MV-CD30 infection did not reduce viability of KM-H2 cells at all during the observation period. In contrast, VSV-CD30 reduced cell viability to 60% after 24 h and to 48% after 48 h. Comparison of both cHL cell lines indicated a slightly higher killing activity of VSV-CD30 on L-428 cells than on KM-H2 cells. Overall, VSV-CD30 was more potent *in vitro* killing both L-428 and KM-H2 cells than MV-CD30.

3.1.3 Specificity of CD30-targeted oncolytic viruses

In this thesis, CD30 on cHL cells was used as a specific entry receptor for MV-CD30 and VSV-CD30. However, CD30 is not a cHL-exclusive tumor marker. For instance, activated T lymphocytes could express CD30 upon viral infections (Horie, R. and Watanabe, T. 1998). Those activated $CD30^+$ T lymphocytes represent a potential target population which can be infected by CD30-targeted oncolytic viruses. Therefore, the infection of $CD30^+$ T lymphocytes with MV-CD30 and VSV-CD30 was investigated first. To do so, CD30 expression upon activation of T lymphocytes was verified and CD25 was stained to monitor the activation of T lymphocytes.

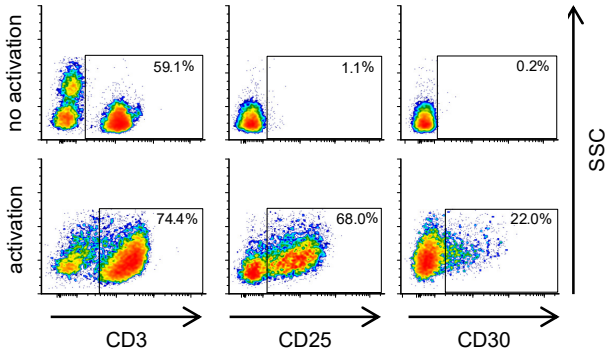

Figure 3.6: CD30 expression on activated T lymphocytes

Flow cytometry analysis of human PBMC that were cultured in absence (upper panel) or presence of the activating agents α-CD3/α-CD28 and IL-2 (lower panel) for CD3, CD25 and CD30 expression. Cells were stained with a Pacific-Blue-labeled mouse CD3 antibody, an APC-Cy7-labeled mouse CD25 antibody and a PE-labeled mouse CD30 antibody. Modified from (Hanauer et al. 2018).

T lymphocytes cultivated in the presence of α-CD3/α-CD28 and IL-2 were successfully activated indicated by detection of CD25 (Figure 3.6). Following activation of T lymphocytes, CD30 was upregulated. Since CD30 expression as described in literature was confirmed, infection of activated T lymphocytes with CD30-targeted viruses and their parental viruses was performed.

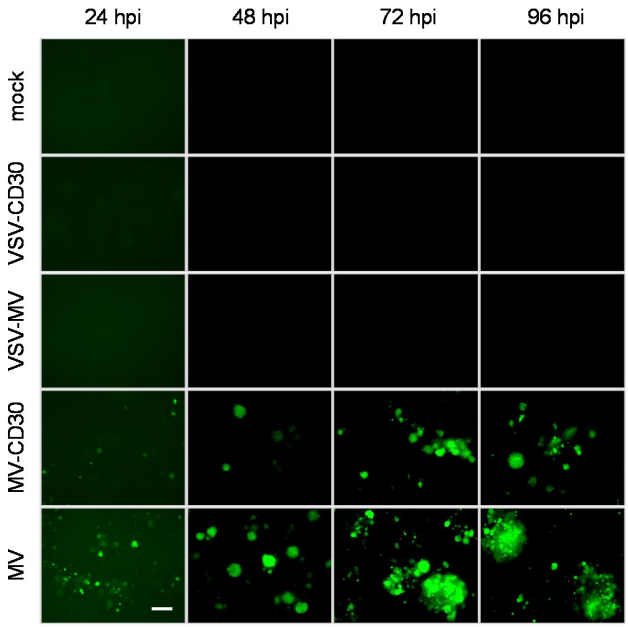

Figure 3.7: Infection of CD30$^+$ T lymphocytes

Activated PBMC expressing CD30 were infected with CD30-targeted viruses or untargeted parental viruses with an MOI of 0.1. GFP expression was monitored by fluorescence microscopy 24–96 h post infection. Scale bar=200 µm. Modified from (Hanauer et al. 2018).

Both VSV-CD30 and VSV-MV did not infect activated T lymphocytes within 96 hpi (Figure 3.7). MV-CD30 infected some cells, which subsequently build syncytia-like structures. Still, the infection seemed not to spread within the culture over time. Only MV infection spread within 96 hpi, leading to the formation of larger syncytia. Flow cytometry analysis of infected cells revealed the same pattern on single cell level (Figure 3.8).

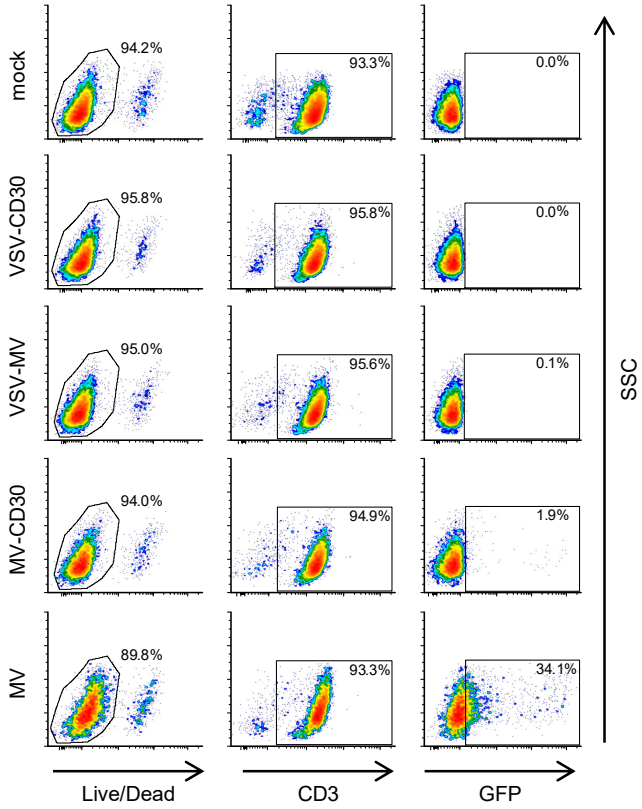

Figure 3.8: Flow cytometry analysis of infected CD30⁺ T lymphocytes

Flow cytometry analysis of activated living PBMC infected with CD30-targeted viruses or untargeted parental viruses (MOI of 1) after 72 hpi for CD3 and GFP expression. Cells were stained with an eFluor™-780-labeled Fixable Viability Dye and a Pacific-Blue-labeled mouse CD3 antibody. Modified from (Hanauer et al. 2018).

To sum up, T lymphocytes were completely protected from VSV-CD30 as well as VSV-MV infection despite the presence of CD30 as entry receptor. Partial susceptibility of T lymphocytes for MV infection is reduced by retargeting MV to CD30.

3.2 Setting up a tumor mouse model for *in vivo* characterization of VSV-CD30

To evaluate the oncolytic potential of VSV-CD30 in comparison to MV-CD30 on cHL cells *in vivo*, a suitable tumor mouse model had to be established. For proof of concept, a s.c. growing human cHL tumor was generated in immunodeficient NSG mice from the previously introduced cell lines.

3.2.1 Tumor growth of subcutaneous L-428 vs KM-H2 tumors

Both cHL cell lines L-428 and KM-H2 were shown to be susceptible for infection with CD30-targeted viruses *in vitro*. However, only VSV-CD30 infection had induced killing of both tumor cell lines, whereas MV-CD30 had not. Therefore, investigation of the oncolytic activity of VSV-CD30 in a tumor mouse model was focused first. L-428 or KM-H2 cells were implanted s.c. into NSG mice. Once tumors reached a size of 100 mm^3, three i.t. injections of 3 x 10^8 $TCID_{50}$ of VSV-CD30 in total were performed within one week.

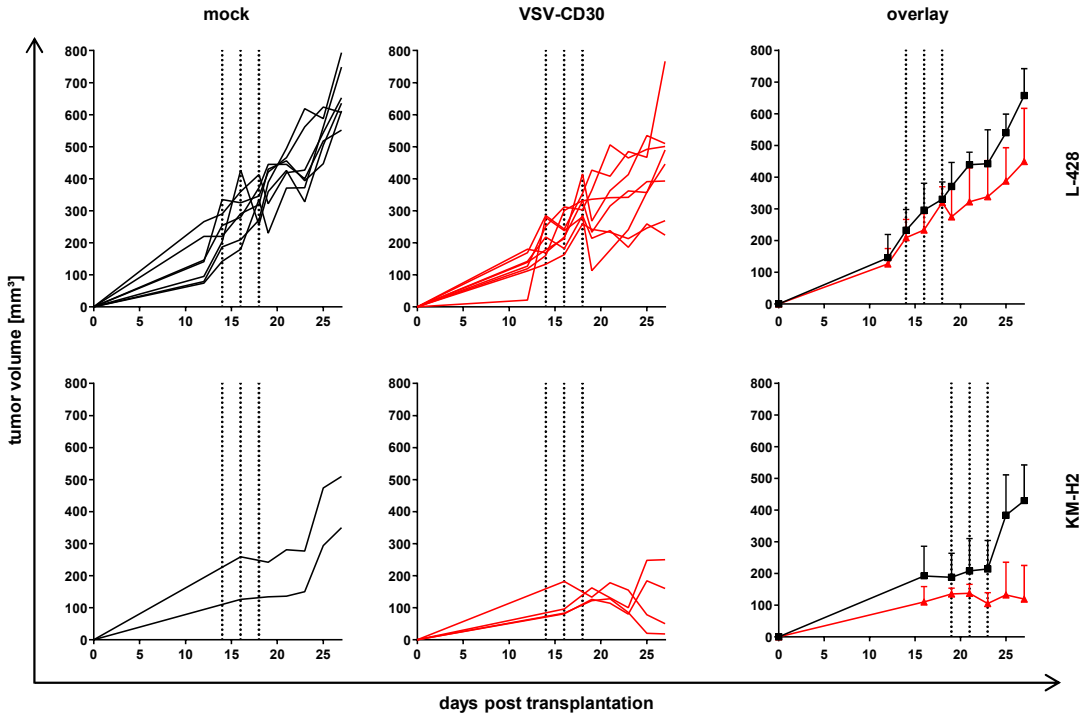

Figure 3.9: Tumor growth curves of s.c. L-428 and KM-H2 tumors

NSG mice were s.c. implanted with 5 x 10^6 L-428 or KM-H2 cells. 14 days post cell transplantation, mice received three i.t. injections of VSV-CD30 over a period of five days covering a total dose of 3 x 10^6 $TCID_{50}$ (dashed lines). Control animals (mock) were injected with an equal volume of VP-SFM. Tumor growth curves of individual mice and an overlay of the mean of both groups (error bars: mean ± SD) are shown. L-428: VSV-CD30 and mock, n=8. KM-H2: VSV-CD30, n=4; mock, n=2.

L-428 tumors grew more homogenously than KM-H2 tumors (Figure 3.9). Only 6 out of 16 (37%) implanted KM-H2 tumors grew, with delayed kinetics compared to L-428 tumors. However, VSV-CD30 treatment induced a strong tumor growth inhibition in KM-H2 tumors, but not in L-428 tumors.

Since tumor sizes were measured manually with a caliper during the experiment, tumor weight and size were measured again at the end of the experiment to obviate any inaccuracies.

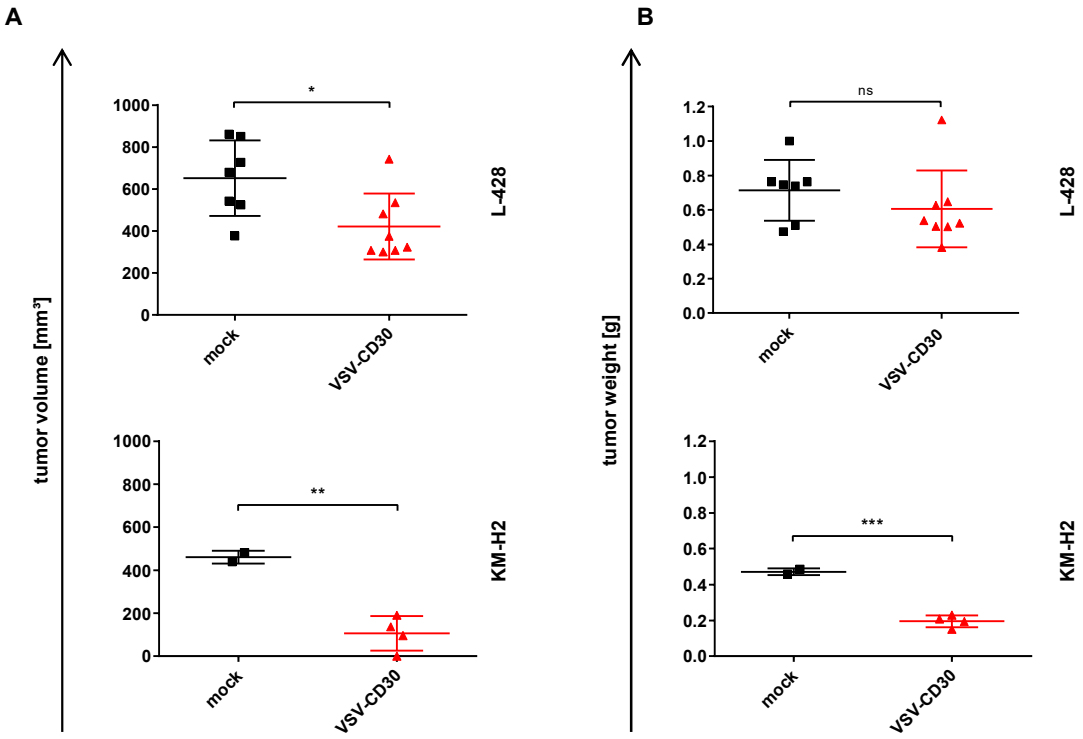

Figure 3.10: Final analysis of s.c. L-428 and KM-H2 tumors treated with VSV-CD30

14 days after the last virus injection, s.c. L-428 and KM-H2 tumors were explanted and analyzed for (A) Tumor volume and (B) Tumor weight. L-428: VSV-CD30 and mock, n=8. KM-H2: VSV-CD30, n=4; mock, n=2. Unpaired t test: *** p <0.001, ** p <0.01, * p<0.05. Error bars: mean ± SD.

Final analysis revealed a slight difference between VSV-CD30 and mock treated L-428 tumors when measuring the tumor volume. Determination of tumor weight however confirmed that this difference was not significant (Figure 3.10). In contrast, volumes of KM-H2 tumors treated with VSV-CD30 were significantly smaller than mock treated tumors. Difference in tumor growth of VSV-CD30 to mock treated KM-H2 tumors proved even greater when the tumor weight was examined. Altogether, the data from final analysis was consistent with the tumor size measurements during the experiment. To verify that VSV-CD30 was present in i.t. treated tumors, L-428 and KM-H2 tumors were dissociated and an overlay of tumor cell suspension on Vero-αHis cells was performed.

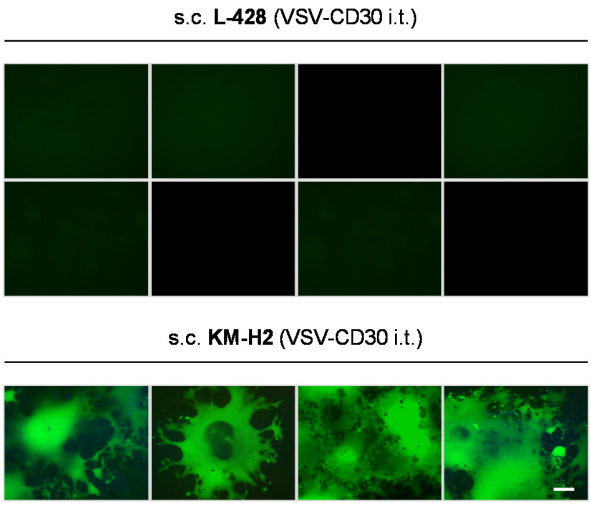

Figure 3.11: Virus recovery from i.t. treated L-428 and KM-H2 tumor tissue

Intratumorally (i.t.) VSV-CD30 treated s.c. L-428 and KM-H2 tumors were explanted 14 days after the last virus injection and dissociated mechanically through a cell strainer. Tumor cell suspensions were overlayed on Vero-αHis cells and analyzed for GFP expression by fluorescence microscopy 48 hours post infection. Scale bar=200 µm.

From none of the VSV-CD30 treated L-428 tumors, virus was recovered (Figure 3.11), indicating that no replicating virus had remained in the tumor tissue. As expected from the tumor growth inhibition, in all four VSV-CD30 treated KM-H2 tumors virus was recovered from tumor cell suspension. To assess the targeting capacity of VSV-CD30 in the KM-H2 tumor mouse model, the experimental set-up was repeated. KM-H2 cells were implanted s.c., but this time, VSV-CD30 was injected intravenously instead of intratumorally.

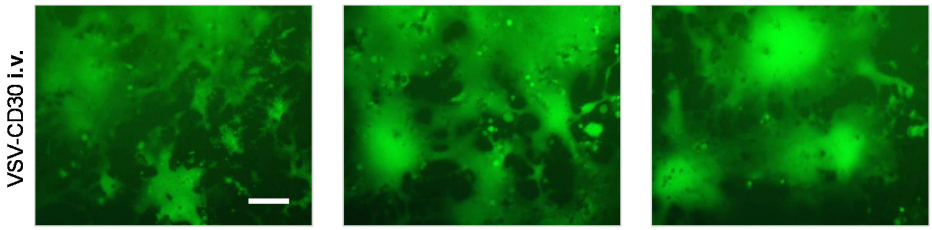

Figure 3.12: Virus recovery from i.v. treated KM-H2 tumor tissue

NSG mice were s.c. implanted with 5 x 10^6 KM-H2 cells. 14 days post cell implantation mice received three i.v. injections of VSV-CD30 over a period of five days covering a total dose of 3 x 10^8 $TCID_{50}$. Treated s.c. KM-H2 tumors were explanted 14 days post last virus injection and dissociated mechanically through a cell strainer. Tumor cell suspension was overlayed on Vero-αHis cells and analyzed for GFP expression by fluorescence microscopy 48 hours post infection. n=3. Scale bar=200 µm.

Remarkably, similar to i.t. treated KM-H2 tumors, replicating VSV-CD30 could also be recovered from of all i.v. treated tumors (Figure 3.12).

Taken together, KM-H2 cells seemed to respond better than L-428 cells to VSV-CD30 treatment *in vivo*, but tumor growth of s.c. KM-H2 had to be optimized.

3.2.2 Improving KM-H2 tumor growth using Matrigel

Antitumoral efficacy of VSV-CD30 was demonstrated to be stronger on s.c. KM-H2 tumors than on L-428 tumors, but the tumor growth was unstable. Subsequently, the next step was to optimize the tumor growth of s.c. KM-H2 tumors. An extracellular matrix-based hydrogel ("Matrigel") was used to stabilize growth of s.c. injected KM-H2 cells at the site of injection. To do so, KM-H2 cells were mixed with Matrigel (1:1) or left untreated as control and subsequently implanted s.c. into NSG mice. In contrast to the previous experimental setting, tumors were already injected three times i.t. with 3 x 10^8 $TCID_{50}$ of VSV-CD30 within one week when they reached a size of 50 mm^3 instead of 100 mm^3.

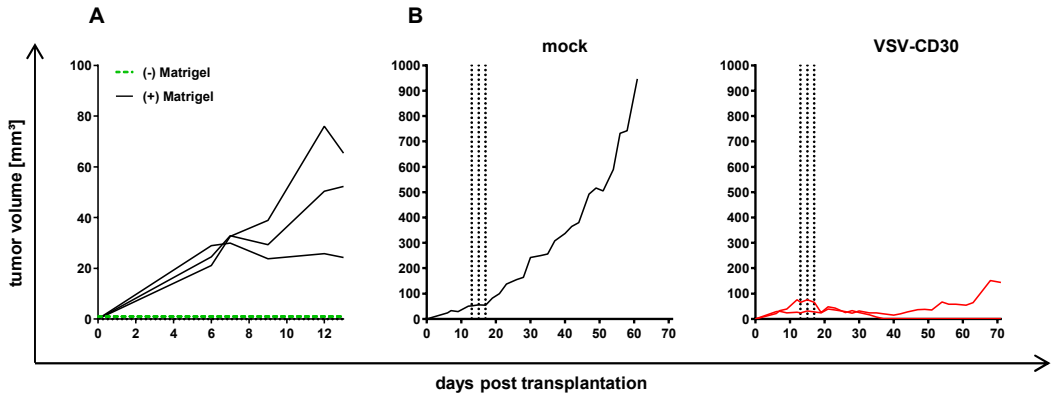

Figure 3.13: Tumor growth of s.c. KM-H2 tumor in combination with Matrigel matrix

NSG mice were s.c. implanted with 1 x 10^7 KM-H2 cells mixed with Matrigel (+) or left untreated as mock control (-). 13 days post cell transplantation, mice ((+) Matrigel) received three i.t. injections of VSV-CD30 over a period of five days covering a total dose of 3 x 10^6 $TCID_{50}$ (dashed lines). Control animal (mock) was injected with an equal volume of VP-SFM. Tumor growth curves of individual mice are shown. VSV-CD30, n=2; mock, n=1.

Tumor growth curves show that s.c. implanted KM-H2 cells without Matrigel did not grow at all (Figure 3.13A). In contrast, all mice implanted s.c. with KM-H2 cells in combination with Matrigel developed a tumor. In addition, s.c. KM-H2 tumors implanted with Matrigel responded to VSV-CD30 treatment with a tumor growth delay (Figure 3.13B), indicating that the Matrigel matrix did not hinder oncolysis.

To further characterize viral replication in KM-H2 Matrigel tumor tissue, VSV-CD30 and blood vessels (CD31) were detected by immunofluorescence. In detail, KM-H2 cells mixed with Matrigel were implanted s.c. into NSG mice. VSV-CD30 was either applied i.t. (1 x 10^6 $TCID_{50}$) or i.v. (1 x 10^8 $TCID_{50}$). Afterwards, VSV-CD30 injected tumors were cut in sections and stained for GFP and CD31.

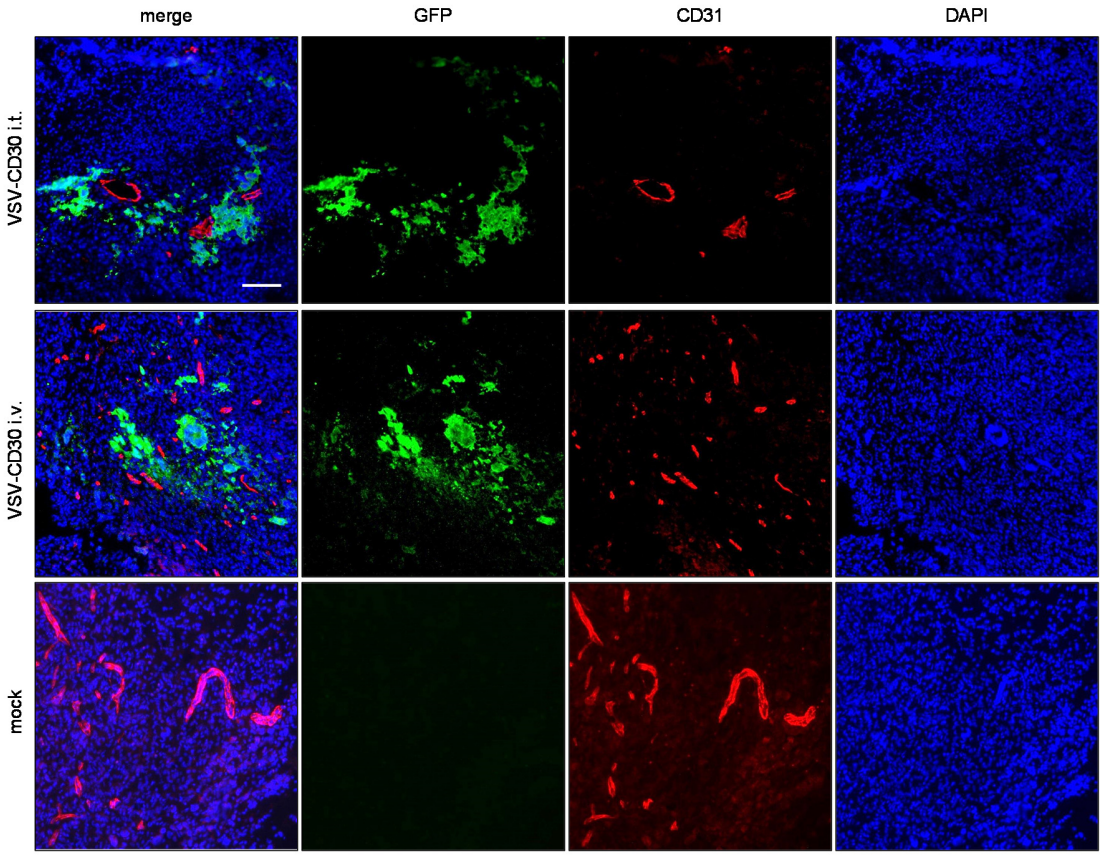

Figure 3.14: Detection of VSV-CD30 in s.c. KM-H2 tumor tissue

Subcutaneously (s.c.) implanted KM-H2 tumors were treated i.t. with 1 x 10^6 $TCID_{50}$ of VSV-CD30 (top row), i.v. with 1 x 10^8 $TCID_{50}$ VSV-CD30 (middle row) or OptiMEM as mock control (bottom row), respectively. 14 days post treatment, tumors were removed and cut in sections. GFP^+ cells were detected by immunofluorescence staining using a polyclonal GFP antibody and a Cy2-labeled secondary antibody. Murine blood vessels were detected by immunofluorescence staining using a polyclonal CD31 antibody and an Alexa-Fluor647-labeled secondary antibody. One representative section out of ten GFP positive sections is shown. Scale bar=200 µm. Adapted from (Hanauer et al. 2018).

Slices of mock treated tumors showed expression of CD31 which indicated blood vessel formation, but no GFP expression for any infectious spots (Figure 3.14). For both virus application routes, GFP expression indicated infectious areas of VSV-CD30 in all sections stained.

Remarkably, infectious areas were equally distributed independent from virus application route. Similar to mock treated tumors, VSV-CD30 treated tumors showed expression of CD31 for blood vessel formation potentially facilitating the spread of VSV-CD30 within the tumor.

In conclusion, s.c. KM-H2 tumors grew more homogenously when implanted with Matrigel. In addition, VSV-CD30 was detected within the tumor tissue independently from Matrigel environment or route of administration.

3.3 Antitumoral activity of CD30-targeted viruses *in vivo*

Based on the aforementioned factors, KM-H2 cells are more suitable than L-428 for analysis of VSV-CD30 *in vivo* as model for cHL. After optimizing the tumor growth, this cHL cell line was used for the subsequent characterization of the antitumoral activity of CD30-targeted viruses in the xenograft mouse model.

3.3.1 Oncolytic activity of CD30-targeted viruses after intratumoral administration

After having established the KM-H2 tumor model, the comparison of antitumoral activities of VSV-CD30 vs MV-CD30 was examined next. For this purpose, KM-H2 cells mixed with Matrigel were implanted s.c. into NSG mice. Once tumors reached a size of 50 mm^3, three i.t. injections of 3 x 10^6 $TCID_{50}$ (MV-CD30 or VSV-CD30) in total were performed within one week. To analyze the impact of the dosage, one group received 3 x 10^8 $TCID_{50}$ of VSV-CD30 in total within one week.

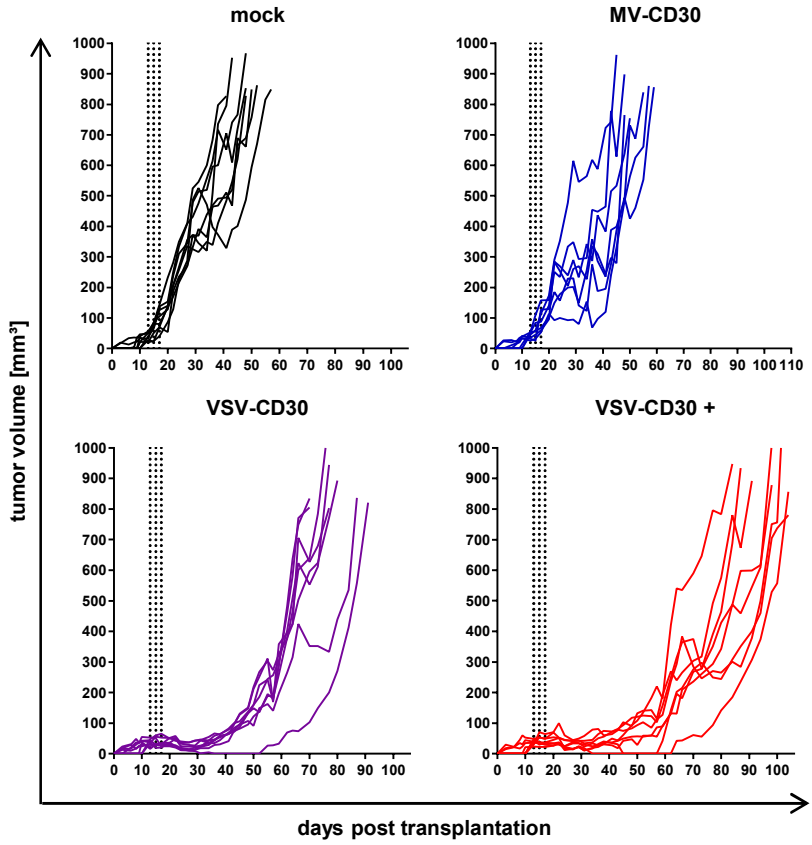

Figure 3.15: Tumor growth curves of s.c. KM-H2 tumors i.t. treated with VSV-CD30 and MV-CD30

NSG mice were s.c. implanted with 1 x 10^7 KM-H2 cells mixed with Matrigel. 13 days post cell transplantation, mice received three i.t. injections over a period of five days covering a total dose of 3 x 10^6 $TCID_{50}$ (MV-CD30, VSV-CD30 low dose) or 3 x 10^8 $TCID_{50}$ (VSV-CD30 high dose (+)) (dashed lines). Control animals (mock) were injected with an equal volume of VP-SFM. Tumor growth curves of individual mice are shown till a tumor size >800 mm^3 was reached. MV-CD30, n=7; VSV-CD30 low dose, n=8; VSV-CD30 high dose (+), n=8; mock, n=8.

Mock treated tumors grew unaffectedly and exponentially (Figure 3.15). MV-CD30 treated tumors showed only a slight tumor growth delay compared to mock treated controls. Remarkably, VSV-CD30 treatment in both doses completely inhibited tumor growth over several weeks. One VSV-CD30 low dose treated mouse went into full remission initially. It relapsed on day 55 post transplantation. Application of VSV-CD30 in the high dose resulted in the strongest tumor growth delay, with two mice that went into full remission initially. One of these mice relapsed on day 59, the other on day 62 post transplantation. Consequently, slowing of tumor growth was not permanent in VSV-CD30 treated mice. To quantify differences between the treatment groups, the differences in area under the curve (AUC) as well as survival of tumor bearing mice were determined.

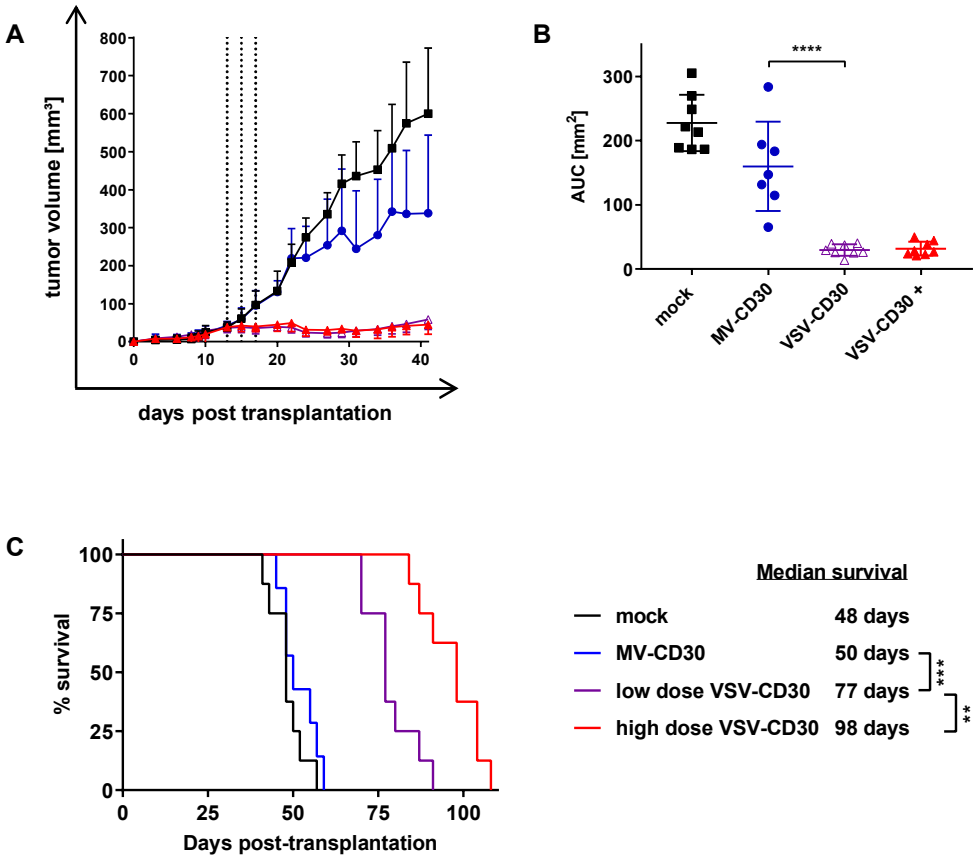

Figure 3.16: Quantification of AUC and survival analysis of KM-H2 tumor-bearing mice

NSG mice were s.c. implanted with 1 x 10^7 KM-H2 cells mixed with Matrigel. 13 days post cell transplantation, mice received three i.t. injections over a period of five days covering a total dose of 3 x 10^6 $TCID_{50}$ (MV-CD30, VSV-CD30 low dose) or 3 x 10^8 $TCID_{50}$ (VSV-CD30 high dose (+)) (dashed lines). Control animals (mock) were injected with an equal volume of VP-SFM. (**A**) Average tumor growth curves of MV-CD30, VSV-CD30 low dose, VSV-CD30 high dose or mock treated mice until day 41 post transplantation. (**B**) Areas under the curves (AUC) shown in (a). One-way ANOVA test (Multiple comparisons), **** p <0.0001. (**C**) Kaplan-Meyer plot survival analysis. Logrank test (Bonferroni adjusted), *** p <0.001, ** p <0.01. MV-CD30, n=7; VSV-CD30 low dose, n=8; VSV-CD30 high dose, n=8; mock, n=8. Error bars: mean ± SEM. Modified from (Hanauer 2015; Hanauer et al. 2018).

AUC determination revealed that the tumor volume of VSV-CD30 treated tumors was significantly smaller than that of MV-CD30 treated tumors when both were treated with an equivalent viral dose (Figure 3.16A, B). In correlation with the tumor growth inhibition, tumor-bearing mice survived significantly longer when treated with VSV-CD30 than MV-CD30 (Figure 3.16C). The prolonged survival of tumor bearing mice was even more pronounced when VSV-CD30 was applied at the higher dose. This data indicate that there is a dose relation of VSV-CD30 treatment.

3.3.2 Oncolytic activity of CD30-targeted viruses after intravenous administration

Since VSV-CD30 was retargeted to CD30$^+$ cells, it was expected that systemic administration would lead to a similar oncolytic effect compared to i.t. application. Previous experiments had already confirmed that VSV-CD30 can be detected in s.c. cHL xenograft tumor tissue when applied intravenously. Subsequently, the oncolytic potential in combination with the targeting capacity of VSV-CD30 was verified. The same s.c. xenograft KM-H2 mouse model as before was used, but VSV-CD30 was applied i.v. instead of i.t.. KM-H2 cells mixed with Matrigel were s.c. implanted into NSG mice. Once tumors reached a size of 50 mm^3, mice received three i.v. injections of 3 x 10^8 $TCID_{50}$ of VSV-CD30 in total within three weeks.

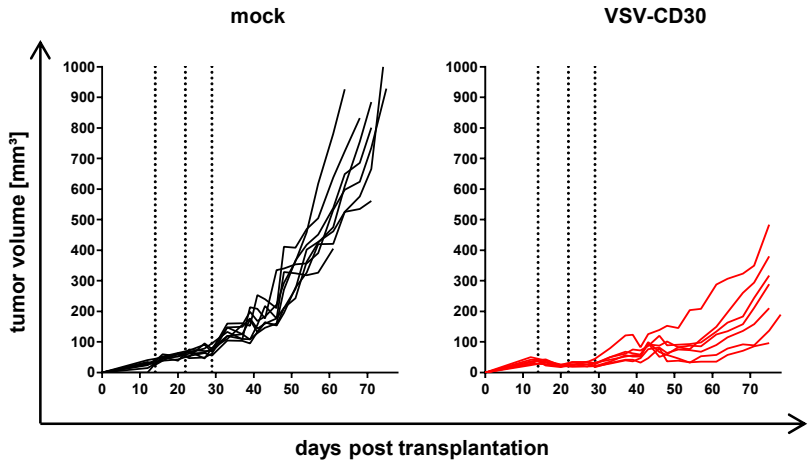

Figure 3.17: Tumor growth curves of s.c. KM-H2 tumors i.v. treated with VSV-CD30

NSG mice were s.c. implanted with 1 x 10^7 KM-H2 cells mixed with Matrigel. 14 days post cell transplantation, a total dose of 3 x 10^8 $TCID_{50}$ of VSV-CD30 split in three aliquots was systemically injected weekly (dashed lines). Control animals (mock) were injected with an equal volume of VP-SFM. Tumor growth curves of individual mice are shown until a tumor size >800 mm^3. VSV-CD30, n=8; mock, n=6.

Again, mock treated tumors grew unaffectedly (Figure 3.17). Remarkably, even after systemic application VSV-CD30 was able to inhibit tumor growth over several weeks compared to mock treated tumors. Similar to the results obtained for i.t. application of VSV-CD30, the slowed down tumor growth was not permanent and mice relapsed around day 32 post transplantation. To quantify the differences, AUCs were determined.

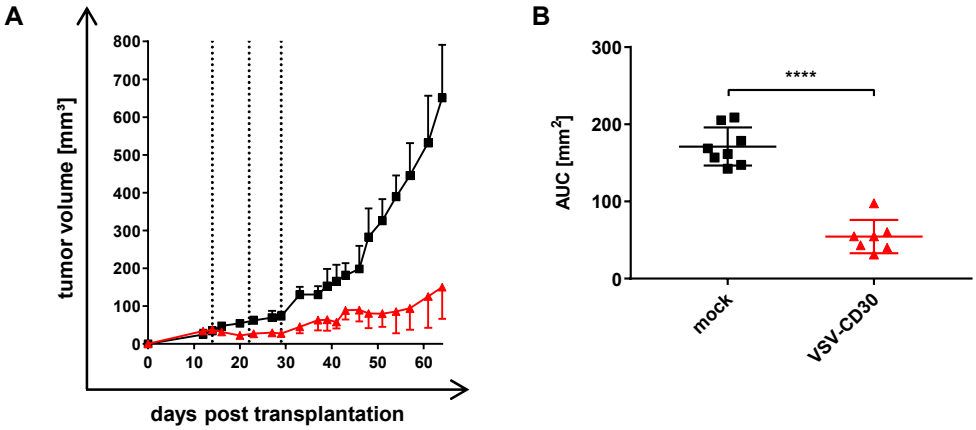

Figure 3.18: Quantification of AUC of KM-H2 tumor-bearing mice

NSG mice were s.c. implanted with 1 x 10^7 KM-H2 cells mixed with Matrigel. 14 days post cell transplantation, a total dose of 3 x 10^8 $TCID_{50}$ of VSV-CD30 split in three aliquots was systemically injected weekly (dashed lines). Control animals (mock) were injected with an equal volume of VP-SFM. (**A**) Average tumor growth curves of VSV-CD30 or mock treated mice until day 64 post transplantation. (**B**) Areas under the curves (AUC) shown in (a). Unpaired t test, **** p <0.0001. VSV-CD30, n=7; mock, n=8. Error bars: mean ± SEM. Modified from (Hanauer 2015; Hanauer et al. 2018).

Quantification of AUC reveled that tumor sizes of i.v. VSV-CD30 treated tumors were significantly smaller than mock treated ones (Figure 3.18). When the last mock treated mouse had to be sacrificed all VSV-CD30 treated mice were still alive. This also indicates a clear survival benefit with VSV-CD30 even with i.v. treatment. Altogether, the tumor growth inhibition pattern was comparable to i.t. treated tumors.

In conclusion, VSV-CD30 showed a high antitumoral efficacy in the s.c. cHL xenograft mouse model independent of the route of administration.

3.4 Analyzing VSV-CD30 in a disseminated KM-H2 tumor model

Up to now, a xenograft tumor mouse model in which cHL cells were growing to large s.c. tumors was used for examining the oncolytic potential of VSV-CD30. However, in early stages cHL is rather affecting peripheral lymph nodes in patients. In late stages, metastasis in liver, lung and bone marrow can be found as well (Küppers 2012). Therefore, a tumor mouse model reflecting the clinically relevant tumor burden was needed to further characterize the potential applications of CD30-targeted VSV. For this purpose, a xenograft model in which KM-H2 tumors are systemically injected for disseminated growth was established. For non-invasive monitoring of tumor growth *in vivo*, KM-H2 cells stably expressing the luciferase gene (luc) had to be generated first.

3.4.1 Generation of KM-H2-luc cells

KM-H2-luc cells were generated by transduction of parental KM-H2 cells with an HIV-1-derived LV pseudotyped with VSV-G, encoding the firefly luciferase and a puromycin resistance. Selection of transduced cells was performed using puromycin. Luciferase expression of KM-H2 cells was afterwards verified in a luciferase assay.

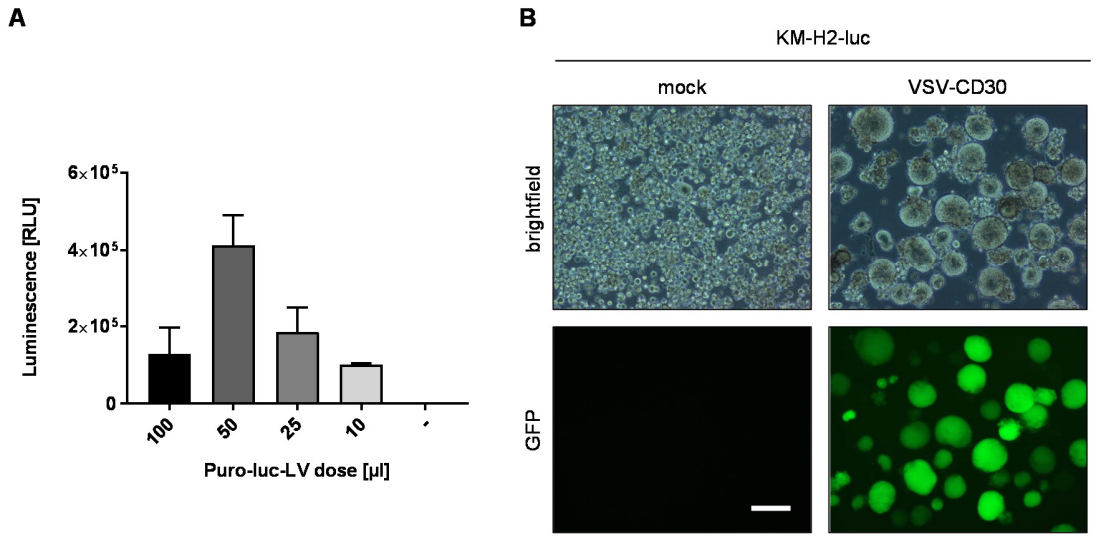

Figure 3.19: Generation of KM-H2-luc cells and infection with VSV-CD30

(**A**) Luciferase signals of KM-H2-luc cells stably expressing the luciferase reporter gene (luc). 100-10 µl of VSV-G-HIV1-Puro-Luc vector (Puro-luc-LV) were used for transduction of parental KM-H2 cells. Transduced cells were lysed and luciferase activity was determined. n=2, error bars: mean ± SD. (**B**) KM-H2-luc were infected with VSV-CD30 at an MOI of 1 and analyzed by fluorescence microscopy 24 hours post infection. Scale bar=200 µm.

KM-H2-luc cells generated using 50 µl of Puro-luc-LV showed the highest luciferase intensity (Figure 3.19A). Therefore, these cells were expanded and used for further experiments. Before investigating the disseminated tumor growth *in vivo*, KM-H2-luc cells were analyzed for their susceptibility for VSV-CD30 *in vitro*. Fluorescence microscopy pictures indicated that the expression of firefly luciferase did not influence the susceptibility of KM-H2-luc cells for VSV-CD30 infection (Figure 3.19B).

3.4.2 Setting up the injection regime in a multifocal KM-H2-luc model

To monitor disseminated tumor growth *in vivo*, KM-H2-luc cells were injected i.v. into NSG mice in two different cell counts. Development of tumor foci was visualized by luciferase *in vivo* imaging over time. When luciferase signals were detectable, both mice implanted with KM-H2-luc cells were injected with 1×10^8 $TCID_{50}$ of VSV-CD30. Luciferase signal intensities were quantified afterwards.

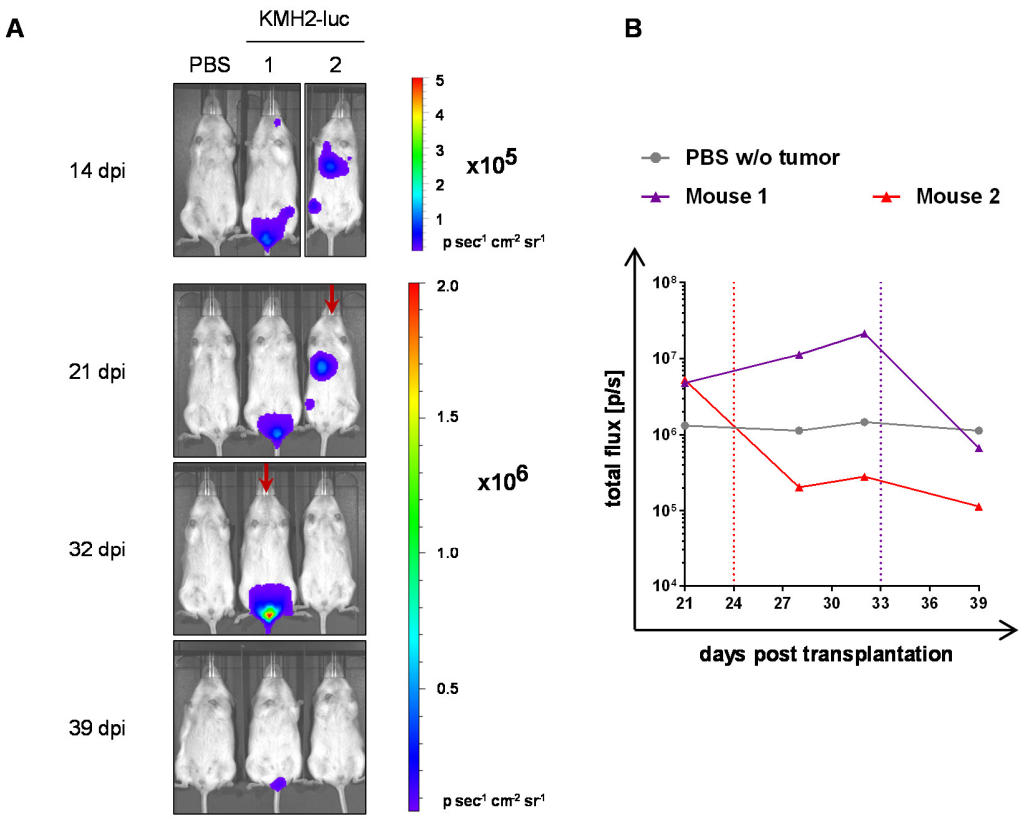

Figure 3.20: Setting up VSV-CD30 injection regime in a multifocal KM-H2-luc model

NSG mice were implanted i.v. with 1 x 10^6 (mouse 1) or 2 x 10^6 (mouse 2) KM-H2-luc cells. Mouse 1 received one i.v. injection of 1 x 10^8 $TCID_{50}$ VSV-CD30 on day 33 post cell transplantation (dpi) (B: purple dashed line). Mouse 2 received one i.v. injection of 1 x 10^8 $TCID_{50}$ VSV-CD30 on 24 dpi (B: red dashed line). Control animal (PBS) was injected with an equal volume of PBS. (**A**) Luciferase imaging pictures of treated mice. Ventral view of all mice included in the experiment recorded at the indicated time points. Red arrows: Injection of VSV-CD30. (**B**) Total luciferase activities over time for each mouse.

Luciferase signals were detected in both mice injected with KM-H2-luc cells, indicating successful tumor growth for both cell intensities used (Figure 3.20A). For mouse 1 tumor foci concentrated close to the injection site and for mouse 2 presumably in the liver and in the bone marrow. Interestingly, independent of tumor site and infused cell number, VSV-CD30 treatment induced a nearly complete tumor remission until the end of the observation period in both mice (Figure 3.20B).

3.4.3 Oncolytic activity of VSV-CD30 in a multifocal KM-H2-luc model

Having shown that KM-H2-luc cells engrafted into NSG mice and tumor sites can be targeted with VSV-CD30, the next step was the analysis of the antitumoral efficacy in larger cohorts. Again, KM-H2-luc cells were i.v. implanted into NSG mice. Luciferase intensities reflecting the tumor burden were measured by *in vivo* imaging over time. When considerable luciferase signals were detected, all mice received three i.v. injections of 3 x 10^8 $TCID_{50}$ of VSV-CD30 in total within 10 days.

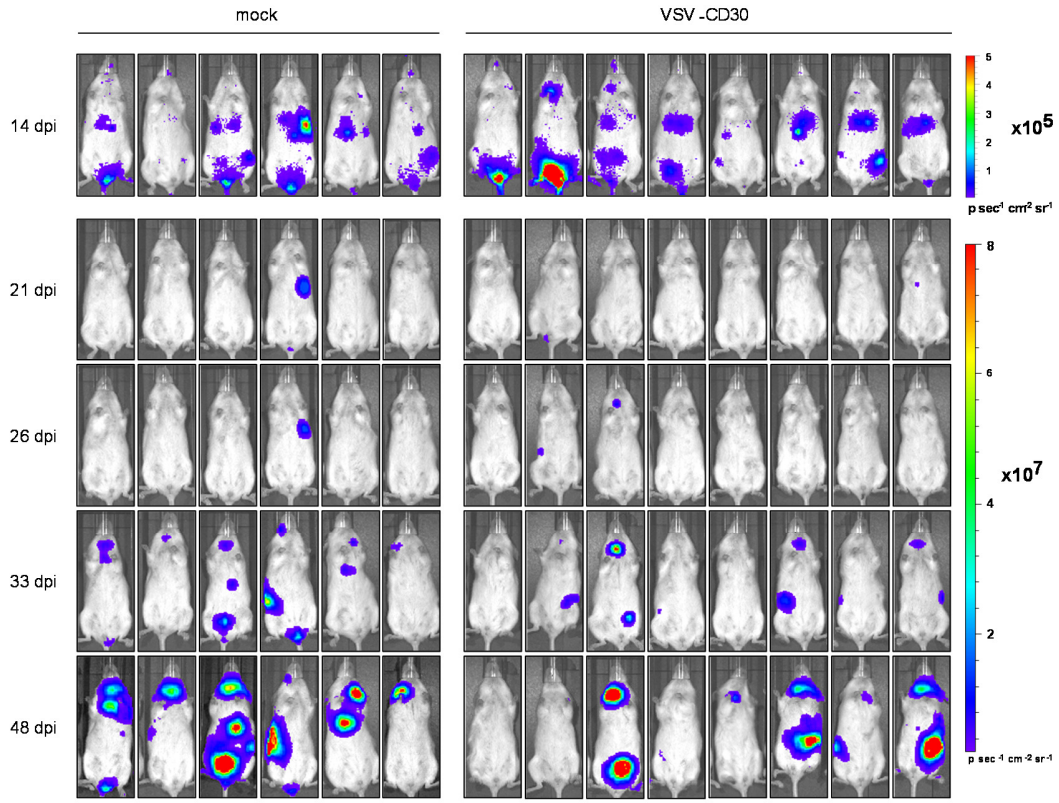

Figure 3.21: Oncolytic activity of VSV-CD30 in a multifocal KM-H2-luc model

Luciferase imaging pictures of NSG mice implanted i.v. with 2 x 10^6 KM-H2-luc cells. Mice received three i.v. injections of VSV-CD30 covering a total dose of 3 x 10^8 $TCID_{50}$ on day 18, 21 and 28 post cell transplantation (dpi). Control animals (mock) were injected with an equal volume of VP-SFM. Ventral view of all mice included in the experiment recorded at the indicated time points (dpi: days post implantation). Modified from (Hanauer 2015; Hanauer et al. 2018).

Luciferase imaging pictures on day 14 post transplantation showed that KM-H2-luc cells had engrafted into all mice and concentrated in different organs (Figure 3.21). For some mice, signals concentrated at the injection site, for others presumably in the liver, in lung or in bone marrow. Up to day 26 post transplantation, tumor signals increased slowly and no differences between both treatment groups were detectable.

First responses to VSV-CD30 treatment were visible on day 33 post cell transplantation in five out of eight mice. On the last day of observation, at least those five mice showed substantial decreased luciferase signals, whereas the remaining three mice showed high luciferase signals concentrating in different organs, similar to mock treated mice.

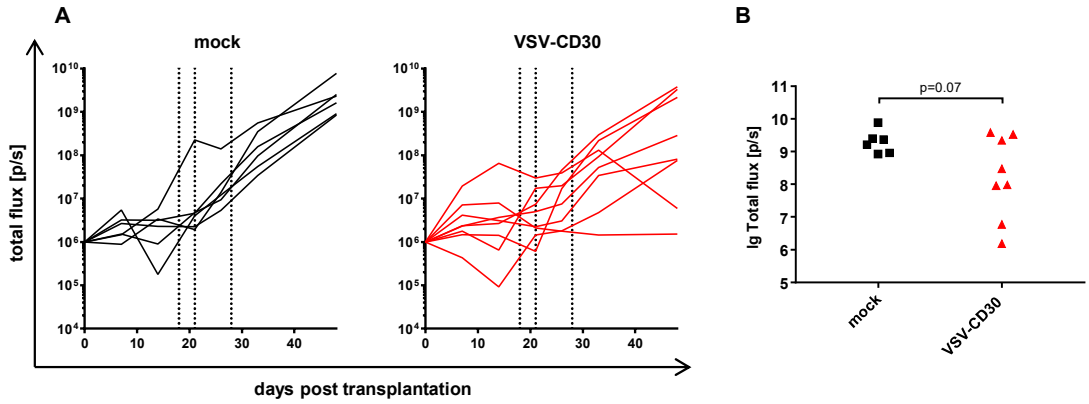

Figure 3.22: Kinetic of KM-H2 luc tumor burden in mock and VSV-CD30 treated mice

NSG mice were intravenously (i.v.) implanted with 2 x 10^6 KM-H2-luc cells. Mice received three i.v. injections of VSV-CD30 covering a total dose of 3 x 10^8 $TCID_{50}$ on day 18, 21 and 28 post cell transplantation (dashed lines). Control animals (mock) were injected with an equal volume of VP-SFM. (**A**) Total luciferase activities over time for each individual mouse are shown as spider plots. (**B**) Quantified luciferase signals on day 46 are shown as logarithm of the total flux (p/sec). Unpaired t test, p=0.07 (ns). VSV-CD30, n=8; mock, n=6. Modified from (Hanauer 2015; Hanauer et al. 2018).

Quantification of the total flux of luciferase intensity over the duration of the experiment demonstrated that VSV-CD30 treatment induced a delayed tumor growth in some mice (Figure 3.22 A). However, comparing the luciferase intensities of VSV-CD30 vs mock treated mice at the endpoint of the experiment, the observed difference narrowly failed to be statistically significant (p=0.07). Still, VSV-CD30 showed oncolytic activity at least in some mice. These results were unexpected compared to the pilot experiment where VSV-CD30 treatment completely eliminated tumor burden. To eliminate inaccuracies, final analysis of KM-H2-luc mice treated with VSV-CD30 involved explantation and imaging of all organs to determine signal origin more precisely.

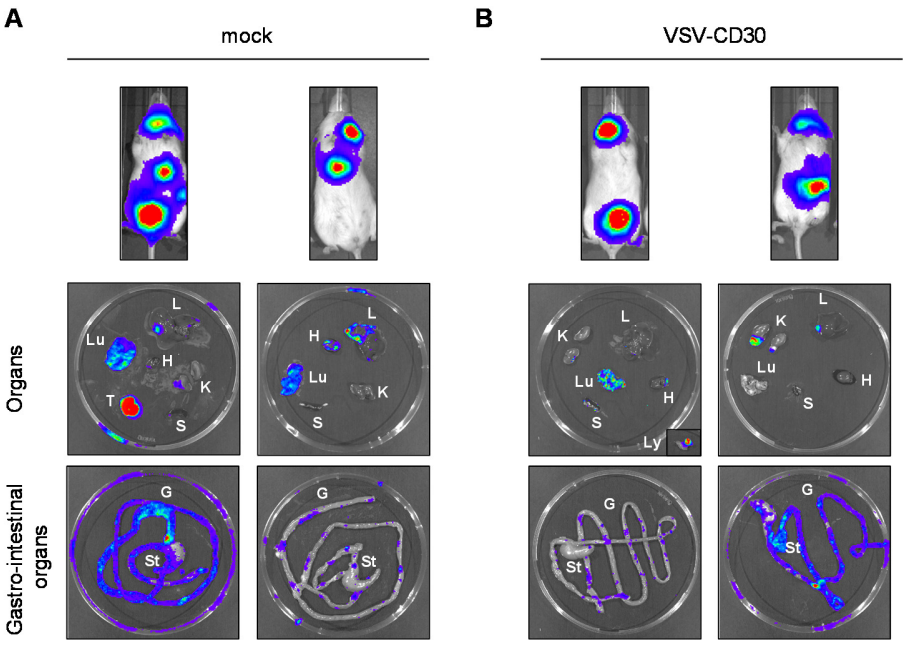

Figure 3.23: Final analysis of KM-H2-luc of mock and VSV-CD30 treated mice

NSG mice were implanted i.v. with 2 x 10^6 KM-H2-luc cells. Mice received three i.v. injections of VSV-CD30 covering a total dose of 3 x 10^8 $TCID_{50}$ on day 18, 21 and 28 post cell implantation. Control animals (mock) were injected with an equal volume of VP-SFM. Luciferase imaging pictures of two treated mice on day 46 dpi with all explanted organs, respectively. (**A**) mock treated mice. (**B**) VSV-CD30 treated mice. Lu: lung, L: liver; H: heart, K: kidney, S: spleen, T: tumor, G: gut, St: stomach.

In the peritoneal cavity of mock treated mouse 1, a large solid tumor nodule was present (Figure 3.23). Additionally, strong luciferase signals were observed in lung and gut. Mock treated mouse 2 mainly showed signals in lung and liver. In contrast, VSV-CD30 treated mouse 1 showed luciferase signals concentrating in the lung again, but also in lymph nodes in the head region. In VSV-CD30 treated mouse 2 KM-H2-luc cells formed a large tumor nodule on one kidney.

To sum up, besides metastasis in different organs, also a large solid tumor structure was found in the peritoneal cavity. Therefore, final luciferase imaging more precisely illustrates the heterogeneous growth of KM-H2-luc tumors in this disseminated tumor model.

To find another explanation for the unexpected results, a competition assay of VSV-CD30 using plasma of KM-H2-luc bearing mice in both treatment groups was performed.

3.4.4 Competition assay of VSV-CD30

For cHL cells a certain amount of CD30 on the cell surface is described as cleaved by metalloproteinases, resulting in the release of soluble CD30 (sCD30) (Josimovic-Alasevic et al. 1989). VSV-CD30 is designed to bind to CD30 with a high affinity through the CD30-scFv targeting domain. If sCD30 is present, as it would be in the plasma of KM-H2-luc bearing mice, the CD30-scFv displayed on VSV-CD30 could potentially be blocked. To analyze if the plasma of KM-H2-luc bearing mice in both treatment groups contained any neutralizing agents for VSV-CD30, a competition assay was performed. In detail, VSV-CD30 was pre-incubated with plasma of tumor bearing mice which were treated either with VSV-CD30 or mock treated. Subsequently, pre-incubated VSV-CD30 was titrated on HT1080-CD30 target cells.

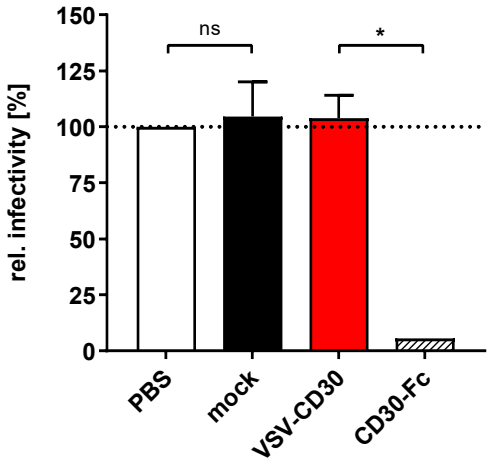

Figure 3.24: Neutralization assay of VSV-CD30 with KM-H2-luc bearing mouse plasma

NSG mice were i.v. implanted with 2 x 10^6 KM-H2-luc cells. Mice received three i.v. injections of VSV-CD30 covering a total dose of 3 x 10^8 $TCID_{50}$ on day 18, 21 and 28 post cell transplantation. Control animals (mock) were injected with an equal volume of VP-SFM. On day 46 (final day), plasma of all treated mice (VSV-CD30, mock) was used for pre-incubation with 1 x 10^6 $TCID_{50}$ VSV-CD30. As positive control for competiton of VSV-CD30, soluble CD30-Fc protein (CD30-Fc) was used, PBS served as negative control. Titration of the pretreated viruses was done on HT1080-CD30 cells. Infectivity [%] is presented as percentage to NSG mouse plasma without KM-H2-luc burden. Unpaired t test, * $p<0.05$, ns $p>0.05$. Error bars: mean ± SD. VSV-CD30, n=8; mock, n=6.

Neither mock nor VSV-CD30 treated KM-H2-luc bearing mouse plasma induced neutralization of VSV-CD30 compared to PBS and CD30-Fc controls (Figure 3.24). This data indicates that there was no blocking agent present in plasma of KM-H2-luc mice.

3.5 Susceptibility of CD30⁺ anaplastic large cell lymphoma cell lines

After successful treatment of cHL xenografts, CD30-targeted viruses were also investigated for their therapeutic potential on another CD30⁺ tumor type. ALCL is a T cell derived NHL characterized by high CD30 expression. Continuous patient-derived cell lines for ALK+ (Karpas 299, SUDHL1) and ALK- (MAC-1) ALCL were used for the subsequent experiments. To start with, expression of CD30 the target receptor on the ALCL cell lines were determined by flow cytometry.

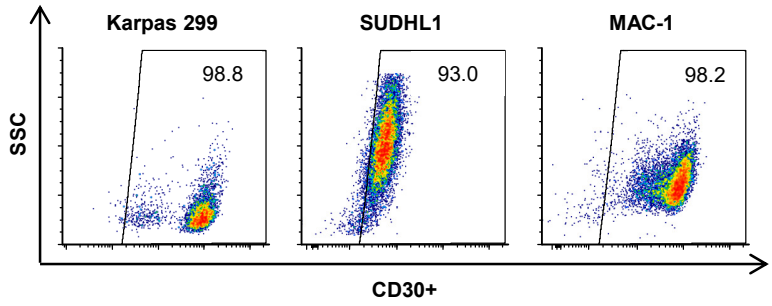

Figure 3.25: CD30 expression in ALCL cell lines

Flow cytometry analysis of human ALCL cell lines Karpas 299, SUDHL1 and MAC-1 for CD30 expression. Cells were stained with a PE-labeled mouse CD30 antibody.

All ALCL cell lines expressed a high amount of CD30 (Figure 3.25). This high expression of the target receptor should result in all cell lines being susceptible for the infection with CD30-targeted viruses. First Karpas299, SUDHL1 and MAC-1 were infected with VSV-CD30.

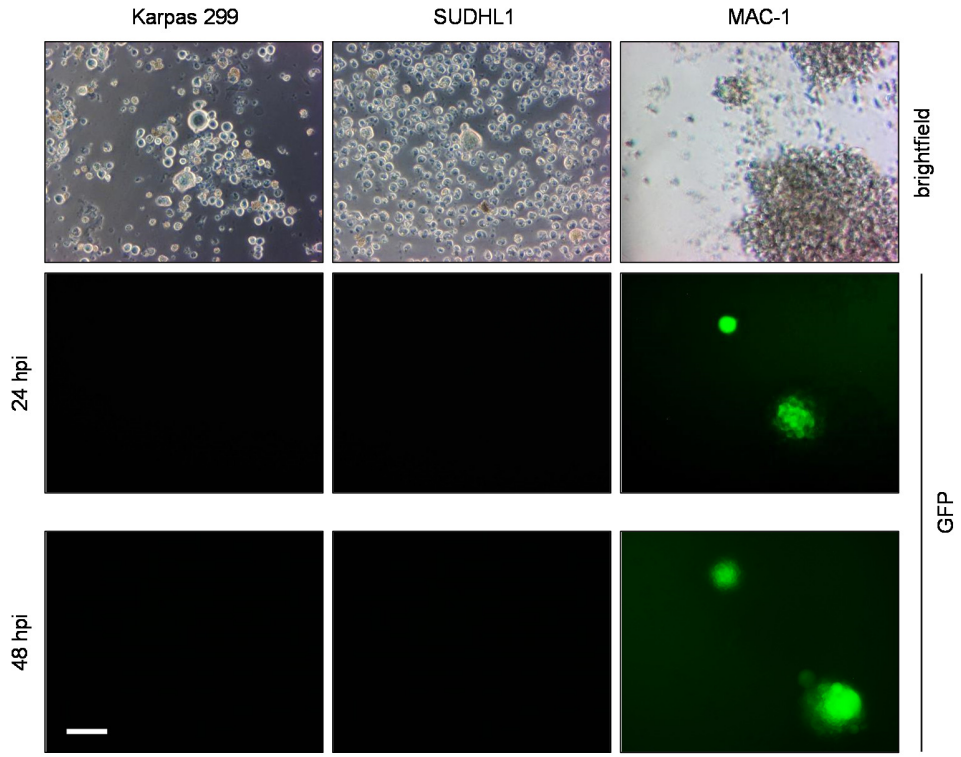

Figure 3.26: VSV-CD30 infection of ALCL cell lines

Human ALCL cell lines Karpas 299, SUDHL-1 and MAC-1 were infected with VSV-CD30 at an MOI of 1 and analyzed by fluorescence microscopy 24 and 48 hours post infection. Scale bar=200 µm.

However, despite the high expression of CD30, Karpas 299 as well as SUDHL1 were not susceptible for VSV-CD30 infection at all (Figure 3.26). Within the MAC-1 cell clusters, two infectious spots were found 24 hpi. However, VSV-CD30 infection seemed not to spread within the culture 48 hpi. Next, Karpas 299 and MAC-1 were infected with MV-CD30.

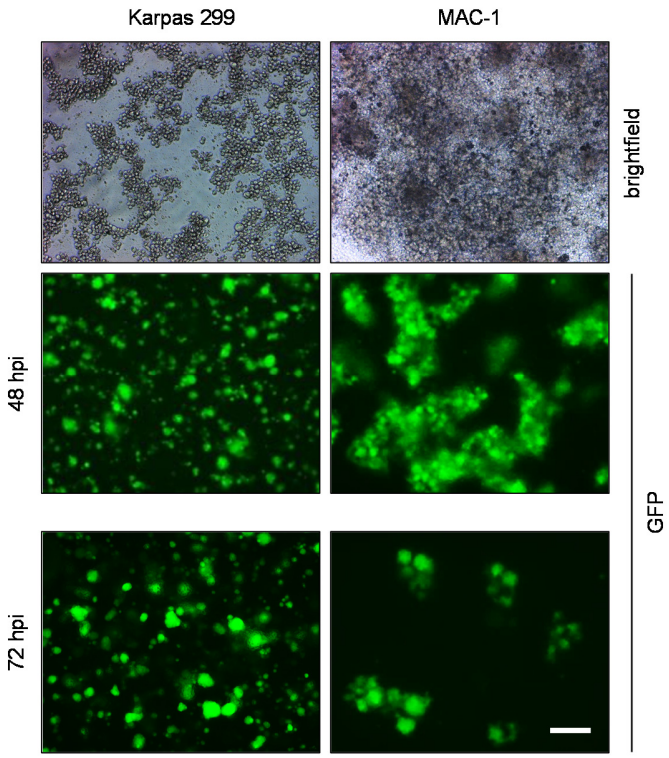

Figure 3.27: MV-CD30 infection of ALCL cell lines

Human ALCL cell lines Karpas 299 and MAC-1 were infected with MV-CD30 at an MOI of 1 and analyzed by fluorescence microscopy 48 and 72 hours post infection, respectively. Scale bar = 200 µm.

Surprisingly, MV-CD30 readily infected both Karpas 299 as well as MAC-1 cells 48 hpi. Infected Karpas 299 cells formed small-sized syncytia, which were still present in the culture 72 hpi. MAC-1 cells showed infectious spots all over the formed clusters 48 hpi, which were also partially still present 72 hpi.

This data demonstrates that cHL cell lines differ from ALCL cell lines in that they seem to be more susceptible for infection with MV-CD30 than with VSV-CD30.

4 Discussion

cHL is a hematopoietic malignancy with a characteristic cellular composition where only 1% of CD30$^+$ tumor cells are embedded in a reactive immune cell infiltrate. Current treatment of cHL patients mainly relies on chemotherapy followed by radiotherapy, while treatment options for relapsed or refractory cHL are still inadequate. Based on the unique histological pattern, immunotherapy based concepts using CD30 as targeting molecule are in focus as new therapy approaches. As part of immunotherapy, oncolytic viruses have an inherent lytic nature and the potential to induce a local inflammation in the tumor microenvironment. CD30-targeted oncolytic viruses could be a powerful new therapy approach for cHL specifically redirected to infect and lyse CD30$^+$ tumor cells.

This thesis depicts the first proof-of-concept study for the therapeutic use of two CD30-targeted oncolytic viruses, MV-CD30 and VSV-CD30, against cHL using preclinical xenograft mouse models. Findings on specificity of MV-CD30 and VSV-CD30, killing capacity *in vitro* and oncolytic activity of CD30-targeted viruses *in vivo* were made. Furthermore, the possibility to expand the system to other CD30$^+$ lymphomas was investigated. This data will support further preclinical testing of VSV-CD30 as a novel therapeutic agent for the treatment of cHL and other CD30$^+$ malignancies.

4.1 CD30 as viral entry receptor

CD30 expression was first discovered in 1982, as Ki-1 antigen found on HRS cells of cHL (Stein et al. 1985). Therefore, CD30 is a characteristic cell surface marker for HRS cells, as well as ALCL and a few NHL (Pierce and Mehta 2017). In this thesis, two oncolytic viruses using CD30 as entry receptor were characterized.

CD30 (also known as TNFRSF8) belongs to the superfamily of tumor necrosis factor (TNF) receptors (Kumar and Younes 2014; Hansen et al. 2016). It is a 120-kDa type I transmembrane protein which encompasses a large elongated extracellular part containing six cysteine-rich pseudo-repeat motifs (Duckett et al. 1997). CD30 is activated by ligand binding of CD30L and leads to trimerization of the receptor, recruitment of signaling proteins and transducing of numerous effects (Horie, R. and Watanabe, T. 1998). CD30 lacks an intrinsic enzymatic domain. Signal transduction is exclusively mediated by several TNF receptor-associated factors (TRAF)-binding domains which are associated with the cytoplasmic domain. Several pathways can be activated including the activation of nuclear

factor kappa-b (NF-κB) and MAP kinases. In contrast to other members of the TNF receptor superfamily, the cytoplasmic domain of CD30 does not contain a death domain. Several pathways including promotion of cell proliferation and cell survival as well as anti-proliferative effects and cell death can be activated depending on cell type and co-stimulatory effects (Schneider and Hübinger 2002).

To use CD30 as viral entry receptor, a CD30-specific scFv was optimized and fused to MV-H. The successful binding of MV-H-α-CD30 to soluble CD30-Fc protein was verified during its optimization (Friedel et al. 2016). This scFv proved to be highly stable and specific in mediating gene delivery by lentiviral vectors pseudotyped with these MV glycoproteins. Specificity of CD30-targeted viruses had been assessed on a panel of transgenic CHO-cells as wells as in a competition assay using soluble CD30-protein before using them for the infection of cHL and ALCL cells lines (Hanauer et al. 2018; Hanauer 2015).

CD30 is not only present on cHL cells but also on activated T lymphocytes upon viral infection or during autoimmune disease (Horie, R. and Watanabe, T. 1998). $CD30^+$ T lymphocytes form a potential off-target population and were therefore investigated for their susceptibility for CD30-targeted viruses. However, in healthy cells, including T lymphocytes, viral infection induces antiviral mechanisms of the innate immune system for example the expression of type I IFN (Katze et al. 2002). In contrast, many tumor cells accumulate defects in the innate immune system to escape the immune response. These defects render them sensitive towards infection especially with RNA viruses (Stojdl et al. 2003). Indeed, T lymphocytes were completely protected from infection with VSV-CD30 and VSV-MV despite the presence of CD30 on the cell surface and cultivation for several days. Only MV_{Nse} infected a few $CD30^+$ cells (Figure 3.7, Figure 3.8). Infection of activated T lymphocytes by MV_{NSe} was not unexpected. Wildtype MV as well as attenuated MV variants have a natural tropism for monocytic and lymphoid cells. Infection of activated T lymphocytes is based on the expression of SLAM as entry receptor which allows the first systemic spread of MV (Tatsuo et al. 2000; Schneider-Schaulies et al. 2001). Thus, CD30 targeting does not extend the tropism of VSV or MV to T lymphocytes.

In this study, two different cHL cell lines covering two different patient cases, as well as three different ALCL cell lines were examined for the infection with CD30-targeted viruses. All cell lines

expressed a high amount of CD30, which rendered them susceptible for the infection. Both cHL cell lines tested L-428 and KM-H2 were equally susceptible for the infection with MV-CD30 and VSV-CD30 *in vitro* (Figure 3.4). VSV-CD30 induced cell killing of both cHL cell lines (Figure 3.5).

However, KM-H2 turned out to be more sensitive for oncolysis mediated by the infection with VSV-CD30 than L-428 *in vivo* (Figure 3.9, Figure 3.10). The classification of these two cHL types is probably not the reason for the different oncolytic effect observed in this study. L-428 belongs to the NSHL type while KM-H2 belongs to the MCHL type. However, the difference between both cHL types is mainly defined by histo-pathological conditions, while little is known about the molecular differences. It is more likely that characteristics of the tumor mouse model used here influenced the result of oncolytic activity of VSV-CD30. First, the tumor growth kinetic could influence the oncolytic activity of VSV-CD30. Growth of s.c. KM-H2 tumors was slower than growth of s.c. L-428 tumors. A slower growing tumor could provide higher accessibility for an oncolytic virus than a faster growing one, because viral particle spread could be higher and reach all tumor sides. Second, the kinetic of oncolysis in both cell lines could influence the oncolytic activity of VSV-CD30. *In vitro*, viability of L-428 cells infected with VSV-CD30 was reduced faster than viability of KM-H2 cells infected with VSV-CD30. Faster oncolysis of L-428 may not be beneficial in a tumor mouse model. Initially infected cells would die too fast before they could release new viral particles to infect neighboring cells. In conclusion, slower oncolysis of KM-H2 cells may lead to a higher spread of VSV into the tumor tissue. CD30-targeted viruses encode for GFP as model transgene to follow up the infection process. To further optimize the therapeutic use of both viruses, therapeutic transgenes could be encoded in the viral genome. Expression of transgenes could benefit from a slower oncolysis in KM-H2 cells.

Using the suitable tumor mouse model, there was no evidence for any impairment of the oncolytic activity by IFN suggesting that cHL may be compatible with VSV-mediated oncolytic activity. VSV-CD30 was highly active and prevented outgrowth of s.c. injected cHL cells after local as well as systemic application (Figure 3.16, Figure 3.18). In the tumor mouse model where cHL cells grew disseminated, a substantial reduction in tumor growth was observed at least for some mice (Figure 3.22).

In contrast, ALCL cell lines were not susceptible for the infection with VSV-CD30, but for the infection with MV-CD30 (Figure 3.26, Figure 3.27). Most likely, ALCL cell lines tested here expressed a higher amount of type I IFN and therefore especially VSV-CD30 cannot infect those cells.

An interesting aspect of using CD30 as viral entry receptor is, that CD30 present on the surface of HRS cells is cleaved by metalloproteinases resulting in sCD30 (Josimovic-Alasevic et al. 1989). Consequently, high serum levels of CD30 are used as diagnostic marker for cHL, ALCL and DLBCL (Schneider and Hübinger 2002). Interestingly, despite the release of sCD30, cHL tumor cells also release CD30 on extracellular vesicles (CD30-EV) for tumor-supporting communication with $CD30L^+$ neighboring bystander cells (Hansen et al. 2014). sCD30 as well as CD30-EV both could potentially bind via the CD30-scFv to CD30-targeted viruses used in this thesis. In theory, this binding could lead to competition for CD30 binding sites and therefore reduce productive infection. For KM-H2 cells used in this thesis, the release of sCD30 and CD30-EV into cell culture supernatant as well as into a Matrigel microenvironment is described in literature (Hansen et al. 2016). The plasma from NSG mice carrying a disseminated KM-H2 tumor was analyzed for the extend of any neutralizing effect on VSV-CD30. No competition of VSV-CD30 pre-incubated with NSG plasma was observed, while recombinant soluble CD30-Fc protein completely blocked infection (Figure 3.24). This could indicate that sCD30 was not present or concentrated highly enough to completely block VSV-CD30 infection. However, presence and amount of sCD30 in NSG mice plasma were not quantified here.

Nevertheless, the presence of sCD30 is only one possible explanation for the partial response to VSV-CD30 treatment observed in the KM-H2 multifocal tumor model. Based on the heterogeneous tumor growth pattern, some tumor niches could be better accessible than others for the infection with VSV-CD30. Furthermore, tumor cells could down regulate CD30 on their cell surface rather than releasing it as sCD30. When no CD30 is present as entry receptor, VSV-CD30 cannot infect cHL cells. Further analysis is needed to gain closer insights into the partial response of VSV-CD30 in this tumor mouse model.

Apart from potential competition between sCD30 with VSV-CD30 for CD30 binding, Hansen el al. demonstrated, that CD30-EV positively contributed to the clinical efficacy of brentuximab vedotin (Hansen et al. 2016). They showed that brentuximab vedotin binds to CD30-EV and is then transported to the $CD30L^+$, but $CD30^-$ surrounding bystander cells in the tumor microenvironment,

where it is internalized and becomes cytotoxically active. Accordingly it can be speculated that the CD30 targeted viruses investigated in this thesis, were transported via CD30-EV to CD30L$^+$ bystander cells as well. The potential infection and killing of bystander cells is another interesting issue for further investigation.

4.2 Increasing oncoselectivity of VSV

To use VSV as an oncolytic virus, modifications of the virus to increase oncoselectivity and decrease neurotoxicity need to be made. Neurotoxicity is mainly associated with the VSV-G glycoprotein (Martinez et al. 2003; Clarke et al. 2007; Cooper et al. 2008). Therefore, pseudotyping VSV with heterologous glycoproteins and an additional layer of tumor-targeting could prevent neurotoxicity (Miest and Cattaneo 2014; Muik et al. 2014).

For this purpose, a VSV-MV pseudotype was recently generated and used as background for VSV-CD30 analyzed in this thesis (Ayala-Breton et al. 2013). This first VSV-MV chimera did not contain an additional layer of tumor targeting. Since MV glycoproteins were inserted, MV-H protein could easily be used to retarget VSV-MV to tumor-associated antigens using the well-established MV retargeting concept. During the work on this thesis two examples of fully targeted VSV were published.

In mid of 2015, Ayala Breton and colleagues described the first example of a fully replication-competent, receptor targeted VSV. They generated a VSV-MV chimera retargeted to the Her2/neu receptor by displaying a scFv on MV-H. To analyze the effect of scFv affinity to its target, they rescued a panel of six VSV-Her2/neu viruses displaying Her2/neu-scFv that bind to the same Her2 epitope but with different K_d values. They found, that a least a K_d of 10^{-8} M was required for the infection of Her2/neu$^+$ tumor cells. All high affinity viruses with a K_d of $>10^{-8}$ M were able to infect Her2/neu$^+$ tumor cells and induced syncytia formation. In a s.c. tumor model of ovarian cancer, all high affinity viruses induced tumor shrinkage with no significant difference between them (Ayala Breton et al. 2015). The findings made there for the affinity threshold could suggest a high oncolytic effect for VSV-CD30 analyzed in this thesis, since its K_d value was determined to be 3.75×10^{-9} M (Friedel et al. 2015).

In 2017, parts of this thesis contributed to the generation of VSV-CD133 as a second example of a fully replication-competent, receptor targeted VSV (Kleinlützum et al. 2017). The chimeric VSV-CD133 was generated as part of enhancing the oncolytic activity of the previously described MV-CD133 against tumor stem cells (Bach et al. 2013). Different MV-CD133 variants were generated using arming techniques (MV^{SCD}-CD133), receptor extension (MV-CD46/CD133) and the chimera between MV-CD133 and VSV (VSV-CD133). To first verify safety of the newly generated viruses, $CD133^+$ hematopoietic stem cells were infected. No productive infection of hematopoietic stem cells was observed, again most likely due to the high sensitivity of VSV against IFN. This is in line with observations made in this thesis regarding the infection of $CD30^+$ activated T lymphocytes which were completely protected from infection. Oncolytic activity of the CD133-retargeted viruses was analyzed on a $CD133^+$ hepatocellular carcinoma cell line *in vitro*. VSV-CD133 showed highest tumor cell killing within 48 hpi. In a s.c. tumor model of hepatocellular cancer, VSV-CD133 exhibited the strongest oncolytic activity and significantly prolonged survival of tumor bearing mice without any signs of neurotoxicity when administered intratumorally or intravenously. The data shown for the oncolytic activity of VSV-CD133 *in vitro* and in the s.c. tumor model of hepatocellular cancer are in line with the data shown for VSV-CD30 here in this thesis. For both retargeted VSV the antitumoral effect was more pronounced compared to retargeted MV *in vitro* and *in vivo*. In contrast, i.t. application of VSV-CD30 in cHL xenografts initially eliminated the tumor in two mice completely while VSV-CD133 only induced delayed tumor growth in hepatocellular xenografts. Differences observed could be based on technical reasons. Application of VSV-CD133 was started when tumors already reached a size of 100 mm^3 while in this thesis the injections started at a size of 50 mm^3. In addition, VSV-CD133 was only applied at a low dose of 4×10^6 $TCID_{50}$ in total, while VSV-CD30 demonstrated here exhibited the best antitumoral effect at a high dose of 3×10^8 $TCID_{50}$ in total. Furthermore, in none of the experiments the expression of target receptors was verified. Tumor resistance based on decreased amounts of target receptors could therefore also explain the differences observed here.

To demonstrate the susceptibility of another $CD133^+$ tumor type, primary glioma cells were infected with CD133-retargeted viruses. All viruses infected glioma tumor spheres and induced syncytia formation. However, 2-3 days after infection with VSV-CD133 tumor spheres started expanding again. Only MV-derived but not VSV-MV derived viruses were able to induce a continuous decrease in cell number. Since glioma spheres contained more than 90% $CD133^+$ cells and VSV-MV did not

infect these cells, both aspects could be excluded. Therefore the hypothesis was made that cells became resistant through post-entry mechanisms e.g. an intact type I IFN response. Most cancer cell lines are described to have a deregulated IFN pathway. However there are many which have partial or complete intact IFN response (Stojdl et al. 2003; Dold et al. 2016). This has to be evaluated before using these cell lines for the treatment with oncolytic VSV. In an orthotopic glioma model using the same glioma tumor spheres, MV-CD46/CD133 and MV^{SCD}-CD133 were most effective to clear tumor burden. Notably, VSV-CD133 caused fatal neurotoxicity in this tumor model, while the use of CD133 as receptor was excluded as being causative. This was surprising and somehow contradictory to the description of VSV-MV in 2013 (Ayala-Breton et al. 2013). There, VSV-MV was described to be highly attenuated to neurotoxicity due to the deletion of VSV-G. Similar findings were made when VSV was pseudotyped with glycoproteins from LCMV, which reduced neurotoxicity (Muik et al. 2011). As a conclusion, different virus types were identified as best treatment option for each tumor type. This data demonstrates that besides the rational tendency for VSV to be oncolytically more effective than MV, this cannot be generalized and has to be separately evaluated for each type of tumor.

VSV-CD30 is now the third example of a receptor targeted VSV. Most importantly, in none of the *in vivo* tumor models investigated, including a multifocal growing tumor model for the first time, signs of neurotoxicity were observed. Severe symptoms of neurotoxicity by VSV-CD133 infection was only observed when applied directly into the brain. In the s.c. hepatocellular model, VSV-CD133 proved to be safe after i.t. as well as i.v. application. However, if VSV-CD30 is inducing neurotoxicity when administered directly into the brain, needs to be considered in further safety studies before envisaging clinical studies.

When using MV derived oncolytic viruses, the presence of neutralizing antibodies in MV vaccinated individuals is a major issue. Since VSV-MV is pseudotyped with MV glycoproteins, it likely would get neutralized too. There are multiple technologies to bypass the neutralization of MV or MV pseudotyped oncolytic viruses and increase serum stability after systemic application. One strategy describes the exchange of the surface proteins of MV since the immune neutralization is mainly associated with the glycoproteins. The glycoproteins from other paramyxoviruses like those of tupaia paramyxvirus (Miest et al. 2011; Hudacek et al. 2013) or Nipah virus are ideal candidates.

Glycoproteins from both viruses have a similar structure to those of MV in terms of separating fusion activity and receptor binding activity in two glycoproteins. Receptor binding proteins of both alternative paramyxoviruses allow the modification by inserting point mutations and fusion of a targeting ligand. In addition, glycoproteins from both viruses were recently tested for pseudotyping of lentiviral vector particles. They mediated specific gene transfer upon blinding of natural binding sites and fusion of a targeting ligand (Enkirch et al. 2013; Bender et al. 2016). Biological shielding of viral particles is another strategy to prevent neutralization. *Ex vivo* infected T lymphocytes (Ong et al. 2007) or mesenchymal stem cells (Mader et al. 2009; Mader et al. 2013) can be used as cell-based carriers in a "trojan horse" approach.

4.3 Therapeutic application of receptor targeted oncolytic viruses

With Imlygic, oncolytic viruses have reached marketing authorization while work on this thesis was ongoing. Authorized for the treatment of advanced melanoma patients, Imlygic is derived from the HSV-1 strain (Pol et al. 2016). Two genes for neurovirulence were inactivated to enhance the safety profile. Finally one cassette encoding GM-CSF was inserted to recruit and activate antigen-presenting cells (Liu et al. 2003). However, in a phase III clinical trial the local injection in metastatic melanoma lesions improved the durable response rate only to 16% compared to sc. injected GM-CSF alone (Andtbacka et al. 2015). Still the administration of Imlygic showed only mild adverse events like fatigue, chills, and pyrexia. In general, OVs are multi-mechanistic therapeutics. They can be considered as mono- or combination-therapy. Especially, combination with checkpoint inhibitors seems very promising.

In a phase 1 clinical trial, the combination of Imlygic with the checkpoint inhibitor ipilimumab, which blocks the cytotoxic T lymphocyte associated antigen 4 (CTLA-4) improved the response rate from 18% (alone) to 39% (combination) (Chesney et al. 2016; Puzanov et al. 2016). In another phase 1b trial, Imlygic was applied locally in combination with i.v. injected pembrolizumab, which blocks PD-1 on T lymphocytes achieving a complete response rate of 33% (Ribas et al. 2017). Intratumoral injection of Imlygic as an *in situ* vaccine attracted immune cells and therefore changed the tumor microenvironment in the injected lesions and increased T lymphocyte infiltration to turn it from "cold to hot" (Ribas et al. 2017). Both studies demonstrate that the oncolytic capacity of Imlygic can be boosted in combination with an immune checkpoint inhibitor. Besides Imlygic a chimeric

adenovirus (Enadenotucirev) in combination with pembrolizumab (ClinicalTrials.gov Identifier: NCT02636036) and a reovirus in combination with α-PD-1 (ClinicalTrials.gov Identifier: NCT02620423) are tested in phase I clinical trials (Breitbach et al. 2016).

Other approaches to use oncolytic virotherapy as combination therapy is the combination with JAK/STAT inhibitors (Dold et al. 2016) or CAR (chimeric antigen receptor) T cells (Ajina and Maher 2017). Both strategies benefit from changed tumor microenvironment induced by oncolysis.

Oncolytic VSV-IFNβ-NIS is currently tested in different clinical trials. Interestingly, VSV-IFNβ-NIS is tested in a phase 1 study for treating patients with relapsed or refractory multiple myeloma, acute myeloid leukemia, or T cell lymphoma (ClinicalTrials.gov Identifier: NCT03017820). T cell lymphomas also include recurrent anaplastic large cell lymphoma. Therefore, VSV seems to have a natural preference for this tumor entity which was also analyzed in this thesis. In a two-part open label phase 1/2 study VSV-IFNβ-NIS is tested in treating patients with refractory solid tumors as i.t. administration in combination with the PD-L1 blocking agent avelumab (ClinicalTrials.gov Identifier: NCT02923466). This demonstrates that the oncolytic power of VSV can be boosted in combination with immune checkpoint inhibitors as well.

All oncolytic viruses tested in clinical trials are non-receptor targeted viruses. Instead, most of them encode immune stimulatory transgenes. However, a variety of receptor targeted oncolytic viruses have been described as promising tools in cancer immunotherapy during the last decades in preclinical studies. Up to now, there is no clinical translation of receptor targeted oncolytic viruses. Initially, receptor targeting of oncolytic viruses was designed to increase the safety profile. However, Imlygic as the first oncolytic virus receiving marketing authorization was not designed to contain an additional layer of receptor targeting. It was tested to be safe and induced only mild adverse events. Currently, the need to improve safety based on restricting cell entry of oncolytic viruses is not a main focus of research. Most oncolytic viruses are oncoselective *per se* because of their natural tumor tropism. There is no additional benefit to include a secondary layer of selectivity. In fact, quite the contrary could result from receptor targeting. Tumors are highly heterogeneous and constantly evolving (Alexandrov et al. 2013). Therefore tumors can develop resistance against targeted therapies based on down regulation of the target receptor. Tumor cells that do no longer express the entry receptor cannot be infected any more. Besides local oncolysis a systemic

activation of the immune system is needed. Using a receptor targeted OV could potentially decrease the attraction of the immune system.

However, in some cases, receptor targeted oncolytic viruses could be beneficial. For the treatment of disseminated cancers and metastasis only a systemic application can theoretically reach all tumor sites. Attempts at systemic delivery have shown limited success until now since the administered virus is immediately diluted in the circulating blood volume (Maroun et al. 2017). As consequence, extremely high doses are needed to achieve circulating titers. Here, the usage of receptor targeted viruses could be beneficial allowing for the administration of higher tumor destructive doses without toxicity to normal tissues.

In a tumor mass where only few tumor cells are embedded in a changing immune cell infiltrate, potentially blocking accessibility, a receptor targeted OV could also be beneficial. Especially for cHL a CD30-targeted therapy approach using oncolytic viruses could be a new therapy approach to investigate. The targeting capacity of engineered MV glycoproteins was demonstrated on pseudotyped lentiviral vectors specific for CD105. CD105-LV discriminated between target cells and lymphocytes and selectively transduced $CD105^+$ endothelial target cells in mixed cultures (Anliker et al. 2010).

Particularly using VSV as a receptor targeted oncolytic virus has several advantages. In general *Rhabdoviridae* show a high safety profile, can be produced to high titers and can infect tumor vasculature (Breitbach et al. 2011). VSV-CD30 which was characterized in this thesis showed a high replication capacity, strong lytic properties and was able to reach disseminated tumor sides. Until now, manufacturing resulting in the production of low titers is one major limitation for a broad clinical application of many OVs. In the clinical trial analyzing MV-NIS 100 ml of virus suspension was infused into the patients to achieve a dose of 10^{11} $TCID_{50}$ (Russell et al. 2014). In contrast, VSV-CD30 can be produced to higher titers out of supernatant of infected cells, representing a suitable virus stock for clinical trials.

Based on the proof-of-concept study in this thesis, VSV-CD30 could also be equipped with immune stimulatory transgenes to further enhance its oncolytic capacity. Combining VSV-CD30 with other cancer therapeutics such as immune checkpoint inhibitors or CAR T cells could be another future option to be explored.

5 References

Ahmed, M.; McKenzie, M. O.; Puckett, S.; Hojnacki, M.; Poliquin, L.; Lyles, D.S. (2003): Ability of the matrix protein of vesicular stomatitis virus to suppress beta interferon gene expression is genetically correlated with the inhibition of host RNA and protein synthesis. *J Virol* 77 (8), 4646–4657. DOI: 10.1128/JVI.77.8.4646-4657.2003.

Ajina, A.; Maher, J. (2017): Prospects for combined use of oncolytic viruses and CAR T-cells. *J Immunother Cancer* 5 (1), 90. DOI: 10.1186/s40425-017-0294-6.

Alexandrov, L. B.; Nik-Zainal, S.; Wedge, D. C.; Aparicio, S. A.; Behjati, S.; Biankin, A. V. et al. (2013): Signatures of mutational processes in human cancer. *Nature* 500 (7463), 415–421. DOI: 10.1038/nature12477.

Ammayappan, A.; Peng, K.-W.; Russell, S. J. (2013): Characteristics of Oncolytic Vesicular Stomatitis Virus Displaying Tumor-Targeting Ligands. *J Virol* 87 (24), 13543–13555. DOI: 10.1128/JVI.02240-13.

Andtbacka, R. H.; Kaufman, H. L.; Collichio, F.; Amatruda, T.; Senzer, N.; Chesney, J. et al. (2015): Talimogene Laherparepvec Improves Durable Response Rate in Patients With Advanced Melanoma. *J Clin Oncol* 33 (25), 2780–2788. DOI: 10.1200/JCO.2014.58.3377.

Anliker, B.; Abel, T.; Kneissl, S.; Hlavaty, J.; Caputi, A.; Brynza, J. et al. (2010): Specific gene transfer to neurons, endothelial cells and hematopoietic progenitors with lentiviral vectors. *Nat Methods* 7 (11), 929–935. DOI: 10.1038/nmeth.1514.

Aref, S.; Bailey, K.; Fielding, A. (2016): Measles to the Rescue: A Review of Oncolytic Measles Virus. *Viruses* 8 (10), E294. DOI: 10.3390/v8100294.

Armitage, J. O.; Gascoyne, R. D.; Lunning, M. A.; Cavalli, F. (2017): Non-Hodgkin lymphoma. *Lancet* 390 (10091), 298–310. DOI: 10.1016/S0140-6736(16)32407-2.

Ayala Breton, C.; Wikan, N. Abbuhl, A.; Smith, D. R.; Russell, S. J.; Peng, K.-W. (2015): Oncolytic potency of HER-2 retargeted VSV-FH hybrid viruses: The role of receptor ligand affinity. *Mol Ther Oncolytics* 2, 15012. DOI: 10.1038/mto.2015.12.

Ayala-Breton, C.; Barber, G. N.; Russell, S. J.; Peng, K.-W. (2012): Retargeting vesicular stomatitis virus using measles virus envelope glycoproteins. *Hum Gene Ther* 23 (5), 484–491. DOI: 10.1089/hum.2011.146.

Ayala-Breton, C.; Russell, L.O.J; Russell, S.J.; Peng, K.-W. (2014): Faster replication and higher expression levels of viral glycoproteins give the vesicular stomatitis virus/measles virus hybrid VSV-FH a growth advantage over measles virus. *J Virol* 88 (15), 8332–8339. DOI: 10.1128/JVI.03823-13.

Ayala-Breton, C.; Suksanpaisan, L.; Mader, E. K.; Russell, S. J.; Peng, K.-W. (2013): Amalgamating oncolytic viruses to enhance their safety, consolidate their killing mechanisms, and accelerate their spread. *Mol Ther* 21 (10), 1930–1937. DOI: 10.1038/mt.2013.164.

Bach, P.; Abel, T.; Hoffmann, C.; Gal, Z.; Braun, G.; Voelker, I. et al. (2013): Specific elimination of CD133+ tumor cells with targeted oncolytic measles virus. *Cancer Res* 73 (2), 865–874. DOI: 10.1158/0008-5472.CAN-12-2221.

Ball, L. A.; White, C. N. (1976): Order of transcription of genes of vesicular stomatitis virus. *Proc Natl Acad Sci USA* 73 (2), 442–446.

Bankamp, B.; Takeda, M.; Zhang, Y.; Xu, W.; Rota, P. A. (2011): Genetic characterization of measles vaccine strains. *J Infect Dis* 204 (Suppl 1), S533-S548. DOI: 10.1093/infdis/jir097.

Barr, J. N.; Whelan, S. P.; Wertz, G. W. (2002): Transcriptional control of the RNA-dependent RNA polymerase of vesicular stomatitis virus. *Biochim Biophys Acta* 1577 (2), 337–353. DOI: 10.1016/S0167-4781(02)00462-1.

Bender, R. R.; Muth, A.; Schneider, I. C.; Friedel, T.; Hartmann, J.; Plückthun, A. et al. (2016): Receptor-Targeted Nipah Virus Glycoproteins Improve Cell-Type Selective Gene Delivery and Reveal a Preference for Membrane-Proximal Cell Attachment. *PLoS Pathog* 12 (6), e1005641. DOI: 10.1371/journal.ppat.1005641.

Berchtold, S.; Lampe, J.; Weiland, T.; Smirnow, I.; Schleicher, S.; Handgretinger, R. et al. (2013): Innate immune defense defines susceptibility of sarcoma cells to measles vaccine virus-based oncolysis. *J Virol* 87 (6), 3484–3501. DOI: 10.1128/JVI.02106-12.

Bishnoi, S.; Tiwari, R.; Gupta, S.; Byrareddy, S.N.; Nayak, D. (2018): Oncotargeting by Vesicular Stomatitis Virus (VSV). Advances in Cancer Therapy. *Viruses* 10 (2), 90. DOI: 10.3390/v10020090.

Blank, O.; Tresckow, B. von; Monsef, I.; Specht, L.; Engert, A.; Skoetz, N. (2017): Chemotherapy alone versus chemotherapy plus radiotherapy for adults with early stage Hodgkin lymphoma. *Cochrane Database Syst Rev*, CD007110. DOI: 10.1002/14651858.CD007110.pub3.

Breitbach, C. J.; Lichty, B. D.; Bell, J. C. (2016): Oncolytic Viruses: Therapeutics With an Identity Crisis. *EBioMedicine* 9, 31–36. DOI: 10.1016/j.ebiom.2016.06.046.

Breitbach, C. J.; Silva, N. S. de; Falls, T. J.; Aladl, U.; Evgin, L.; Paterson, J. et al. (2011): Targeting tumor vasculature with an oncolytic virus. *Mol Ther* 19 (5), 886–894. DOI: 10.1038/mt.2011.26.

Calain, P.; Roux, L. (1993): The rule of six, a basic feature for efficient replication of Sendai virus defective interfering RNA. *J Virol* 67 (8), 4822–4830.

Cattaneo, R.; Rebmann, G: Schmid, A: Baczko, K; Meulen, V. ter; Billeter, M. A. (1987): Altered transcription of a defective measles virus genome derived from a diseased human brain. *EMBO J* (6), 681–688.

Chen, R.; Gopal, A. K.; Smith, S. E.; Ansell, S. M.; Rosenblatt, J. D.; Savage, K. J. et al. (2016): Five-year survival and durability results of brentuximab vedotin in patients with relapsed or refractory Hodgkin lymphoma. *Blood* 128 (12), 1562–1566. DOI: 10.1182/blood-2016-02-699850.

Chesney, J.; Collichio, F.; Andtbacka, R.H.I.; Puzanov, I.; Glaspy, J.; Milhem, M. et al. (2016): Interim safety and efficacy of a randomized (1:1), open-label phase 2 study of talimogene laherparepvec (T) and ipilimumab (I) vs I alone in unresected, stage IIIB-IV melanoma. *Annals of Oncology* 27 (Suppl_6), 1108PD. DOI: 10.1093/annonc/mdw379.04.

Clarke, D. K.; Nasar, F.; Lee, M.; Johnson, J. E; Wright, K.; Calderon, P. et al. (2007): Synergistic attenuation of vesicular stomatitis virus by combination of specific G gene truncations and N gene translocations. *J Virol* 81 (4), 2056–2064. DOI: 10.1128/JVI.01911-06.

Cooper, D.; Wright, K. J.; Calderon, P. C.; Guo, M.; Nasar, F.; Johnson, J. E. et al. (2008): Attenuation of recombinant vesicular stomatitis virus-human immunodeficiency virus type 1 vaccine vectors by gene translocations and g gene truncation reduces neurovirulence and enhances immunogenicity in mice. *J Virol* 82 (1), 207–219. DOI: 10.1128/JVI.01515-07.

Devaux, P.; Messling, V. von; Songsungthong, W.; Springfeld, C.; Cattaneo, R. (2007): Tyrosine 110 in the measles virus phosphoprotein is required to block STAT1 phosphorylation. *Virology* 360 (1), 72–83. DOI: 10.1016/j.virol.2006.09.049.

Dold, C.; Rodriguez Urbiola, C.; Wollmann, G.; Egerer, L.; Muik, A.; Bellmann, L. et al. (2016): Application of interferon modulators to overcome partial resistance of human ovarian cancers to VSV-GP oncolytic viral therapy. *Mol Ther Oncolytics* 3, 16021. DOI: 10.1038/mto.2016.21.

Dörig, R. E.; Marcil, A.; Chopra, A.; Richardson, C. D. (1993): The human CD46 molecule is a receptor for measles virus (Edmonston strain). *Cell* 75 (2), 295–305. DOI: 10.1016/0092-8674(93)80071-L.

Duan, F.; Simeone, S.; Wu, R.; Grady, J.; Mandoiu, I.; Srivastava, P. K. (2012): Area under the curve as a tool to measure kinetics of tumor growth in experimental animals. *J Immunol Methods* 382 (1-2), 224–228. DOI: 10.1016/j.jim.2012.06.005.

Duckett, C. S.; Gedrich, R. W.; Gilfillan, M. C.; Thompson, C. B. (1997): Induction of nuclear factor kappaB by the CD30 receptor is mediated by TRAF1 and TRAF2. *Mol Cell Biol* 17 (3), 1535–1542. DOI: 10.1128/MCB.17.3.1535.

Duprex, W. P.; McQuaid, S.; Hangartner, L.; Billeter, M. A.; Rima, B. K. (1999): Observation of measles virus cell-to-cell spread in astrocytoma cells by using a green fluorescent protein-expressing recombinant virus. *J Virol* 73 (11), 9568–9575.

Edge, R. E.; Falls, T. J.; Brown, C. W.; Lichty, B. D.; Atkins, H.; Bell, J. C. (2008): A let-7 MicroRNA-sensitive vesicular stomatitis virus demonstrates tumor-specific replication. *Mol Ther* 16 (8), 1437–1443. DOI: 10.1038/mt.2008.130.

Emerson, S. U. (1982): Reconstitution studies detect a single polymerase entry site on the vesicular stomatitis virus genome. *Cell* 31 (3 Part 2), 635–642. DOI: 10.1016/0092-8674(82)90319-1.

Enders, J. F.; Peebles, T. C. (1954): Propagation in tissue cultures of cytopathogenic agents from patients with measles. *Proc Soc Exp Biol Med* 86 (2), 277–286.

Enkirch, T.; Kneissl, S.; Hoyler, B.; Ungerechts, G.; Stremmel, W.; Buchholz, C. J.; Springfeld, C. (2013): Targeted lentiviral vectors pseudotyped with the Tupaia paramyxovirus glycoproteins. *Gene Ther* 20 (1), 16–23. DOI: 10.1038/gt.2011.209.

Ferreri, A. J.; Govi, S.; Pileri, S. A.; Savage, K. J. (2012): Anaplastic large cell lymphoma, ALK-positive. *Crit Rev Oncol Hematol* 83 (2), 293–302. DOI: 10.1016/j.critrevonc.2012.02.005

Ferreri, A. J.; Govi, S.; Pileri, S. A.; Savage, K. J. (2013): Anaplastic large cell lymphoma, ALK-negative. *Crit Rev Oncol Hematol* 85 (2), 206–215. DOI: 10.1016/j.critrevonc.2012.06.004

Fishelson, Z.; Donin, N.; Zell, S.; Schultz, S.; Kirschfink, M. (2003): Obstacles to cancer immunotherapy. Expression of membrane complement regulatory proteins (mCRPs) in tumors. *Mol Immunol* 40 (2-4), 109–123. DOI: 10.1016/S0161-5890(03)00112-3.

Friedel, T.; Hanisch, L. J.; Muth, A.; Honegger, A.; Abken, H.; Plückthun, A. et al. (2015): Receptor-targeted lentiviral vectors are exceptionally sensitive toward the biophysical properties of the displayed single-chain Fv. *Protein Eng Des Sel* 28 (4), 93–106. DOI: 10.1093/protein/gzv005.

Friedel, T.; Jung-Klawitter, S.; Sebe, A.; Schenk, F.; Modlich, U.; Ivics, Z. et al. (2016): CD30 Receptor-Targeted Lentiviral Vectors for Human Induced Pluripotent Stem Cell-Specific Gene Modification. *Stem Cells Dev* 25 (9), 729-739. DOI: 10.1089/scd.2015.0386.

Friedrich, K.; Hanauer, J. R. H.; Prüfer, S.; Münch, R. C.; Völker, I.; Filippis, C. et al. (2013): DARPin-targeting of measles virus: unique bispecificity, effective oncolysis, and enhanced safety. *Mol Ther* 21 (4), 849–859. DOI: 10.1038/mt.2013.16

Galanis, E. (2010): Therapeutic Potential of Oncolytic Measles Virus: Promises and Challenges. *Clin Pharmacol Ther* 88 (5), 620–625. DOI: 10.1038/clpt.2010.211.

Galanis, E.; Bateman, A.; Johnson, K.; Diaz, R. M.; James, C. D.; Vile, R.; Russell, S. J. (2001): Use of viral fusogenic membrane glycoproteins as novel therapeutic transgenes in gliomas. *Hum Gene Ther* 12 (7), 811–821. DOI: 10.1089/104303401750148766.

Gao, Y.; Whitaker-Dowling, P.; Watkins, S. C.; Griffin, J. A.; Bergman, I. (2006): Rapid adaptation of a recombinant vesicular stomatitis virus to a targeted cell line. *J Virol* 80 (17), 8603–8612. DOI: 10.1128/JVI.00142-06.

Guo, Z. S.; Liu, Z.; Kowalsky, S.; Feist, M.; Kalinski, P.; Lu, B. et al. (2017): Oncolytic Immunotherapy: Conceptual Evolution, Current Strategies, and Future Perspectives. *Front Immunol* 8, 555. DOI: 10.3389/fimmu.2017.00555.

Hallak, L. K.; Merchan, J. R.; Storgard, C. M.; Loftus, J. C.; Russell, S. J. (2005): Targeted measles virus vector displaying echistatin infects endothelial cells via alpha(v)beta3 and leads to tumor regression. *Cancer Res* 65 (12), 5292–5300. DOI: 10.1158/0008-5472.CAN-04-2879.

Hammond, A. L.; Plemper, R. K.; Zhang, J.; Schneider, U.; Russell, S. J.; Cattaneo, R. (2001): Single-chain antibody displayed on a recombinant measles virus confers entry through the tumor-associated carcinoembryonic antigen. *J Virol* 75 (5), 2087–2096. DOI: 10.1128/JVI.75.5.2087-2096.2001.

Hanauer, J. (2015): Optimierte Virusvarianten zur Onkolyse des Hodgkin Lymphoms. Diploma thesis. Johann Wolfgang Goethe Universität, Frankfurt a.M. Paul-Ehrlich-Institut.

Hanauer, J. D. S.; Rengstl, B.; Kleinlützum, D.; Reul, J.; Pfeiffer, A.; Friedel, T. et al. (2018): CD30-targeted oncolytic viruses as novel therapeutic approach against classical Hodgkin lymphoma. *Oncotarget* 9 (16), 12971-12981. DOI: 10.18632/oncotarget.24191.

Hansen, H. P.; Engels, H. M.; Dams, M.; Paes Leme, A. F.; Pauletti, B. A.; Simhadri, V. L. et al. (2014): Protrusion-guided extracellular vesicles mediate CD30 trans-signalling in the microenvironment of Hodgkin's lymphoma. *J Pathol* 232 (4), 405–414. DOI: 10.1002/path.4306.

Hansen, H. P.; Trad, A.; Dams, M.; Zigrino, P.; Moss, M.; Tator, M. et al. (2016): CD30 on extracellular vesicles from malignant Hodgkin cells supports damaging of CD30 ligand-expressing bystander cells with Brentuximab-Vedotin, in vitro. *Oncotarget* 7 (21), 30523–30535. DOI: 10.18632/oncotarget.8864.

Hastie, E.; Grdzelishvili, V. Z. (2012): Vesicular stomatitis virus as a flexible platform for oncolytic virotherapy against cancer. *J Genl Virol* 93 (12), 2529–2545. DOI: 10.1099/vir.0.046672-0.

Hilleman, M. R. (2001): Current overview of the pathogenesis and prophylaxis of measles with focus on practical implications. *Vaccine* 20 (5-6), 651–665. DOI: 10.1016/S0264-410X(01)00384-X.

Hodgkin, T. (1832): On some Morbid Appearances of the Absorbent Glands and Spleen. *Med Chir Trans* 17, 68–114.

Horie, R. and Watanabe, T. (1998): CD30: expression and function in health and disease. *Semin Immunol* 10 (6), 457–470. DOI: 10.1006/smim.1998.0156.

Hsu, E. C.; Iorio, C.; Sarangi, F.; Khine, A. A.; Richardson, C. D. (2001): CDw150(SLAM) is a receptor for a lymphotropic strain of measles virus and may account for the immunosuppressive properties of this virus. *Virology* 279 (1), 9–21. DOI: 10.1006/viro.2000.0711.

Hudacek, A. W.; Navaratnarajah, C. K.; Cattaneo, R. (2013): Development of measles virus-based shielded oncolytic vectors. Suitability of other paramyxovirus glycoproteins. *Cancer Gene Ther* 20 (2), 109–116. DOI: 10.1038/cgt.2012.92.

Hughes, T.; Coffin, R. S.; Lilley, C. E.; Ponce, R.; Kaufman, H. L. (2014): Critical analysis of an oncolytic herpesvirus encoding granulocyte-macrophage colony stimulating factor for the treatment of malignant melanoma. *Oncolytic Virother* 3, 11–20. DOI: 10.2147/OV.S36701.

Iverson, L. E.; Rose, J. K. (1981): Localized attenuation and discontinuous synthesis during vesicular stomatitis virus transcription. *Cell* 23 (2), 477–484.

Iwasaki, M.; Takeda, M.; Shirogane, Y.; Nakatsu, Y.; Nakamura, T.; Yanagi, Y. (2009): The matrix protein of measles virus regulates viral RNA synthesis and assembly by interacting with the nucleocapsid protein. *J Virol* 83 (20), 10374–10383. DOI: 10.1128/JVI.01056-09.

Johnson, J. E.; Nasar, F.; Coleman, J. W.; Price, R. E.; Javadian, A.; Draper, K. et al. (2007): Neurovirulence properties of recombinant vesicular stomatitis virus vectors in non-human primates. *Virology* 360 (1), 36–49. DOI: 10.1016/j.virol.2006.10.026.

Josimovic-Alasevic, O.; Dürkop, H.; Schwarting, R.; Backé, E.; Stein, H.; Diamantstein, T. (1989): Ki-1 (CD30) antigen is released by Ki-1-positive tumor cells in vitro and in vivo. I. Partial characterization of soluble Ki-1 antigen and detection of the antigen in cell culture supernatants and in serum by an enzyme-linked immunosorbent assay. *Eur J Immunol* 1989 19 (1), 157–162. DOI: 10.1002/eji.1830190125.

Kadin, M. E.; Cavaille-Coll, M. W.; Gertz, R.; Massagué, J.; Cheifetz, S.; George, D. (1994): Loss of receptors for transforming growth factor beta in human T-cell malignancies. *Proc Natl Acad Sci USA* 91 (13), 6002–6006. DOI: 10.1073/pnas.91.13.6002.

Kasamon, Y. L.; Claro, R. A. de; Wang, Y.; Shen, Y. L.; Farrell, A. T.; Pazdur, R. (2017): FDA Approval Summary. Nivolumab for the Treatment of Relapsed or Progressive Classical Hodgkin Lymphoma. *Oncologist* 22 (5), 585–591. DOI: 10.1634/theoncologist.2017-0004.

Katze, M. G.; He, Y.; Gale, M. Jr. (2002): Viruses and interferon. A fight for supremacy. *Nat Rev Immunol* 2 (9), 675-687. DOI: 10.1038/nri888.

Kirn, D.; Martuza, R. L.; Zwiebel, J. (2001): Replication-selective virotherapy for cancer: Biological principles, risk management and future directions. *Nat Med* 7 (7), 781–787. DOI: 10.1038/89901.

Kleinlützum, D.; Hanauer, J. D. S.; Muik, A.; Hanschmann, K.-M.; Kays, S. K.; Ayala-Breton, C. et al. (2017): Enhancing the Oncolytic Activity of CD133-Targeted Measles Virus. Receptor Extension or Chimerism with Vesicular Stomatitis Virus Are Most Effective. *Front Oncol* 7, 127. DOI: 10.3389/fonc.2017.00127.

Kumar, A.; Younes, A. (2014): Role of CD30 targeting in malignant lymphoma. *Curr Treat Options Oncol* 15 (2), 210–225. DOI: 10.1007/s11864-014-0275-7.

Küppers, R. (2012): New insights in the biology of Hodgkin lymphoma. *Hematology Am Soc Hematol Educ Program* 2012 (1), 328–334. DOI: 10.1182/asheducation-2012.1.328.

Leber, M. F.; Baertsch, M.-A.; Anker, S. C.; Henkel, L.; Singh, H. M.; Bossow, S. et al. (2018): Enhanced Control of Oncolytic Measles Virus Using MicroRNA Target Sites. *Mol Ther Oncolytics* 9, 30–40. DOI: 10.1016/j.omto.2018.04.002.

Lichty, B. D.; Power, A. T.; Stojdl, D. F.; Bell, J. C. (2004): Vesicular stomatitis virus. Re-inventing the bullet. *Trends Mol Med* 10 (5), 210–216. DOI: 10.1016/j.molmed.2004.03.003.

Liu, B. L.; Robinson, M.; Han, Z. Q; Branston, R. H.; English, C.; Reay, P. et al. (2003): ICP34.5 deleted herpes simplex virus with enhanced oncolytic, immune stimulating, and anti-tumour properties. *Gene Ther* 10 (4), 292–303. DOI: 10.1038/sj.gt.3301885.

Mader, E. K.; Butler, G.; Dowdy, S. C.; Mariani, A.; Knutson, K. L.; Federspiel, M. J. et al. (2013): Optimizing patient derived mesenchymal stem cells as virus carriers for a phase I clinical trial in ovarian cancer. *J Transl Med* 11 (1), 20. DOI: 10.1186/1479-5876-11-20.

Mader, E. K.; Maeyama, Y.; Lin, Y.; Butler, G. W.; Russell, H. M.; Galanis, E. et al. (2009): Mesenchymal stem cell carriers protect oncolytic measles viruses from antibody neutralization in an orthotopic ovarian cancer therapy model. *Clin Cancer Res* 15 (23), 7246–7255. DOI: 10.1158/1078-0432.CCR-09-1292.

Maroun, J.; Muñoz-Alía, M.; Ammayappan, A.; Schulze, A.; Peng, K.-W.; Russell, S. (2017): Designing and building oncolytic viruses. *Future Virol* 12 (4), 193-213. DOI: 10.2217/fvl-2016-0129.

Martinez, I.; Rodriguez, L. L.; Jimenez, C.; Pauszek, S. J.; Wertz, G. W. (2003): Vesicular stomatitis virus glycoprotein is a determinant of pathogenesis in swine, a natural host. *J Virol* 77 (14), 8039–8047. DOI: 10.1128/JVI.77.14.8039-8047.2003.

Mathas, S.; Hartmann, S.; Küppers, R. (2016): Hodgkin lymphoma: Pathology and biology. *Semin Hematol* 53 (3), 139–147. DOI: 10.1053/j.seminhematol.2016.05.007.

Mathas, S.; Janz, M.; Hummel, F.; Hummel, M.; Wollert-Wulf, B.; Lusatis, S. et al. (2006): Intrinsic inhibition of transcription factor E2A by HLH proteins ABF-1 and Id2 mediates reprogramming of neoplastic B cells in Hodgkin lymphoma. *Nat Immunol* 7 (2), 207–215. DOI: 10.1038/ni1285.

Miest, T. S.; Cattaneo, R. (2014): New viruses for cancer therapy: meeting clinical needs. *Nat Rev Microbiol* 12 (1), 23–34. DOI: 10.1038/nrmicro3140.

Miest, T. S.; Yaiw, K.-C.; Frenzke, M.; Lampe, J.; Hudacek, A. W.; Springfeld, C. et al. (2011): Envelope-chimeric entry-targeted measles virus escapes neutralization and achieves oncolysis. *Mol Ther* 19 (10), 1813–1820. DOI: 10.1038/mt.2011.92.

Moss, W. J.; Griffin, D. E. (2006): Global measles elimination. *Nat Rev Micro* 4 (12), 900–908. DOI: 10.1038/nrmicro1550.

Mühlebach, M. D.; Mateo, M.; Sinn, P. L.; Prüfer, S.; Uhlig, K. M.; Leonard, V. H. J. et al. (2011): Adherens junction protein nectin-4 is the epithelial receptor for measles virus. *Nature* 480 (7378), 530–533. DOI: 10.1038/nature10639.

Mühlebach, M. D.; Leonard, V. H. J.; Cattaneo, R. (2008): The measles virus fusion protein transmembrane region modulates availability of an active glycoprotein complex and fusion efficiency. *J Virol* 82 (22), 11437–11445. DOI: 10.1128/JVI.00779-08.

Muik, A.; Dold, C.; Geiß, Y.; Volk, A.; Werbizki, M.; Dietrich, U.; Laer, D. von (2012): Semireplication-competent vesicular stomatitis virus as a novel platform for oncolytic virotherapy. *J Mol Med* 90 (8), 959–970. DOI: 10.1007/s00109-012-0863-6.

Muik, A.; Kneiske, I.; Werbizki, M.; Wilflingseder, D.; Giroglou, T.; Ebert, O. et al. (2011): Pseudotyping vesicular stomatitis virus with lymphocytic choriomeningitis virus glycoproteins enhances infectivity for glioma cells and minimizes neurotropism. *J Virol* 85 (11), 5679–5684. DOI: 10.1128/JVI.02511-10.

Muik, A.; Stubbert, L. J.; Jahedi, R. Z.; Geiß, Y.; Kimpel, J.; Dold, C. et al. (2014): Re-engineering vesicular stomatitis virus to abrogate neurotoxicity, circumvent humoral immunity, and enhance oncolytic potency. *Cancer Res* 74 (13), 3567–3578. DOI: 10.1158/0008-5472.CAN-13-3306.

Nakamura, T.; Peng, K.-W.; Harvey, M.; Greiner, S.; Lorimer, I. A.; James, C. D.; Russell, S. J. (2005): Rescue and propagation of fully retargeted oncolytic measles viruses. *Nat Biotechnol* 23 (2), 209–214. DOI: 10.1038/nbt1060.

Noyce, R. S.; Bondre, D. G.; Ha, M. N.; Lin, L.-T.; Sisson, G.; Tsao, M.-S. et al. (2011): Tumor Cell Marker PVRL4 (Nectin 4) Is an Epithelial Cell Receptor for Measles Virus. *PLoS Pathog* 7 (8), e1002240. DOI: 10.1371/journal.ppat.1002240.

Obuchi, M.; Fernandez, M.; Barber, G. N. (2003): Development of recombinant vesicular stomatitis viruses that exploit defects in host defense to augment specific oncolytic activity. *J Virol* 77 (16), 8843–8856. DOI: 10.1128/JVI.77.16.8843-8856.2003.

Ong, H. T.; Hasegawa, K.; Dietz, A. B.; Russell, S. J.; Peng, K-W (2007): Evaluation of T cells as carriers for systemic measles virotherapy in the presence of antiviral antibodies. *Gene Ther* 14 (4), 324–333. DOI: 10.1038/sj.gt.3302880.

Parks, C. L.; Lerch, R. A.; Walpita, P.; Wang, H.-P.; Sidhu, M.S.; Udem, S. A. (2001): Analysis of the noncoding regions of measles virus strains in the Edmonston vaccine lineage. *J Virol* 75 (2), 921–933. DOI: 10.1128/JVI.75.2.921-933.2001.

Patterson, J. B.; Thomas, D.; Lewicki, H.; Billeter, M. A.; Oldstone, M. B. (2000): V and C proteins of measles virus function as virulence factors in vivo. *Virology* 267 (1), 80–89. DOI: 10.1006/viro.1999.0118.

Petersen, J. M.; Her, L. S.; Varvel, V.; Lund, E.; Dahlberg, J. E. (2000): The matrix protein of vesicular stomatitis virus inhibits nucleocytoplasmic transport when it is in the nucleus and associated with nuclear pore complexes. *Mol Cell Biol* 20 (22), 8590–8601. DOI: 10.1128/MCB.20.22.8590-8601.2000.

Pierce, J. M.; Mehta, A. (2017): Diagnostic, prognostic and therapeutic role of CD30 in lymphoma. *Expert Rev Hematol* 10 (1), 29–37. DOI: 10.1080/17474086.2017.1270202.

Pileri, S. A.; Ascani, S.; Leoncini, L.; Sabattini, E.; Zinzani, P. L.; Piccaluga, P. P. et al. (2002): Hodgkin's lymphoma: the pathologist's viewpoint. *J Clin Pathol* 55 (3), 162–176.

Plumet, S.; Duprex, W. P.; Gerlier, D. (2005): Dynamics of viral RNA synthesis during measles virus infection. *J Virol* 79 (11), 6900–6908. DOI: 10.1128/JVI.79.11.6900-6908.2005.

Pol, J.; Kroemer, G.; Galluzzi, L. (2016): First oncolytic virus approved for melanoma immunotherapy. *Oncoimmunology* 5 (1), e1115641. DOI: 10.1080/2162402X.2015.1115641.

Puzanov, I.; Milhem, M. M.; Minor, D.; Hamid, O.; Li, A.; Chen, L. et al. (2016): Talimogene Laherparepvec in Combination With Ipilimumab in Previously Untreated, Unresectable Stage IIIB-IV Melanoma. *J Clin Oncol* 34 (22), 2619–2626. DOI: 10.1200/JCO.2016.67.1529.

Radecke, F.; Spielhofer, P.; Schneider, H.; Kaelin, K.; Huber, M.; Dötsch, C. et al. (1995): Rescue of measles viruses from cloned DNA. *EMBO J* 14 (23), 5773–5784.

Reed, D. (1902): On the pathological changes in Hodgkin's disease with special reference to its relation to tuberculosis. *John Hopkins Hosp* 10, 133–193.

Ribas, A.; Dummer, R.; Puzanov, I.; VanderWalde, A.; Andtbacka, R. H. I.; Michielin, O. et al. (2017): Oncolytic Virotherapy Promotes Intratumoral T Cell Infiltration and Improves Anti-PD-1 Immunotherapy. *Cell* 170 (6), 1109-1119.e10. DOI: 10.1016/j.cell.2017.08.027.

Russell, S. J.; Federspiel, M. J.; Peng, K.-W.; Tong, C.; Dingli, D.; Morice, W. G. et al. (2014): Remission of disseminated cancer after systemic oncolytic virotherapy. *Mayo Clin Proc* 89 (7), 926–933. DOI: 10.1016/j.mayocp.2014.04.003.

Russell, S. J.; Peng, K.-W.; Bell, J. C. (2012): Oncolytic virotherapy. *Nat Biotechnol* 30 (7), 658–670. DOI: 10.1038/nbt.2287.

Savage, K. J.; Harris, N. L.; Vose, J. M.; Ullrich, F.; Jaffe, E. S.; Connors, J. M. et al. (2008): ALK- anaplastic large-cell lymphoma is clinically and immunophenotypically different from both ALK+ ALCL and peripheral T-cell lymphoma, not otherwise specified: report from the International Peripheral T-Cell Lymphoma Project. *Blood* 111 (12), 5496–5504. DOI: 10.1182/blood-2008-01-134270.

Schmitz, R.; Stanelle, J.; Hansmann, M. L.; Küppers, R. (2009): Pathogenesis of classical and lymphocyte-predominant Hodgkin lymphoma. *Annu Rev Pathol* 4, 151–174. DOI: 10.1146/annurev.pathol.4.110807.092209.

Schneider, C.; Hübinger, G. (2002): Pleiotropic signal transduction mediated by human CD30: a member of the tumor necrosis factor receptor (TNFR) family. *Leuk Lymphoma* 43 (7), 1355–1366. DOI: 10.1080/10428190290033288.

Schneider, U.; Bullough, F.; Vongpunsawad, S.; Russell, S. J.; Cattaneo, R. (2000): Recombinant measles viruses efficiently entering cells through targeted receptors. *J Virol* 74 (21), 9928–9936. DOI: 10.1128/JVI.74.21.9928-9936.2000.

Schneider-Schaulies, J.; Meulen, V. ter; Schneider-Schaulies, S. (2001): Measles virus interactions with cellular receptors: consequences for viral pathogenesis. *J Neurovirol* 7 (5), 391–399. DOI: 10.1080/135502801753170246.

Schnell, M. J.; Mebatsion, T.; Conzelmann, K. K. (1994): Infectious rabies viruses from cloned cDNA. *EMBO J* 13 (18), 4195–4203.

Scott, L. J. (2017): Brentuximab Vedotin. A Review in CD30-Positive Hodgkin Lymphoma. *Drugs* 77 (4), 435–445. DOI: 10.1007/s40265-017-0705-5.

Shinozaki, K.; Ebert, O.; Suriawinata, A.; Thung, S. N.; Woo, S. L. (2005): Prophylactic alpha interferon treatment increases the therapeutic index of oncolytic vesicular stomatitis virus virotherapy for advanced hepatocellular carcinoma in immune-competent rats. *J Virol* 79 (21), 13705–13713. DOI: 10.1128/JVI.79.21.13705-13713.2005.

Steidl, C.; Shah, S. P.; Woolcock, B. W.; Rui, L.; Kawahara, M.; Farinha, P. et al. (2011): MHC class II transactivator CIITA is a recurrent gene fusion partner in lymphoid cancers. *Nature* 471 (7338), 377–381. DOI: 10.1038/nature09754.

Stein, H.; Foss, H. D.; Dürkop, H.; Marafioti, T.; Delsol, G.; Pulford, K. et al. (2000): CD30(+) anaplastic large cell lymphoma. A review of its histopathologic, genetic, and clinical features. *Blood* 96 (12), 3681–3695.

Stein, H.; Mason, D. Y.; Gerdes, J.; O'Connor, N.; Wainscoat, J.; Pallesen, G. et al. (1985): The expression of the Hodgkin's disease associated antigen Ki-1 in reactive and neoplastic lymphoid tissue. Evidence that Reed-Sternberg cells and histiocytic malignancies are derived from activated lymphoid cells. *Blood* 66 (4), 848–858.

Sternberg, C. (1898): Über eine eigenartige unter dem Bilde der Pseudoleukämie verlaufende Tuberkulose des lymphatischen Apparates. *Heilkunde* 19, 21–90.

Stojdl, D. F.; Lichty, B. D.; tenOever, B. R.; Paterson, J. M.; Power, A. T.; Knowles, S. et al. (2003): VSV strains with defects in their ability to shutdown innate immunity are potent systemic anti-cancer agents. *Cancer Cell* 4 (4), 263–275. DOI: 10.1016/S1535-6108(03)00241-1.

Sun, X.; Roth, S. L.; Bialecki, M. A.; Whittaker, G. R. (2010): Internalization and fusion mechanism of vesicular stomatitis virus and related rhabdoviruses. *Future Virol* 5 (1), 85–96. DOI: 10.2217/FVL.09.72.

Sun, X.; Yau, V. K.; Briggs, B. J.; Whittaker, G. R. (2005): Role of clathrin-mediated endocytosis during vesicular stomatitis virus entry into host cells. *Virology* 338 (1), 53–60. DOI: 10.1016/j.virol.2005.05.006.

Takeda, M.; Takeuchi, K.; Miyajima, N.; Kobune, F.; Ami, Y.; Nagata, N. et al. (2000): Recovery of Pathogenic Measles Virus from Cloned cDNA. *J Virol* 74 (14), 6643–6647. DOI: 10.1128/JVI.74.14.6643-6647.2000.

Tatsuo, H.; Ono, N.; Tanaka, K.; Yanagi, Y. (2000): SLAM (CDw150) is a cellular receptor for measles virus. *Nature* 406 (6798), 893–897. DOI: 10.1038/35022579.

Tiacci, E.; Döring, C.; Brune, V.; Noesel, C.J. van; Klapper, W.; Mechtersheimer, G. et al. (2012): Analyzing primary Hodgkin and Reed-Sternberg cells to capture the molecular and cellular pathogenesis of classical Hodgkin lymphoma. *Blood* 120 (23), 4609–4620. DOI: 10.1182/blood-2012-05-428896.

White, J.; Matlin, K.; Helenius, A. (1981): Cell fusion by Semliki Forest, influenza, and vesicular stomatitis viruses. *J Cell Biol* 89 (3), 674–679. DOI: 10.1083/jcb.89.3.674.

Zhang, K. X.; Matsui, Y.; Hadaschik, B. A.; Lee, C.; Jia, W.; Bell, J. C. et al. (2010): Down-regulation of type I interferon receptor sensitizes bladder cancer cells to vesicular stomatitis virus-induced cell death. *Int J Cancer* 127 (4), 830–838. DOI: 10.1002/ijc.25088.

6 List of figures

7 List of tables

8 Abbreviations

α	anti
ALCL	Anaplastic large cell lymphoma
ANOVA	N-way analysis of variance
APC	Allophycocyanin
APS	Ammonium persulfate
ATCC	American type cell culture
AUC	Area under the curve
BSA	Bovine serum albumin
CAR	Chimeric antigen receptor
CD	Cytosine deaminase
CD(number)	Cluster of differentiation
cDNA	Complimentary DNA
cHL	Classical Hodgkin lymphoma
CHO	Chinese hamster ovary
CHOP	Multi-agent chemotherapy
CMV	Cytomegalovirus
CT	Computed tomography
CTLA-4	Cytotoxic T lymphocyte associated antigen 4
Cy2/7	Cyanine dye 2/7
C-terminus	Carboxy terminus
DAPI	4 ,6-diamidino-2-phenylindole
DARPin	Designed Ankyrin repeat protein
DLBCL	Diffuse large B-cell lymphoma
DMEM	Dulbecco's modified Eagle's medium
DMSO	Dimethyl sulfoxide
DNA	Deoxyribonucleic acid
dpi	Days post implantation/transplantation
dsRNA	Double stranded ribonucleic acid
EDTA	Ethylenediaminetetraacetic acid
EGFR	Epidermal growth factor receptor
EpCAM	Epithelial cell adhesion molecule
et al.	And others
EV	Extracellular vesicles
F (protein)	Fusion protein
F_0, F_1, F_2	F_0: precursor of the F protein, F_1, F_2: processed, active F protein
FACS	Fluorescence-activated cell sorting
Fc	Fragment crystallizable
FCS	Fetal calf serum

FDA	U.S. Food and drug administration
FITC	Fluorescein isothiocyanate
g	Gravity force
G (protein)	Glycoprotein
GFP	Green fluorescent protein
GM-CSF	Granulocyte macrophage colony-stimulating factor
H (protein)	Hemagglutinin protein
H6	Hexa-His-tag
HEPES	4-(2-hydroxyethyl)-1-piperazineethanesulfonic acid
Her2-neu	Human epidermal growth factor 2
HIV	Human immune-deficiency virus
HL	Hodgkin lymphoma
H_{mut}	Hemagglutinin protein blinded for its native receptors
HSV-1	Herpes simplex virus type 1
hpi	Hours post infection
HRP	Horseradish peroxidase
HRS	Hodgkin- and Reed-Sternberg cells
i.p.	Intraperitoneal
i.t.	Intratumoral
i.v.	Intravenous
IF	Immunofluorescence
IFN	Interferon
Ig	Immunoglobulin
IgG	Immunoglobulin G
IL-2	Interleukin-2
IVIS	In vivo imaging system
JAK/STAT	Janus kinases/Signal transducer and activator of transcription
L (protein)	Large protein
LCMV	Lymphocytic choriomeningitis virus
LDL	Low density lipoprotein
LUC	Luciferase
LV	Lentiviral vector
M (protein)	Matrix protein
MEM	Minimal essential medium
miRNA	Micro RNA
MOI	Multiplicity of infection
mRNA	Messenger RNA
MSCs	Mesenchymal stem cells
MV	Measles virus
N (protein)	Nucleocapsid protein

n.s.	Not significant
NIS	Sodium-iodine symporter
NK cell	Natural killer cell
NSe	*NarI*- and *SpeI*-eliminated
NSG	NOD.Cg.Prkdc^{scid}IL2rg^{tmWjl}/Sz]
N-terminus	Amino terminus
NF-κB	Nuclear factor kappa-b
NHL	Non-Hodgkin lymphoma
OS	Overall survival
OV	Oncolytic virus
P (protein)	Phosphoprotein
PBMC	Peripheral blood mononuclear cells
PBS	Phosphate-buffered saline
PD-1	Programmed cell death protein-1
PD-L1	Programmed cell death ligand-1
PE	Phycoerythrin
PenStrep	Penicillin - Streptomycin
pi	Post infection
PI3K	Phosphatidylinositol-4,5-bisphosphate 3-kinase
poly-A	Poly adenosine monophosphate
Puro	Puromycin
RdRp	RNA-dependent RNA-polymerase
RNA	Ribonucleic acid
RNP	Ribonucleoprotein
RPMI	Roswell Park Memorial Institute
s.c.	Subcutaneous
sCD30	Soluble CD30
scFv	Single-chain variable fragment
SCID	Severe combined immune-deficiency
SD	Standard deviation
SDS	Sodium dodecyl sulfate
SDS-PAGE	SDS-Polyacrylamide gel electrophoresis
SEM	Standard error of the mean
SLAM	Signaling lymphocyte activation molecule
SN	Supernatant
SPECT	Single-photon emission computed tomography
ss(-)RNA	Single-stranded, negative sense RNA
SuperCD/SCD	Super cytosine deaminase
TBS	Tris-buffered saline
$TCID_{50}$	Tissue culture infective dose 50

TEMED	N,N,N',N'-Tetramethylethylendiamin
TIC	Tumor initiating cell
TNF	Tumor necrosis factor
TRAF	TNF receptor-associated factors
VP-SFM	Virus production serum free medium
VSV	Vesicular stomatitis virus
w/o	without
WB	Western blot
WHO	World health organization

9 Curriculum Vitae

Persönliche Informationen

Name:	Julia Dorothea Sophie Hanauer
Geburtsdatum:	22.12.1989
Geburtsort:	Frankfurt am Main

Wissenschaftlicher Werdegang

09/2018	Abgabe der Doktorarbeit am Fachbereich Biologie der Technischen Universität Darmstadt Titel: Increasing oncoselectivity of virotherapy: Receptor targeted viruses against CD30-positive malignancies
02/2015 – 10/2018	Promotionsstudentin in der Abteilung "Molekulare Biotechnologie und Gentherapie" geleitet durch Prof. Dr. Christian Buchholz am Paul-Ehrlich-Institut in Langen
02/2015 – 12/2016	Promotionsstipendium des Zell- und Gentherapie Zentrums der Landesoffensive zur Entwicklung Wissenschaftlich-ökonomischer Exzellenz (LOEWE)
09/2010 – 02/2015	Studium der Biochemie an der Goethe-Universität in Frankfurt am Main, Studienabschluss: Diplom-Biochemikerin
06/2009	Allgemeine Hochschulreife an der Heinrich Böll Schule in Hattersheim am Main

10 Publications

Parts of this thesis are published in peer-reviewed Paper:

CD30-targeted oncolytic viruses as novel therapeutic approach against classical Hodgkin lymphoma

Hanauer JDS, Rengstl B, Kleinlützum D, Reul J, Pfeiffer A, Friedel T, Schneider S, Newrzela S, Hansmann ML, Buchholz CJ and Muik AG,

Oncotarget, 2018, 9 (16), 12971-12981

Enhancing the Oncolytic Activity of CD133-Targeted Measles Virus: Receptor Extension or Chimerism With Vesicular Stomatitis Virus Are Most Effective"

Kleinlützum D, Hanauer JDS, Muik AG, Hanschmann KM, Kays SK, Ayala-Breton C, Peng KW, Mühlebach M, Abel T and Buchholz CJ

Frontiers in Oncology, 2017, 7, 127

Parts of this thesis were orally presented at scientific conferences:

CD30-targeted oncolytic viruses as novel therapeutic approach against Hodgkin lymphoma

Hanauer JDS, Rengstl B, Friedel T, Schneider S, Newrzela S, Buchholz CJ and Muik AG

Annual PEI Retreat, Ronneburg, 2018

CD30-targeted oncolytic viruses as novel therapeutic approach against Hodgkin lymphoma

Hanauer JDS, Rengstl B, Friedel T, Schneider S, Newrzela S, Buchholz CJ and Muik AG

27. Annual Meeting of the Society for Virology (GfV), Marburg, 2017

CD30-targeted oncolytic viruses as novel therapeutic approach against Hodgkin lymphoma

Hanauer JDS, Rengstl B, Friedel T, Schneider S, Newrzela S, Buchholz CJ and Muik AG

7. UCT Science Day, Frankfurt a.M., 2016

Parts of this thesis were presented by a poster at scientific conferences:

CD30-targeted oncolytic viruses as novel therapeutic approach against Hodgkin lymphoma

Hanauer]DS, Rengstl B, Friedel T, Schneider S, Newrzela S, Buchholz CJ and Muik AG

25. Annual Meeting of the European Society of Gene & Cell Therapy, Berlin, 2017

CD30-targeted oncolytic viruses as novel therapeutic approach against Hodgkin lymphoma

Hanauer]DS, Rengstl B, Friedel T, Schneider S, Newrzela S, Buchholz CJ and Muik AG

3. CRI-CIMT-EATI-AACR International Cancer Immunotherapy Conference, Mainz, 2017

CD30-targeted oncolytic viruses as novel therapeutic approach against Hodgkin lymphoma

Hanauer]DS, Rengstl B, Friedel T, Schneider S, Newrzela S, Buchholz CJ and Muik AG

24. Annual Meeting of the European Society of Gene & Cell Therapy, Florenz, 2016

CD30-targeted oncolytic viruses as novel therapeutic approach against Hodgkin lymphoma

Hanauer]DS, Rengstl B, Friedel T, Schneider S, Newrzela S, Buchholz CJ and Muik AG

22. Annual Meeting of the German Society for Gene Therapy (DGGT), Heidelberg, 2016

11 Danksagung

Mein besonderer Dank geht allen voran an Christian Buchholz für die angenehme Betreuung meiner Doktorarbeit in seiner Arbeitsgruppe. Ich bedanke mich für Diskussionsbereitschaft und stetige Gelassenheit. Alexander Muik danke ich für das spannende Thema und die finanzielle Möglichkeit meine Doktorarbeit in dieser Arbeitsgruppe beginnen zu können.

Seitens der TU Darmstadt danke ich Beatrix Süß und Alexander Löwer für die freundliche und unkomplizierte Betreuung am Fachbereich Biologie.

Als Teil meines Thesis Committees möchte ich mich bei Veronika von Messling und Michael Mühlebach für konstruktive Diskussionen, die maßgeblich zum Gelingen dieser Arbeit beigetragen haben, bedanken.

Für eine Perspektive abseits vom Labor ein herzliches Dankeschön an meine Mentorin Petra Arndt und meine Peer Gruppe als Teil von Mentoring Hessen.

Ganz besonders möchte ich mich bei allen aktuellen und ehemaligen Kollegen der Arbeitsgruppe Molekulare Biotechnologie und Gentherapie bedanken. Danke im speziellen an Johanna, Dina, Anett, Annika, Laura, Tatjana, Frederic, Jessi, Thorsten, Gundi und Manu. Die tolle Arbeitsatmosphäre, der Teamgeist, sowie die unermüdliche Hilfs- und Diskussionsbereitschaft haben mich immer inspiriert. Ich werde gerne an gemeinsame Mittagspausen mit Kaffeetrinken, viel Lachen und diverse Unternehmungen nach Feierabend zurückdenken. Durch euch werde ich meine Zeit am PEI nie vergessen und immer in guter Erinnerung behalten.

Der größte Dank gilt meiner Familie Do & Roland, Jan, Ruth & Anna, Elke, sowie Nabla & Quabla für den uneingeschränkten Rückhalt in allen Lebenslagen. Meinem zukünftigen Mann Stefan möchte ich insbesondere für seine bedingungslose Unterstützung und sein unendliches Verständnis danken. Danke, dass du mich erdest und mich immer optimistisch in die Zukunft blicken lässt.

Abschließend danke ich an dieser Stelle allen Mäusen, die ihr Leben für diese wissenschaftliche Arbeit gelassen haben.

Ohne euch wäre das alles nicht möglich gewesen!

12 Ehrenwörtliche Erklärung

Ich erkläre hiermit ehrenwörtlich, dass ich die vorliegende Arbeit entsprechend den Regeln guter wissenschaftlicher Praxis selbstständig und ohne unzulässige Hilfe Dritter angefertigt habe.

Sämtliche aus fremden Quellen direkt oder indirekt übernommenen Gedanken sowie sämtliche von Anderen direkt oder indirekt übernommenen Daten, Techniken und Materialien sind als solche kenntlich gemacht. Die Arbeit wurde bisher bei keiner anderen Hochschule zu Prüfungszwecken eingereicht.

Darmstadt, den .....

.....

Julia Hanauer